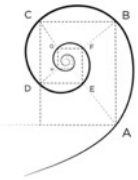


UNIVERSITÀ DEGLI STUDI
DI MILANO



DOTTORATO DI MEDICINA MOLECOLARE E TRASLAZIONALE

CICLO XXXII

Anno Accademico 2019/2020

TESI DI DOTTORATO DI RICERCA

MED/04

Development of an *in-vitro* humanized microfluidic platform to study neuronal tau aggregation and propagation

Dottorando: Elena FICULLE

Matricola N°: R11693

TUTORE: Prof. Mario Salvatore CLERICI

CO-TUTORE: Dott.ssa Suchira BOSE

COORDINATORE DEL DOTTORATO: Prof. Michele SAMAJA

INDEX

INDEX ..... *I*

LIST OF ABBREVIATIONS ..... *I*

RESEARCH INTEGRITY ..... *V*

SOMMARIO ..... *VI*

ABSTRACT ..... *VIII*

1. INTRODUCTION *1*

1.1 Alzheimer's disease *1*

1.1.1 Forms of AD 3

1.1.2 Amyloid β and senile plaques 7

1.1.3 Neurofibrillary tangles 13

1.2 Tau *16*

1.2.1 Tau mutations 20

1.2.2 Tau aggregation 25

1.2.3 Tau propagation 29

1.3 Microfluidic Devices *48*

1.3.1 Trans-neuronal tau propagation 51

1.3.2 The role of synapses in tau propagation 53

1.3.3 MFDs to develop tau targeted therapeutics 55

1.4 Tau modulators and related Clinical Trials *58*

1.4.1 Modulating tau post translational modifications 60

1.4.2 Stabilising microtubules 62

1.4.3 Tau aggregation inhibitors 62

1.4.4 Tau immunotherapy 64

AIMS OF THE STUDY.....68

2. MATERIALS AND METHODS.....70

2.1 hAD Seed Preparation: sarkosyl extraction of tau aggregates from human AD brains.....70

2.1.1 Standard Preparation.....70

2.1.2 AlphaScreen protocol for determining the concentration of tau.....72

2.1.3 Sarkosyl extraction of intracellular tau aggregates and Western blotting.....74

2.2 Rat primary Cortical Neuron cultures, 96-well assay.....77

2.2.1 RCN dissociation and plating protocols.....77

2.2.2 Plating and treating RCN in 96-well plates.....79

2.2.3 Immunocytochemistry and imaging.....81

2.3 Microfluidic Xona Assay.....82

2.3.1 Plasma bonding of MFDs to glass-bottom plates.....82

2.3.2 Poly-D-Lysine coating of Xona MFDs.....82

2.3.3 Plating Rat Cortical Neurons in Xona MFDs.....83

2.3.4 Treating neurons in Xona MFDs.....83

2.3.5 Immunocytochemistry and imaging.....85

2.3.6 Image analysis of Xona MFDs.....85

2.3.7 Xona MFDs assay: characterization of tau aggregates released in the propagation side.....86

2.3.8 Calcium imaging in Xona devices.....88

2.4 High Throughput (HT) microfluidic assay.....90

2.4.1 Plasma bonding of HT devices on glass surfaces.....90

2.4.2 Plating Rat Cortical Neurons in HT devices.....91

2.4.3 Treating neurons in HT devices.....91

2.4.4 Immunocytochemistry, imaging and image analysis.....92

2.5 Humanized High Throughput microfluidic assay 94

2.5.1 Genotyping.....94

2.5.2 hTau neurons preparation protocol 97

2.5.3 Humanized HT microfluidic assay 99

2.5.4 Immunocytochemistry and imaging.....99

2.6 Statistical Analysis 102

3. RESULTS.....103

3.1 hAD seed preparation 103

3.1.1 Sarkosyl extraction of human Alzheimer's disease seed generates concentrated tau extract which can cause endogenous tau aggregation 103

3.1.2 Sarkosyl extracted human AD seed recruits rodent Tau to form insoluble aggregates 105

3.2 RCN Tau aggregation assay 108

3.2.1 RCNs assay characterization: seeding neurons with hAD seed.....108

3.2.2 RCN assay characterization: the effect of hAD seed on endogenous rodent tau.....110

3.2.3 RCN tau aggregation assay: effect of Anle138b on tau aggregation...112

3.3 Xona microfluidic devices, RCN tau propagation assay.....113

3.3.1 Using microfluidic devices to study propagation of h AD templated rodent Tau.....114

3.3.2 Propagation of endogenously aggregated rodent tau is a real effect and not a device artefact. 119

3.3.3 Xona MFDs assay: image analysis and quantification method of T49 propagated thread-like inclusions.....125

3.3.4 Xona MFDs assay: optimization of experimental conditions 128

3.3.5 Xona MFDs assay: seeding and propagation of aggregated tau is hAD seed concentration-dependent 129

3.3.6 Xona MFDs assay: the aggregation and propagation of endogenous tau that result from hAD seeding can be pharmacologically inhibited.....132
3.3.7 Xona MFD assay: characterization of tau thread-like inclusions released in the propagation side.....135
3.3.8 Xona MFD assay: functional studies can be run in this platform.....137

3.4 High throughput (HT) microfluidic assay as a miniaturized platform to study tau propagation.....142

3.4.1 HT microfluidic assay: inhibiting tau propagation with a tool compound 147
3.4.2 HT microfluidic assay: inhibiting tau propagation by modulating neuronal mGluR receptors.....148

3.5 Development of a humanized, high throughput, microfluidic assay platform.....151

3.5.1 hTau HT microfluidic assay: inhibiting tau propagation with a tool compound 160
3.5.2 hTau HT microfluidic assay: the role of astrocytes in tau propagation and aggregation 161

4. DISCUSSION & CONCLUSION.....165

5. BIBLIOGRAPHY.....184

6. SCIENTIFIC PRODUCTS 226

7. RINGRAZIAMENTI..... *Error! Bookmark not defined.*

8. ACKNOWLEDGEMENTS..... *Error! Bookmark not defined.*

9. DISCLOSURE INFORMATION 229

10. PhD THESIS EVALUATION.....230

LIST OF ABBREVIATIONS

AA	*Amino acids*
Aβ	*Amyloid-beta*
AD	*Alzheimer's disease*
ApoE	*Apolipoprotein E*
APP	*Amyloid precursor protein*
BACE	*β site-APP cleaving enzyme*
BBB	*Blood brain barrier*
BCA	*Bicinchoninic acid assay*
BiFC	*Bimolecular fluorescence complementation*
$Ca2^{+}$	*Calcium ion*
CBD	*Corticobasal degeneration*
CFP	*Cyan fluorescent protein*
CNS	*Central nervous system*
CRC	*Concentration response curve*
CSF	*Cerebrospinal fluid*
DIV	*Days in vitro*
DMEM	*Dulbecco's modified eagle's medium*
DMSO	*Dimethyl sulfoxide*
DPBS	*Dulbecco's phosphate-buffered saline*
DS	*Down Syndrome*
EC	*Entorhinal cortex*
EDTA	*Ethylenediaminetetraacetic acid*
EM	*Electron microscopy*
fAD	*Familial Alzheimer's disease*

FBS	*Foetal bovine serum*
FD	*Final/Fixing day*
FL	*Full lenght*
FRET	*Fluorescence resonance energy transfer*
FTD	*Frontotemporal dementia*
FTDP-17	*Frontotemporal dementia with parkinsonism linked to chromosome 17*
GFAP	*Glial fibrillary acidic protein*
GFP	*Green fluorescent protein*
GuHCl	*Guanidine hydrochloride*
HBSS	*Hank's balanced salt solution*
HCI	*High-content imaging*
HT	*High Throughput*
hAD seed	*Human Alzheimer's disease seed*
ICC	*Immunocytochemistry*
IF	*Immunofluorescence*
IHC	*Immunohistochemistry*
iPSC	*Induced pluripotent stem cell*
LRP1	*Lipoprotein receptor protein 1*
LTD	*Long term depression*
LTP	*Long term potentiation*
LVs	*Lentiviruses*
MAPT	*Microtubule associated protein tau*
MeOH	*Methanol*
MFDs	*Microfluidic devices*
MG	*Microglia*

MT	*Microtubule*
MVB	*Multivesicular body*
NFTs	*Neurofibrillary tangles*
NTs	*Neuropil threads*
NO	*Nitric oxide*
PAGE	*Polyacrylamide gel electrophoresis*
PDL	*Poly-D-lysine*
PDMS	*Polydimethylsiloxane*
PF	*Protofibrils*
PFA	*Paraformaldehyde*
PHFs	*Paired helical filaments*
PiD	*Pick's disease*
PLO	*Poly-L-ornithine*
PMSF	*Phenylmethylsulphonyl fluoride*
PRD	*Proline-rich domain*
PS1	*Presenilin-1*
PS2	*Presenilin-2*
PSD95	*Postsynaptic density protein 95*
PSP	*Progressive supranuclear palsy*
PTMs	*Post translational modifications*
QC	*Quality control*
RCNs	*Rat cortical neurons*
RD	*Repeat domain*
ROI	*Region of interest*
ROS	*Reactive oxygen species*
RT	*Room temperature*

sAD	*Sporadic Alzheimer's sisease*
SD	*Seeding day*
SDS	*Sodium dodecyl sulphate*
SFs	*Straight filaments*
SOD1	*Superoxide dismutase 1*
SP	*Senile plaques*
TBS	*Tris buffer saline*
TEC	*Transentorhinal cortex*
TD	*Tangle-only dementia*
Thio-T	*Thioflavin T*
TL	*Total lysate*
TM	*Transmembrane*
TNTs	*Tunnelling nanotubes*
WB	*Western blot*
WT	*Wild type*
YFP	*Yellow fluorescent protein*

RESEARCH INTEGRITY

All data reported in this work are compliant to the fundamental principles of research integrity, according to The European Code of Conduct for Research Integrity (ALLEA, Berlin, 2018), as follows:

- Data are **reliable** in reflecting quality research based on the appropriate design, methodology, the analysis and the use of resources

- Data are developed, undertaken, reviewed, reported and communicated in a transparent fair, full and unbiased way, reflecting research **honesty**

- Data are produced, elaborated and communicated **respecting** colleagues, research participants, society, ecosystems, cultural heritage and the environment

Data are synonymous of **accountability** for the research from idea to publication, for its management and organisation, for training, supervision and mentoring, and for its wider impacts.

SOMMARIO

***Introduzione**: la patologia di Alzheimer (AD) è la causa più comune di demenza ed è caratterizzata da depositi extracellulari di β-amiloide e da aggregati intracellulari chiamati grovigli neurofibrillari (NFTs) formati dalla proteina tau iperfosforilata. Poiché è stato dimostrato che il declino cognitivo dei pazienti di AD correla con la diffusione degli aggregati di tau più che con la presenza di β-amiloide, è fondamentale capire i meccanismi molecolari che causano la propagazione di tau.*
Studi hanno dimostrato come la diffusione temporale e spaziale degli NFTs sia costante nei vari pazienti e che sia dovuta alla propagazione attraverso il network assonale tra neuroni connessi a livello sinaptico. Ad oggi infatti, alcuni degli "early phase Clinical Trials" e degli studi si stanno concentrando sulla propagazione di tau al fine di poter prevenire la sua internalizzazione da parte delle cellule riceventi, ancora sane, sia con uso di molecole che con anticorpi.
Ci sono stati diversi studi per riprodurre in vitro un modello di network neuronale al fine di valutare in maniera appropriata delle terapie mirate prima che esse venissero testate in vivo, e la maggior parte di questi si basano sull'uso di microfluidica. Tuttavia, in questi modelli spesso sono stati utilizzati degli approcci poco fisiologici come l'over-espressione o la mutazione di tau o l'utilizzo di tags fluorescenti che possono compromettere l'affidabilità di questi sistemi. Per questo motivo è necessario lo sviluppo di una nuova metodologia che possa migliorare questo approccio e che potrà in fine essere utilizzata per un efficiente ed affidabile screening di nuove terapie per la malattia di Alzheimer.

***Scopo del lavoro:** il principale obiettivo di questa ricerca è stato quello di stabilire una nuova piattaforma neuronale umanizzata di microfluidica, che potesse modellare e che permettesse lo studio, dell'aggregazione e propagazione di tau in modo sia qualitativo che quantitativo.*
I dispositivi di microfluidica rappresentano un'alternativa miniaturizzata per ricapitolare la propagazione di aggregati proteici come quelli di tau; infatti, essi permettono la coltura di popolazioni neuronali sinapticamente connesse ma fisicamente isolate che possono essere indotte allo sviluppo di aggregati e, conseguentemente, alla loro propagazione. Questo modello potrebbe essere ideale per testare gli effetti di potenziali terapie contro tau che vadano a contrastare la propagazione trans neuronale.

***Materiali & Metodi:** al fine di sviluppare un modello di propagazione nei dispositivi di microfluidica, è stato in primo luogo validato un protocollo per stimolare l'aggregazione di tau endogena in neuroni corticali di ratto (RCN)*

utilizzando come induttore del materiale derivato da cervelli umani di pazienti AD (hAD seed). Successivamente, usando le stesse condizioni, sono stati sviluppati diversi protocolli di microfluidica per RCN che hanno mostrato non solo aggregazione ma anche propagazione di tau utilizzando tecniche quali High Content Imaging (HCI) ed un software di immagine che è stato sviluppato internamente. Infine, è stato sviluppato una versione umanizzata e miniaturizzata di questo protocollo al fine di avere una piattaforma fisiologicamente rilevante per poter testare terapie contro tau umana.

Risultati: *in questo progetto è stato sviluppato un modello cellulare umanizzato che permette lo studio della propagazione endogena di tau, da neurone a neurone, usando dispositivi di microfluidica.*
Dopo una prima fase di ottimizzazione, è stato dimostrato che utilizzando hAD seed è possibile indurre in neuroni corticali piastrati in dispositivi di microfluidica, l'aggregazione della proteina tau endogena e la sua propagazione in maniera trans-neuronale in modo quantificabile.
Inoltre, questo modello è stato validato statisticamente ed è stato successivamente convertito in uno miniaturizzato per aumentare il "throughput" della piattaforma passando così da 6 a 16 unità di microfluidica contenute in una piastra.
Infine, questo metodo è stato umanizzato al fine di studiare l'aggregazione e la propagazione della forma umana di tau usando una cultura primaria di neuroni murini che esprimono solo la proteina tau umana.
E' stato dimostrato che Anle 138b, una molecola conosciuta in letteratura per le sue capacità antiaggreganti, può bloccare l'aggregazione e il trasferimento trans-neuronale di tau, suggerendo che questo nuovo sistema possa essere usato per valutare i meccanismi di propagazione di tau e trovare nuove terapie.

Conclusioni: *In questo lavoro è stato sviluppato con successo un metodo di microfluidica quantitativo e riproducibile che può modellare le taupatie sporadiche umane come la malattia di Alzheimer. Usando sia RCN che neuroni corticali hTau trattati ed indotti con hAD seed, è stata osservata e quantificata la formazione e la propagazione di aggregati endogeni di tau ed è stato testato l'effetto di una molecola inibitoria su questi due meccanismi. È stato inoltre dimostrato come questi modelli possano essere anche utilizzati per condurre studi esplorativi come quelli volti al monitoraggio dell'attività e della connettività neuronale e gli studi sul ruolo dei diversi tipi cellulari presenti in cultura, nell'aggregazione e propagazione di tau. Soprattutto, è stato dimostrato come questo modello possa essere utilizzato come piattaforma di screening per testare potenziali inibitori della propagazione di tau murina ed umana.*

ABSTRACT

Background: *Alzheimer's disease (AD) is the most common cause of dementia, characterized by the presence of extracellular β-amyloid plaques and intracellular neurofibrillary tangles (NFTs) composed of aggregated and hyperphosphorylated tau. Since it has been shown that tau aggregates correlate with cognitive decline much better than β-amyloid formations, it is important to understand how tau can spread in the brain. Moreover, the spatiotemporal spread of tau observed during clinical manifestation suggests that it propagates along the axonal network between synaptically connected neurons. On these bases, some early-phase Clinical Trials are aiming to target tau during transcellular spreading in order to prevent its internalization by recipient neurons, using both compounds and antibodies. For the experimental evaluation of candidates before in vivo studies, there have been many attempts to replicate this network in vitro, most of which used microfluidic approaches; however, these experiments have often utilized parameters that may reduce the physiological relevance of the assay, such as by overexpressing tau, using fluorescent tags, or by introducing MAPT mutations. New methods that can improve these assays are required to help the screening of efficient and effective treatments.*

Aim of the work: *The main purpose of this research project has been to establish a humanized, in vitro neuronal microfluidic platform to recapitulate and study tau aggregation and propagation in a qualitative and quantitative way. Microfluidic devices represent a miniaturized alternative tool to recapitulate tau spreading conditions, by enabling the culture of synaptically connected, but environmentally isolated, neuronal populations that can be seeded, thereby inducing endogenous tau aggregation and subsequent propagation. This model system could be ideal for testing the effect of potential tau therapeutics that modulate transneuronal tau propagation.*

Material & Methods: *Before developing the microfluidic propagation assay, a rat cortical neuron (RCN) aggregation assay that uses seeding-competent material from human AD brains (hAD seed) to induce endogenous aggregation was validated. Subsequently, the same conditions were used to develop a RCN microfluidic assay that can show endogenous tau aggregation, and consequent propagation, using High Content Imaging (HCI) and a proprietary interactive computer program for image quantification. Finally, using a transgenic mouse line that expresses human MAPT, a humanized and miniaturized version of the assay has been developed in order to have a physiologically relevant, medium-throughput platform to test tau therapies.*

Results: *After a phase of optimization, it has been shown that hAD seed induces endogenous rodent tau aggregation and transneuronal propagation in a quantifiable manner in a microfluidic culture model. Moreover, this assay was statistically validated and further converted to a medium-throughput format allowing the user to handle 16 two-chamber devices simultaneously in the footprint of a standard 96 well plate. Furthermore, this assay was humanized in order to study hTau aggregation and propagation using primary neurons from a mouse model that expresses human tau only. It has been proved that Anle 138b, a literature small molecule that has been previously shown to impair protein aggregation, can block the transneuronal transfer of tau aggregates, suggesting that this novel system can be used to evaluate mechanisms of tau spreading and to find therapeutic interventions. Moreover, preliminary experiments have shown that the aggregation of endogenous tau induces not only an increase of neuronal excitability but also an activation of astrocytes which might also have a role in tau pathology.*

Conclusions: *This work has been successfully developed a robust and quantitative microfluidic assay that can model an isolated mechanism of tau propagation. Using both RCNs and hTau mouse cortical neurons seeded with hAD seed, it was possible to quantify the formation and propagation of endogenous tau inclusions and demonstrate that a putative inhibitor of tau propagation is active in this assay. It was also shown that these models can be further employed for exploratory studies, such as monitoring the functional activity and connectivity of the neuronal cultures, as well as investigating the role of different cell types in tau aggregation and propagation. Most importantly, this manuscript exhibits the latent potential of microfluidic assays as screening platforms for the preclinical evaluation of tau propagation inhibitors.*

1. INTRODUCTION

1.1 Alzheimer's disease

Ageing is a physiological process that is associated to several body changes throughout the lifespan of human beings; in this frame, the brain is highly affected since important changes in neurons, molecules, vasculature and tissue morphology occur ultimately leading to neurodegeneration [1]. Recent studies have demonstrated that neurogenesis and synaptogenesis in humans continue into and throughout adult life contributing to the ability of the adult brain to function normally and that they can be induced in response to cerebral diseases for self-repair; however, these processes decline with advancing age [2].

Presently, average life expectancy is much longer than in the past due to improvements in healthcare, medicine, and technology, but this has also led to an increased prevalence of age-related pathologies, such as dementia-causing diseases.

Dementia is a condition that currently affects 40-50 million people; it is characterized by a group of symptoms including memory loss, confusion, mood changes, and a gradual loss of independence [3].
The most common form of dementia (50-70%) is Alzheimer's Disease (AD), a neurodegenerative disease clinically characterized by cognitive decline and memory impairment, which is caused by a reduction of dendritic spines and synapses that lead to neuronal

degeneration. Substantial neuronal death causes macroscopic changes in the brain morphology that results in atrophic areas and in ventricular enlargement. In particular, the brain areas affected by AD are involved in memory, including the entorhinal cortex and hippocampus, and, in a latter phase of the pathology, areas of the cerebral cortex responsible for language, reasoning, and social behaviour [4,5].

The characteristic lesions associated with AD are extracellular senile plaques (SP) mostly composed of amyloid-beta aggregates, and intracellular neurofibrillary tangles (NFTs) composed of misfolded and hyperphosphorylated tau protein [6].

A systematic revision published in The Lancet [7] shows that there are over 9.9 million new cases of dementia each year worldwide, which can be calculated as one new case every 3.2 seconds. This pathology is most common in the elderly population and its incidence increases with age up to 40% of people over 80 [8].
It has been predicted that the current worldwide cost for dementia is £600 billion/year, which will increase by 85% by 2030.
Considering the massive socioeconomic impact that this pathology has, and will have in the future, we must study multiple ways to approach and characterize it, in order to find the best way to translate preclinical findings into disease-modifying treatments.

1.1.1 Forms of AD

Alzheimer's disease is a severe neurodegenerative disease characterized by the formation and accumulation of very stable, insoluble protein aggregates in the brain: amyloid fibrils [9].

For this reason, AD is defined as an amyloidosis, a group of pathologies that is characterized by accumulation of proteins that have adopted the characteristic amyloid beta-sheet-rich structure and are detectable by Congo Red birefringence [10]. They are formed by the aggregation of normally soluble amyloid proteins that accumulate progressively in deposits that disrupt normal tissue architecture, damaging the function of tissues and organs. Moreover, they are often related to defects in protein clearance so amyloid deposits are usually removed very slowly from the cells [11]. Many proteins are known to form amyloid fibrils and they are implicated in multiple pathologies, including Huntington's disease or Creutzfeldt–Jakob disease. In particular, AD is a conformational pathology since in this case the accumulation is favoured by a misfolding of the protein themselves. Moreover, aggregated amyloid proteins can act as a template to induce further aggregation by recruiting endogenous protein. The cellular damage then is not only related to the cytotoxicity caused directly by the aggregates, but also from the loss of function of the misfolded proteins [12].

There are different forms of AD:

- Sporadic with late onset
- Familial with early onset

- Familial with late onset
- Forms associated with Down syndrome

Sporadic forms (sAD) are the most common (85-90% of cases) but the causes are not yet fully understood. In the small percentage of cases where the causes are known, they can be due to viruses, cerebral traumas, chronic circulatory insufficiency, and natural ageing. The average duration of the pathology is 7-10years [13].

Familial forms (fAD) are pathologies that are caused by autosomal dominant genetic mutations. The most common genes related to fAD are APP (amyloid precursor protein), PS1 (presenilin-1) and PS2 (presenilin-2), which are all involved in the biosynthesis pathway of Aβ, the main peptide component of senile plaques [14].

APP is a type I transmembrane (TM) glycoprotein expressed in both neuronal and non-neuronal cells in different isoforms, arisen from alternative splicing, and it is the precursor of amyloidogenic peptides that form senile plaques. Its gene is on chromosome 21 and neurons predominantly express the APP695 isoform, for which the role is still not fully understood[15]. It has been shown that this protein is important in regulating neuronal survival, neurite development and synaptic plasticity. In fact, its expression is upregulated during neuronal development [16].

APP is sequentially cleaved by different secretase enzymes and, based on the type of secretase that processes it, amyloidogenic or non-amyloidogenic peptides are formed. Mutations of this genes are

rare, but they have been found close to the cleavage sites; these mutations preferentially drive certain amyloidogenic cleavage -i.e. some of them increase the production of amyloidogenic peptides [17]. PS1 is a protein that composes the catalytic site of γ-secretase and the mutations of this gene cause an increase of Aβ production, an alteration of Ca^{2+} homeostasis, and tau hyperphosphorylation. Compared to APP mutations, the onset of PS1-mutant fAD is much earlier, in fact the first signs appear before 55 years [18].

PS2 is also part of the catalytic site of γ-secretase and is a homolog of PS1. Its mutations cause similar effects to PS1 mutations with the only difference being a later onset of pathology. Presenilin mutations are the most common cause of fADs [19].

AD onset is not always due to mutations that directly cause the pathology (APP/PS1/PS2) but there are other genetic factors that don't necessarily cause AD, but they increase the risk.

Apolipoprotein E (ApoE) is a polymorph gene on chromosome 17 that exists in 3 variants: ε2, ε3, and ε4. ApoE is a plasmatic lipoprotein with a role in cholesterol transportation and it promotes receptor-mediated clearance of lipoprotein remnants from the circulation. One of its targets that it helps to eliminate is Aβ. ε4 polymorphism is associated with a greater abundance of Aβ because it both enhances Aβ production, by affecting the activity of gamma-secretase, and decreases Aβ clearance, because of its reduced ability to transport Aβ across the blood–brain barrier (BBB); it also impairs the lysosomal degradation of Aβ [20].

So far ApoE4 is considered the most important risk factor for late onset AD [21,22]. Despite other polymorphisms associated with genes related to inflammation, lipid metabolism, and intracellular trafficking having been described in AD, none of them are as common nor as severe as ApoE [23].

Another form of AD is the one associated with Down syndrome [24]. Down syndrome (DS), described in 1866 by J. Langdon Down [25] and identified as a chromosome 21 trisomy by Lejeune in 1959, is one of the most common causes of intellectual disability. Since APP's gene is located on chromosome 21, the trisomy causative of DS is characterised by an overexpression of APP that leads to the presence of elevated levels of Aβ peptides [26,27]. Pathologically this is reflected in the extracellular accumulation of amyloid and the appearance of senile plaques after the age of 30 years that are usually detected and diagnosed at the age of 40 [28]. Nevertheless autopsy studies of younger individuals with DS have shown that intracellular Aβ can be observed also in young 15 year old patients [29].

People with DS not only show Aβ plaques and NFTs, but also higher levels of oxidative stress at all ages compared with age matched controls. Moreover, on the chromosome 21 there are also inflammation-related genes as SOD1, IFNAR1 and 2, IFNGR2 and CXADR. Due to the trisomy, the overexpression of these genes influences neuroinflammation that plays a very important roles in AD [30].

1.1.2 Amyloid β and senile plaques

Senile plaques (SP) are polymorphous β-amyloid protein deposits found in the brain in Alzheimer's disease and normal aging [31]. SP morphology and size (from 6 to 10 nm) is dependent on the anatomical region in which they accumulate, and they are composed of short peptides (39-42 amino acids) derived from APP protein.

To explore in more detail the formation of SPs and, consequently, their role in neurodegeneration, it's important to analyse the amyloidogenic cleavage of APP.

APP processing is mediated by three different enzymatic complexes: α, β, and γ secretases. Depending on the secretase that mediates the cleavage, APP will undergo either amyloidogenic (β-secretase) or non-amyloidogenic (α-secretase) processing (*Fig 1.1*).

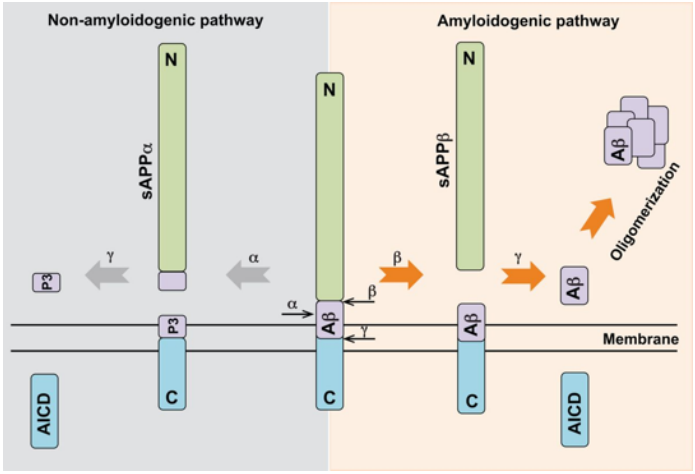


***Figure 1.1**: APP processing into amyloidogenic or non-amyloidogenic pathways. Image adapted from* [32].

In the non-amyloidogenic pathway, the first enzyme to act on APP is the α-secretase that hydrolyses APP on the extracellular side and generates two fragments: soluble APP-α, and C38 that is anchored to the membrane, and that is further hydrolysed by γ-secretase. This sequential processing of C38 results in the formation of the soluble fragment P3, and the intracellular peptide AICD (APP Intracellular Domain) that can translocate into the nucleus where it has transcriptional factor functions that regulate calcium-mediated signals [33].

In the amyloidogenic pathway, the first enzyme that acts on APP is β-secretase named BACE (β site-APP Cleaving Enzyme) that hydrolyses APP on the extracellular, N-terminal region of the transmembrane protein generating sAPP-β and C99 that remains within the membrane. C99 is subsequently processed by the γ-secretase that, in this case, has multiple binding sites that can generate many Aβ fragments of various lengths – from 39 to 42aa – which possess differing fibrillogenic characteristics, and the AICD peptide.

As mentioned previously, the γ-secretase, differently from α and β-secretases that are cytoplasmic enzymes, is a transmembrane enzymatic complex with a catalytic domain constructed by PS1 and PS2. It's now more evident that mutations of PS1 or PS2 modify the catalytic domain of the γ-secretase complex, which then favours the generation of longer fragments, such as Aβ40 and Aβ42, which are the monomeric units that form SPs.

To form toxic, insoluble fibrils, Aβ-peptides assemble in small, prefibrillar and low molecular weight aggregates. These are still soluble and have a β-sheet structure, which can form intermediate structures named protofibrils (PF) that form 1-2 nm strings [34] with curved appearance and generally shorter than fully formed fibrils.
Negative stain EM of protofibrils formed from Aβ1–40 and 1–42 show flexible fibres rolled into coils [35] formed by a double β-sheet structure. Protofibrils then may assemble into protofilaments with the bidirectional addition of monomers and lateral incorporation of 3-6 protofibrils [36]. Finally, multiple protofibrils form large, mature amyloid fibres, linear structures that are 6-12 nm wide, and aggregate to form SPs.

Fibrillogenesis is a mechanism that is related to two factors: length and concentration of Aβ peptides. The organisation of the soluble Aβ peptides in protein micelles depends on their amphipathic surface-area, whereby the more apolar surfaces that are exposed, the more readily peptides will collapse into a thermodynamically stable conformation to minimise interaction with the environment [37].
Since Aβ-42 is longer than Aβ-40, its aggregation is physically favoured. In vivo there is an equilibrium of Aβ40 monomers, dimers, trimers and tetramers whereas Aβ42 is initially present only as monomers that quickly oligomerise in pentamers and hexamers without a proper structure therefore named paranuclei. The critical aa

residue that drives their formation is Ile-4. Its lateral chain promotes the self-assembly of paranuclei into bigger oligomers [38].
APP protein is transported anterogradely through the axon to the synaptic bouton, where it is processed, suggesting that synapses are the sites where Aβ peptides are released and oligomers can accumulate. The effect of the formation of these species can be found in the declining integrity and functionality of both pre- and post-synaptic terminals that represent the sites where the neuronal failure probably starts [39].

Several mechanisms have been proposed for Aβ clearance as receptor-mediated Aβ transport across the blood–brain barrier, enzyme-mediated Aβ degradation and immune responses [40]. 10-15% of soluble Aβ can be removed slowly, via interstitial fluid bulk flow, into the bloodstream [41] but the majority is removed via receptor-mediated transport to the blood system across the BBB. The transport of Aβ across the BBB is mainly mediated by lipoprotein receptor-related protein (LRP). The interaction between Aβ and LRP mediates Aβ brain capillary binding, endocytosis and transcytosis across the BBB into blood [42]. Another mechanism that has been suggested to be involved in Aβ clearance involves the ATP-binding cassette transporter p-glycoprotein that can act as an Aβ efflux pump at the BBB [43]. Finally there are evidences that Aβ is degraded by several peptidases, principally two zinc metallo-endopeptidases referred to as neprilysin, a rate-limiting Aβ -degrading enzyme [44], and insulin-degrading enzyme (IDE) which levels decrease during aging [45].

In 1992, Hardy and Higgins, for the first time, posited the 'Amyloid Cascade Hypothesis' that suggests that the accumulation of Aβ peptides in the brain parenchyma is the earliest event in the pathogenesis of Alzheimer's disease [46]. The toxicity exerted by Aβ was suggested to be driven by two different mechanisms:

- **Direct mechanism:** Aβ interacts with components of the neuronal cell membrane increasing its susceptibility to factors such as excitotoxicity, hypoglycaemia, and oxidative stress [47].
- **Indirect mechanism:** Aβ induces the activation of microglia and astrocytes that, consequently, produce toxic and inflammatory molecules as nitric oxide (NO), pro-inflammatory cytokines and ROS that can induce apoptosis and necrosis [48][49].

Moreover, the pathological accumulation of Aβ, often associated with clearance defects, can lead to an inhibition of LTP (Long term potentiation) but the synaptic elements that mediate this effect remain unclear.

LTP is a form of synaptic plasticity related to memory formation that consists of increased synaptic transmission between two neurons. On the other hand, the weakening of synaptic connections produced by low-frequency stimulation is called long-term depression (LTD) [50]. To test the role of Aβ in altering synaptic function, many studies used

exogenous application of various Aβ peptides (i.e., Aβ42, Aβ40, or Aβ25–35) showing that it induced an LTP inhibition without affecting basal synaptic transmission [51]. Moreover, this effect is due to soluble Aβ oligomers but not to monomeric Aβ or Aβ fibrils [52].

In addition, at postsynaptic level, Aβ40 peptides can selectively augment NMDAR current [53]. Many studies focused on the role of Aβ peptides on NMDAR function demonstrating that Aβ peptides affect downstream Calcium (Ca^{2+}) dependent signalling pathways possibly via the activation of Calcineurin, a Ca^{2+} -activated protein phosphatase, as well as preventing the activation of CaMKII, a Ca2+-dependent protein kinase necessary for LTP [54].

Ca^{2+} is a universal second messenger that regulates the most important activities of all eukaryotic cells as cell growth and metabolic activities and it is of critical importance to neurons. Its main effects in fact are not only to alter their electrical activity, by modifying the opening and closing of Na and K channels inducing depolarisation, but also to stimulate the release of transmitter substance [55,56].

Amyloid peptides have been shown to increase Ca^{2+} influx either via voltage-dependent Ca^{2+} channels, deactivating Ca^{2+} ATPases on the neuronal membrane, or by directly forming aspecific channels in neuronal membranes [57]. Amyloid peptides can also affect Ca^{2+} influx through AMPA and NMDA receptors [58]. The influx of this ion causes ionic disequilibrium that can induce damage through the hyperactivation of Ca^{2+}-dependent kinases that can

hyperphosphorylate, and consequently cause the aggregation of, tau protein [14,59].
In support of this theory, neurons containing NFTs show an increase in intracellular Ca^{2+}. The failure of neuronal calcium regulation, which is essential for LTP, is an aspect of AD that seems to be related to synaptic dysfunction and neuronal death [60].

1.1.3 Neurofibrillary tangles

The diagnosis of Alzheimer's disease is predicated on the presence of both amyloid plaques and neurofibrillary tangles (NFTs) in a patient's brain.
The dynamic of Aβ deposition and tau pathology is still controversial; while some literature suggests that tau pathology precedes Aβ deposition, some other authors, mainly looking at biomarkers, showed an opposite effect [61,62].

As postulated by the Amyloid Cascade Hypothesis [24], it was initially believed that amyloid deposits were the most important feature for the pathological progression of AD. However, there is now evidence to suggest that the abundance of NFTs, and the anatomical location of these NFTs, better correlate with neuronal loss, disease severity and cognitive impairment than amyloid deposits [63].

Tau proteins in NFTs are hyperphosphorylated and abnormally folded. The aggregates can themselves induce toxicity, but also exert loss-of-

function toxicity through the sequestration of native tau proteins, which cannot bind and stabilize microtubules in the axon [64].

Neurofibrillary tangles form thick bundles near the cell surface of affected neurons, which can be visualized using Bielschowsky silver stain, or Thioflavin-S or -T staining. Since they are associated with neuronal death and lead to “disintegration” of the cell, they result in what are now called extracellular or “ghost” tangles that have been observed in post-mortem tissues. [65].

NFTs are composed of hyperphosphorylated and misfolded tau protein that assemble in “paired helical filaments” (PHFs) [66], structures composed of two intertwined filaments of 10nm diameter that twist around one another as shown by electron microscopy.

In AD, the PHF structure is uniform and it has been possible to resolve the structural folding of the core peptide with cryo-electron microscopy at 3.5Å [67] (Fig 1.2).

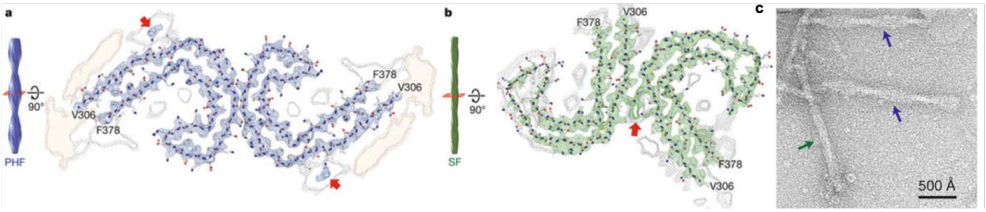


Figure 1.2: PHF and SF cryo-EM structures. *Atomic models of PHFs (a) and SFs (b); red arrows point at additional densities in contact with K317 and K321. Negatively stained electron micrograph of purified Tau filaments, in which PHFs (blue arrows) and SFs (green arrows) are readily distinguished (c). Image adapted from* [67].

In this work, it was also shown that in AD brains there are other species of tau aggregates known as straight filaments (SFs) that exhibit less periodicity than PHFs. These also differ from straight helical filaments observed in other tauopathies and filaments generated *in-vitro* using recombinant tau.

In addition to NFTs, neuropil threads (NTs) have also been observed in AD patient brains, which are comprised of both dendritic and axonal PHFs and SFs aggregates probably originating from neurons containing NFTs [68].

NFTs formation comprises several stages. Initially, tau forms “pre-tangles” that contain aggregates in dendrites and cell bodies. Subsequently, these formations will mature into aggregated filaments in the perikaryal and proximal cell processes regions. Their morphology differs from neuron to neuron and is dependent on the type of neuron that is affected. For example, hippocampus pyramidal neurons show “flame-shaped tangles”, whereas neurons in the substantia nigra and locus coeruleus express “globose tangles” [69].

Overall, independent of the morphology, NFTs can displace the nucleus and other vital cellular components leading to neuronal death. Consequently, tau aggregates will be released into the extracellular space where they can affect other cell types, such as microglia and astrocytes, or associate with extracellular proteins (e.g., Aβ).

1.2 Tau

Tau is a microtubule (MT)-binding protein that stabilizes and promotes the assembly of MTs [70]. Through this interaction, tau plays important roles in neuronal morphogenesis, axonal extension, as well as axonal vesicle and protein transport in neurons [71]. Tau function is regulated by the degree of its phosphorylation. Excessive phosphorylation leads tau to detach from microtubules with a consequent disruption to the structure of the neuronal cytoskeleton [72].

Tau protein is encoded by the MAPT gene on chromosome 17q21 and it is prevalently expressed in neurons [73]. In human brains, tau mRNA undergoes alternative splicing at exons 2, 3, and 10 resulting in the formation of 6 isoforms ranging from 352 to 441 amino acids in length, that differ by the presence or absence of one or two inserts in the N-terminal part (projection domain of 29 amino acids, 0N-1N-2N) and for the presence of either three (3R) or four (4R) C-terminal repeat domains (tubulin binding motif of 31 amino acids encoded by exon 10) (*Fig. 1.3*).

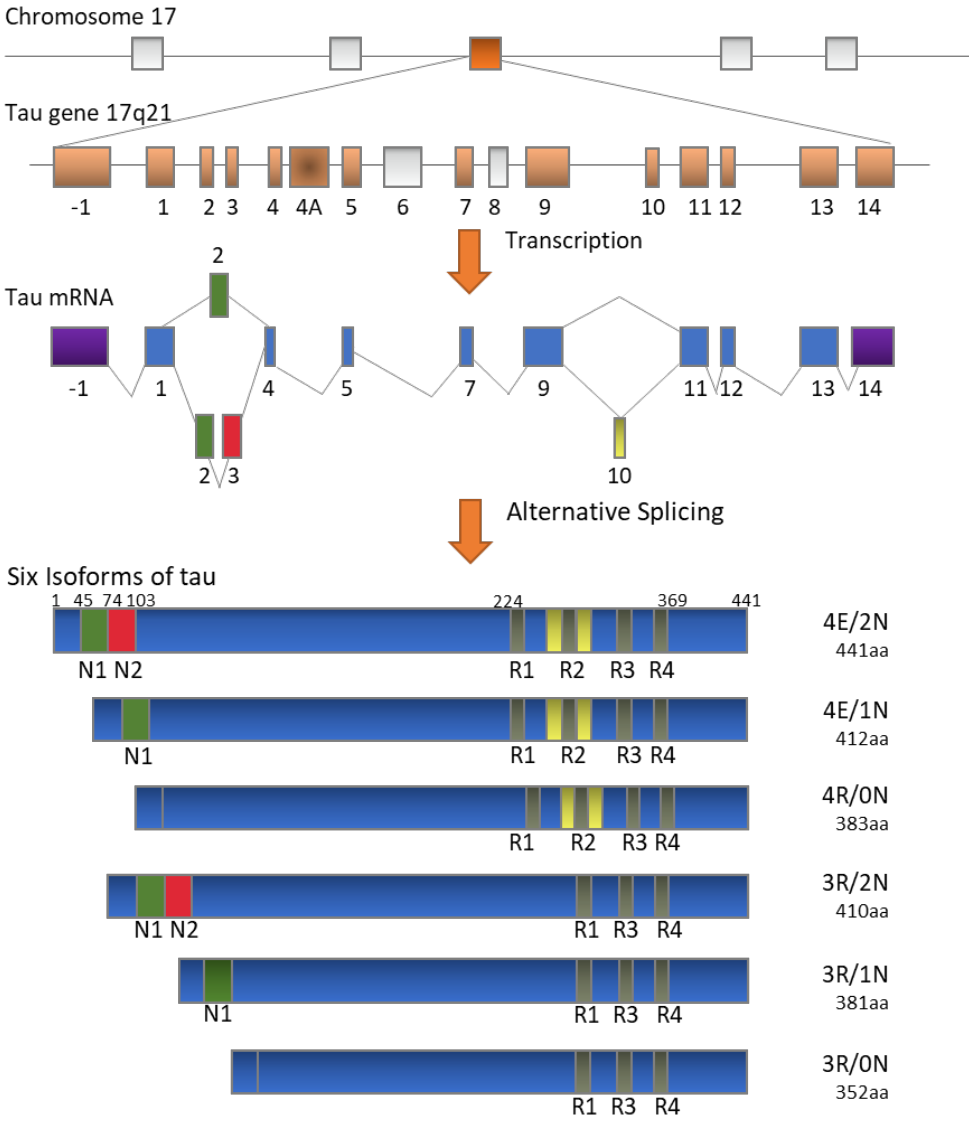


Figure 1.3: MAPT gene and the six isoforms of human tau found in the brain. *Illustration of the six isoforms of human tau derived from alternative splicing of MAPT mRNA. The incorporation of exons 2 and 3 determine the expression of N-terminus inserts of 28 amino acids (0N,1N and 2N) whereas the inclusion of exon 10 determines the expression of a C-terminus insert that produces either 3R or 4R tau. Adapted from* [74].

The N-terminal and the C-terminal portions are separated by a central proline-rich region (PRD) (*Fig 1.4*).

Within the whole sequence, 45 phosphorylation sites have been identified, and they cluster in the PRD and in the C-terminal region, with few sites evident within the microtubule-binding domain of tau (*Fig 1.4*) [43].

In a healthy brain, the various isoforms are differentially expressed during development, and adult humans express equal amounts of 3R-tau and 4R-tau, a ratio that is lost in most of the neurodegenerative tauopathies. Nevertheless, tau protein level is two times higher in the neocortex than in white matter and cerebellum, possibly explaining the differential vulnerability of brain regions to tau pathology [75].

Tau is a naturally unfolded soluble protein which, under normal condition, lacks a secondary structure. It has a preference for adopting a paperclip-like shape in which the N-terminal, C-terminal and repeat domains are in close proximity which may protect tau from aggregation [76]. However, its conformation can change from random coil to highly ordered β-sheet structures as it assembles into SFs and PHF, where the repeat domains constitute the beta-sheet core, and the short C-terminal and the long N-terminal domains form a “fuzzy coat” which supposedly stabilises the PHFs [77]. (*Fig 1.4*)

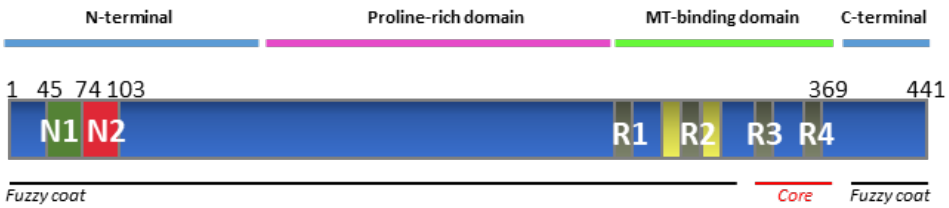


Figure 1.4: Primary structure of the longest tau isoform in human brain. *Tau protein can be divided into an N-terminal region that contains sites from alternative splicing of exon 2 and 3; the proline rich mid-domain; the microtubule-binding domain that contains sites from alternative splicing in exon 10; and the distal C-terminal region. The N-terminal, the PRD and C-terminal form the fuzzy coat of the three-dimensional structure of Tau in PHF and SFs while the R3 and R4 domains of the MT- binding domain form the core domain of the insoluble structures.*

In AD, all 6 isoforms of tau are present in NFTs, but in other tauopathies such as cortico-basal degeneration, globular glial tauopathy, and progressive supranuclear palsy only 4R has been found in the fibrils as in the. Conversely, the characteristic Pick's bodies, of Pick's disease, consist only of 3R tau [78].
This suggests that different molecular conformers of aggregated tau exist, and it has been shown that tau can adopt distinct folds in different diseases [79].

Using cryo-EM it has been possible to resolve the atomic structure of PHFs and SFs showing that even though the protofilaments that compose them are the same, with similar C-shape forms, and in the same environment, their structures are different. In particular, in PHFs two protofilaments form identical structures related by helical symmetry with the interface being the residues ^{332}PGGGQ^{336}, whereas

in SFs the two protofilaments pack asymmetrically (residues ^{321}KCGS^{324} – ^{313}VDLSK^{317}) [79]. Overall, the core component of these two filaments includes tau residues 306-378, which corresponds to the R3 and R4 domains, and is composed of a combination of cross-β packing and β helices, a structure very dissimilar to the hairpin that tau forms when it it bound to the MTs (*Fig 1.2*).

The N and C termini of both PHFs and SFs have a disordered structure. In PHFs, the N-terminal regions of both protofilaments fold back in to form weak β-sheets that will interact with the core, whereas only one protofilament can form this additional β-sheet in SFs.

1.2.1 Tau mutations

AD is defined by the presence of extracellular β-amyloid plaques and intraneuronal neurofibrillary lesions composed of tau. Similar tau aggregates, in the absence of extracellular amyloid deposits, have also been found in other neurodegenerative diseases, including progressive supranuclear palsy (PSP), cortico-basal degeneration (CBD) and Pick's disease (PiD). Initially, there was no genetic evidence implicating tau protein in the neurodegenerative process. However, it has since been shown that *MAPT* mutations are causal of familial forms of frontotemporal dementia and parkinsonism[80,81].
Different tau mutations exert different effects. Most of them influence protein expression, alternative splicing, or reduce the ability of tau protein to interact with MTs, thereby increasing its propensity to assemble into abnormal filaments [82,83]. Indeed, many of the

missense mutations are in the MT-binding site, for example: G272V; N279K; ΔK280; P301L; V337M; and R406W. Some other mutations, away from the MT-binding domain like A152T or R5H, may still cause loss of tau function by decreasing the binding of tau to microtubules and causing microtubule disassembly [84].

Finally, the splicing mutations affect the mRNA processing of tau, and perturb the normal ratio of 3R:4R tau. Most of them are within or near intron 10 and they increase the expression of 4R tau, which is more prone to aggregate that 3R [85]. Other mutations – such as ΔK280, L266V and G272V – decrease the expression of 4R tau, triggering specific aggregation of 3R tau as this isoform has a lower microtubule-stabilizing capacity [86] (*Fig 1.5*).

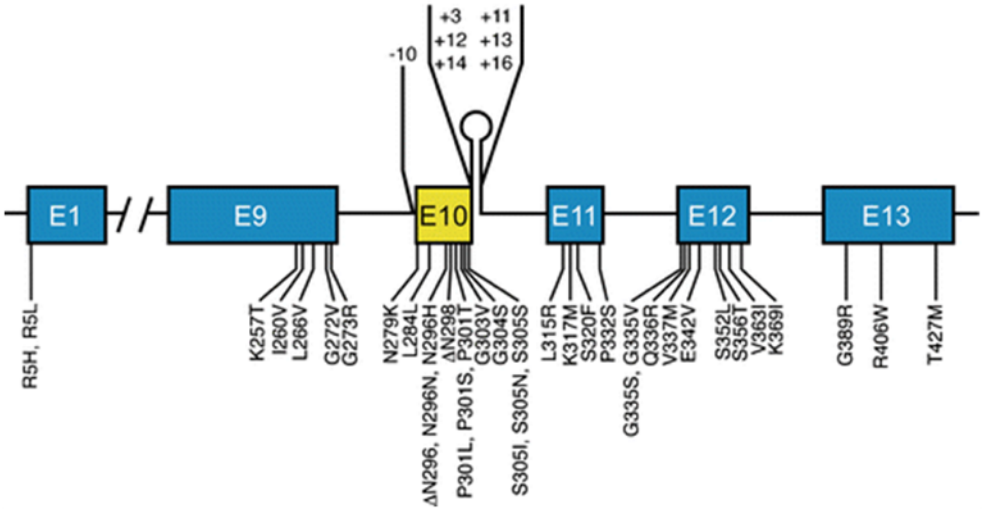


Figure 1.5: Mutations in MAPT in frontotemporal dementia and parkinsonism linked to chromosome 17 (FTDP-17T). *Thirty-seven coding region mutations in E1, E9, E10, E11, E12 and E13 of MAPT and seven intronic mutations flanking E10 are shown. Figure and caption taken from* [87].

Irrespective of the mutations or the pathological conditions that lead to the detachment of tau from microtubules, the resulting events are toxic: loss-of-function, gain-of-function, and mis-localisation have been identified as the main mechanisms of tau-mediated neurodegeneration.

1.2.1.1 Loss of function neurotoxicity

The function of tau is to stabilise the structure of MTs; when mutations occur that impair this function, neurons incur structural and functional impairments of microtubules in axons and, consequently, a deficit in axonal transport.

Moreover, knock-out animal models suggest that tau function can only be partly compensated by other, microtubule-associated proteins, as the animals show an impaired phenotype, suggesting that tau is necessary for normal neuronal and brain function [88].

When aggregation occurs, monomeric tau is recruited into the deposits creating a deficit of free-tau, which may result in microtubule disassembly [89].

Even if it is still unclear why tau aggregates, evidence from AD patient brains and transgenic mice has led to the hypothesis that phosphorylation drives tau aggregation since most of the aggregated tau is phosphorylated. However, it has also been demonstrated that tau phosphorylation alone is not sufficient for its aggregation [90] and that, even if phosphorylation in some sites could favour the detachment from MTs, phosphorylation of other residues, for example in the repeat domain, can protect against aggregation [91].

One of the key features of AD is synapse degeneration, mainly due to defects in axonal transport, as well as energy deprivation and oxidative stress due to mitochondria failure. These events are possibly related to tau loss of function. Indeed, tau, as well as regulating microtubule dynamics, affects the activity of motor proteins. In particular, tau reduces dynein and kinesin mobility and binding frequency to microtubules, slowing both anterograde and retrograde axonal transport of cargo [92].

This will not only affect the axonal transport of proteins and organelles, including transport of cargo to synapses, but may also lead to an accumulation of organelles, such as mitochondria, in the neuronal soma, resulting in axonal swellings and spheroids observed in neurodegenerative diseases [93].

1.2.1.2 Gain of function neurotoxicity

Aggregated tau gain-of-function toxicity is pleiotropic, involving aberrant interactions between tau aggregates and either intracellular organelles or extracellular objects, such as other proteins, receptors or cells.

It has been shown that AD severity and neuronal death correlates better with NFTs than with other biomarkers such as Aβ deposits, which supports the notion that NFTs and PHFs are directly neurotoxic. However, growing evidence has challenged this view, by showing that NFT formation is neither necessary nor sufficient for neurodegeneration [94]. In fact, another hypothesis is that in order to clear tau monomers or oligomers and protect neurons from acute

harms [95], neurons make PHFs and NFTs to remove the toxic agents from the environment and contain them [96]. On the other hand, even if cells produce NFTs to protect themselves from toxic oligomeric species, they have an indirect toxicity by sequestering and depleting other functionally significant proteins and cell components and by affecting the localization of subcellular organelles and cytoplasm organization.

1.2.1.3 Mis-localization of tau induces neurotoxicity

In adult neurons, tau is mainly distributed in axons, where it interacts with microtubules; however, in AD and other tauopathies, it has been found mislocalized to presynaptic terminals, dendrites and postsynaptic spines, resulting in synaptic dysfunction, destabilisation of microtubules, as well as abnormal translocation of other proteins and enzymes [97].

For example, in rat hippocampal neurons, mutated tau binds to synaptic vesicles via its N-terminal domain and interferes with presynaptic functions, such as synaptic vesicle mobility and release rate, thereby lowering neurotransmission [98].

Overall, it is still not clear if the neurotoxicity related to aggregated tau is due to loss of function or gain of function. It is likely that both mechanisms contribute to neurodegeneration to different extents, and play separate, though complementary, roles in driving the damage, which ultimately leads to onset and progression of tauopathies.

1.2.2 Tau aggregation

It has been shown via NMR that when tau protein is in a soluble form, bound to MTs, the residues 268-284 and 300-312 adopt a hairpin conformation and the rest of the structure appears disordered [99]. The first step that starts the aggregation process is the detachment from the MTs [100] probably due to factors including gene mutations or covalent post-translational modifications, such as phosphorylation. There is a physiological phosphorylation pattern of tau, which is highly regulated by kinases and phosphatases, and that is fundamental for tau to remain bound to MTs. The MT-binding domain is rich in positively-charged lysine that can easily bind the negatively charged MTs [101]. However, when phosphorylation increases, especially on serine and threonine, the charge balance is disrupted and the efficiency of the binding decreases [102].

Once soluble tau dissociates from MTs, the concentration of free intracellular monomer increases, as does the likelihood of pathogenic conformational changes. Moreover, at cytoplasmic level tau can be cleaved into smaller fragments that can aggregate much faster than the full length protein, probably due to the loss of the paperclip structure that promotes the stability of the monomer in solution [103–105].

As described before monomeric and/or truncated tau initially assemble into pre-tangles that will form PHF structures that, ultimately, will aggregate to form NFTs.

1.2.2.1 Tau aggregation models

The mechanism of tau aggregation can be modelled *in-vitro* and it has been studied in order to reproduce, and better understand, physiological tau aggregation [106].

Aggregated tau has the capacity to seed and induce aggregation of native proteins, propagating its amyloid state in a prion-like manner. The aggregation mechanism can then be schematized in a kinetic model that is composed by different phases (*Fig 1.6*).

The first phase is a long, slow lag phase called nucleation that start with the dimerization of tau monomer. These then form a dimer of dimers, so four proteins, which go on to form oligomers. This reaction is thermodynamically unfavoured and exists in kinetic equilibrium with the reverse, disaggregation reaction, as oligomer fragmentation can occur at this stage. Once oligomers have formed, they can act as aggregation nuclei, which increase the kinetic rate of the aggregation reaction. Indeed, the second phase is a thermodynamically favoured elongation phase in which monomers are rapidly recruited into growing aggregates. In this phase, additional fragmentation events occur, where regions of the growing aggregates can detach and form new nuclei that can be used to recruit new monomers and create more aggregates. This mechanism will plateau when local monomer is depleted.

The reaction kinetics can be changed by using preformed fibrils “seeds” that provide the templates (nuclei) that can recruit tau monomers, thereby skipping the nucleation phase (*Fig 1.6 A*) [107].

This mechanism can be measured *in-vitro* with Thioflavin T (Thio-T) assays, which utilise the differential fluorescence exhibited by Thio-T upon binding to β-sheet structures. At a high concentration, tau monomers aggregate into amyloid-like structures spontaneously. *In-vitro* tau fibrillization can be accelerated using inducers, such as heparin or *in-vitro* aggregated tau (seed). During aggregate formation, Thio-T binds the newly formed β-sheet structures and undergoes a shift in fluorescence (excitation: 450 nm; peak emission: 485 nm). It is possible then to estimate the degree of tau aggregation over time by assessing Thio-T fluorescence [108].

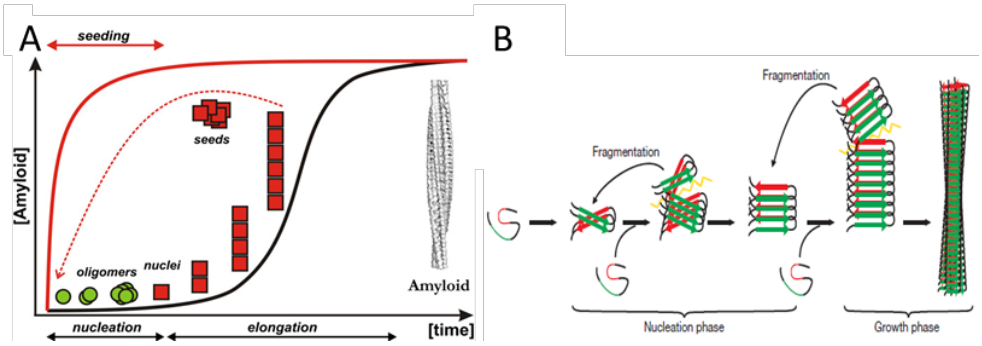


Figure 1.6: Tau aggregation kinetics*. The kinetics of amyloid fibril formation is dependent on the nucleation, growth, and fragmentation rates (A). Amyloid formation starts with a slow nucleation phase that requires a series of intermediate states until the seed is formed. Monomers or oligomers are then bonded to the ends of the initial seed by conformational conversion (prionic effect/seeding). With increasing length, and depending on the conformational stability of the fibril, it can eventually break (fragmentation), either spontaneously or actively through cellular processes (B). This event will increase the availability of new seed ends inducing the formation of more aggregates (A). Moreover, the "seeding" becomes self-propagating through the generation and spread of new amyloid seeds. Remarkably, the lag time that precedes protein aggregation in vitro can be greatly shortened by the addition of pre-formed exogenous seeds (A). Image adapted from* [107,109].

Many methods have been used to recapitulate tau aggregation. However, a disadvantage of these methods is that, due to tau solubility and its natively unfolded structure, it is not easy to produce aggregates similar to those observed in tauopathies.

Multiple strategies have been adopted to monitor aggregation in cell systems, including: the overexpression of truncated forms of tau that aggregate more rapidly than the full-length tau [110,111]; the use of aggregation inducers, such as Congo red, to overcome the kinetic barrier of fibrillization within cells expressing full length tau isoform [112]; and the use of aggregation-prone tau mutants, such as $MAPT^{P301L}$ [113], or tau overexpression [82,114,115].

In some cases, viral transfection was used to induce protein overexpression whilst, in other cases, expression of exogenous tau was regulated by an inducible promoter, to avoid cytotoxicity associated with chronic overexpression.

This highlights how these models are incompletely recapitulating AD pathology, because most of the MAPT mutations employed are causal of frontotemporal dementia only (FTD), and such acute toxicity of tau aggregates is not reflective of these human diseases.

Another approach requires the exogenous addition of recombinant tau fibrils (seed) that can skip the nucleation phase and directly induce aggregation of the endogenous tau expressed by the cells[116,117].

Often, recombinant human 4R-tau fibrils were used as 4R tau has a higher propensity for self-aggregation than 3R tau, despite also having a higher affinity for MTs [118–120]. Tau fragments of the microtubule-

binding region of tau (K18) have also been used for this purpose, as they show a higher aggregation rate than full length tau [121].

Even if recombinant and synthetic tau fibrils have been widely used to propagate tau pathology in transgenic mice overexpressing mutant tau [122,123], they are inefficient at templating the fibrillization of non-overexpressed WT tau [124]. In 2016, Guo et al. demonstrated that authentic tau fibrils purified from AD brains (hAD seed) were superior to synthetic tau fibrils – generated with or without heparin – at seeding the aggregation of WT tau *in vivo* [125]. This aggregation model has also been positively used to screen compounds that inhibit tau pathology [126].

1.2.3 Tau propagation

During the clinical course of AD, tau pathology shows a very characteristic spatiotemporal spreading indicating that, once the aggregation has initiated, it propagates between neighbouring neuronal cells, possibly by spreading along the axonal network.
To describe tau propagation, in 1991, Heiko and Eva Braak introduced a 6-tiered system of disease, also known as Braak Staging [127], based on silver-stained, hyperphosphorylated tau aggregates that are widely used to describe AD neuropathology [128] (*Fig 1.7*).

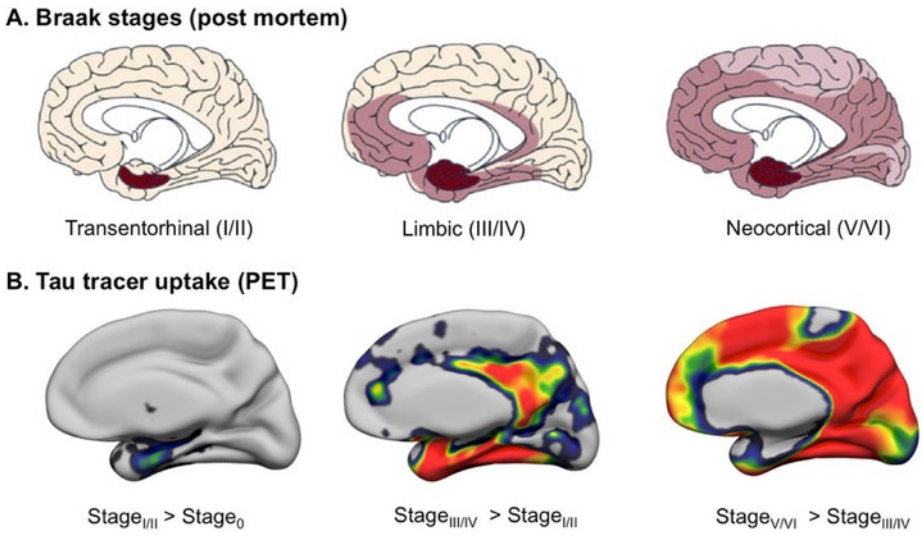


Figure 1.7: Tau tracer uptake patterns recapitulate post-mortem Braak stages*. Schematic of Braak stages in the development of AD-associated tau pathology based on post-mortem data. Tau pathology starts within the entorhinal cortex, progresses to the hippocampal area, and spreads throughout the isocortical areas as the disease progresses (A). PET images from AD patients using the tau PET tracer Flortaucipir resemble the Braak stages of tau pathology observed in post-mortem tissues (B). Image from* [129]*.*

The first Braak stages, I and II, are not associated with clinical dementia; however, NFTs can be found at the level of transentorhinal (TEC) and entorhinal cortex (EC). From stage III and IV, also termed the “limbic stages”, clinical symptoms appear due to robust tau pathology that has extended from the EC and TEC into the hippocampus, the fusiform gyrus and temporal cortex. The most severe pathology is observed in patients at Braak V-IV that meet the neuropathological criteria for the diagnosis of AD; at these stages NFTs are found into isocortical association areas, accompanied by severe dementia.

Interestingly tau inclusions seem to appear in human brains much earlier than Aβ plaques [127,130], and also in in the locus coeruleus

of the majority of children and young adults, in the absence of Aβ deposits [131,132].

So, there must be an event – or, indeed, a series of events – that exacerbates pathology by inducing the spread of hyperphosphorylated tau from the locus coeruleus to the transentorhinal cortex via anterograde axonal transport. Downstream neuron-to-neuron transmission of hyperphosphorylated tau to other brain regions will eventually give rise to the cognitive deficits and alterations associated with AD.

One study suggests that the instigating event could be the accumulation of β-amyloid deposits in the isocortical regions [133].

The distribution of pathological tau in the brains of individuals with Alzheimer's disease follows highly predictable spatiotemporal patterns but, interestingly, the distribution of Aβ pathology follows a different trajectory. Aβ pathology first develops in the orbitofrontal neocortex and basal temporal cortex, and then spreads throughout the neocortex before finally reaching the hippocampus, midbrain, brainstem and cerebellum [127,134,135].

Numerous studies have attempted to elucidate the reason why proteins spread in different ways in neurodegenerative disease, however the precise mechanisms are not yet fully understood.

It has been hypothesised that the stereotypical distribution of pathological proteins in the brain was the result of differences in vulnerability between brain regions [136]. However, during the past decade, it has been demonstrated that another reason for the

particular involvement of different brain regions is due to the spreading of pathological proteins between anatomically connected brain areas (transmission hypothesis) [137].
This second theory is somewhat limited by the fact that not all patients show the stereotypical spreading pattern and not all the areas that are anatomically connected contain pathological proteins [136].
Therefore, it is possible that the selective vulnerability of different neuronal populations, that could derive from differences in the release or uptake of pathological seeds or in the intracellular environment that modulates the templated amplification process initially hypothesised, could be a crucial regulatory step for the transmission process [136].
It has been recently demonstrated that tau aggregates predominantly accumulate in excitatory neurons compared to inhibitory neurons, not only in the primary affected region but also in secondary regions, suggesting that excitatory neurons are vulnerable to both cell autonomous and non-cell-autonomous accumulations of tau as tauopathy propagates. Transcriptomics analysis has shown that this selective vulnerability of excitatory neurons to tau aggregation is due to an intrinsic susceptibility to protein homeostasis dysregulation, which is a consequence of an elevated expression of aggregation-prone proteins and tau aggregation promoters, as well as a decreased expression of tau aggregation protectors [138].

The processes of tau propagation highly depend on the nature of the aggregates that propagate. Indeed, not all aggregates have the same seeding capacity, so it is important to identify what characteristics

render one aggregate more seeding competent than another. Aggregates with a higher seeding ability are likely to have a greater role in the spreading of pathology and, therefore, might be the more propitious target for interventional therapies. The first characteristic that influences tau seeding ability is the size [139]. Many studies have tried to determine the influence that size has on the ability of aggregates to recrute non-pathological monomer in recipient cells. Size is important as aggregates must be able to undergo transport between cells while maintaining the ability to induce templated amplification, so it is unlikely that very large mature aggregates can mediate transneuronal propagation.

Different studies have demonstrated that the seeding species are relatively small; different models have been used so the results are not always in accordance, but all have shown that pathological tau seed are composed by few monomers. They can range from as little as 3 tau monomers [140] to 10 tau monomers [139]. Moreover, a more recent study observed that in the presence of lipofectamine, even the tau monomer can exist in different conformations and when derived from sonicated tau fibrils (recombinant or from hAD brains) is able to trigger tau aggregation [141].

Another important feature of the pathological seed is the conformation. It has been shown that many pathological proteins, including tau, exist in multiple different conformations and that, depending on the conformation, a protein can have different seeding and spreading

properties, which consequently determine specific pathology [142–144] (*Table 1.1*).

Evidence of transmission in humans	Evidence of transmission in experimental models						
Human-derived growth hormone treatment	Type of seed	In Vitro		In Vivo			
		Non-Neuronal cells	WT Neurons	Intracerebral injection in transgenic mouse models of disease	Intracerebral injection WT mice	Transmission to glial cells following intracerebral injection in WT mice	Peripheral injection in transgenic mouse models of disease and WT mice
	Synthetic Fibrils	Yes	Yes	Yes	No	No	Not Tested
	Mouse Brain Lysates	Not Tested	Not Tested	Yes	Not Tested	Not Tested	Yes
	Human Brain Lysates	Yes	Yes	Yes	Yes	Yes	Not Tested

Table 1.1: *In vitro and in vivo models of tau transmission. Adapted from*[145].

For example, pathological tau isolated from PSP was conformationally different from tau isolated from AD brains, and it had greater seeding ability [125]. Another finding is that pathological proteins isolated from diseased brains have a greater seeding ability than recombinant fibrils, indicating that the environment in diseased brains leads to the formation of unique protein conformations. For example, pathological tau isolated from tauopathy brains induced more pathology than synthetic tau fibrils when injected into wild-type mouse brains [125,142]. In line with these findings, it has been demonstrated that the heparin-induced tau aggregates have a different cryo-EM structure when compared to the aggregates derived from AD and Picks brains raising questions about the relevance of *in vitro* assembly [146].

Different conformations might induce pathology in specific cell types. For example, pathological tau derived from hAD brains injected into tau transgenic or wild-type mice only induce tau pathology in neurons,

whereas tau from PSP brains induces pathology in neurons, as well as astrocytes and oligodendrocytes, recapitulating the glial inclusions observed in post-mortem human brains [142,143].

1.2.3.1 Mechanisms of tau spreading

Finding therapies that can target tau aggregation is impeded by the complexity of the aggregation mechanism, and as such, several studies are focused instead on targeting the mechanisms of tau spreading. This process involves the initial aggregation and amplification of the pathological seeds in the donor cell. Subsequently, the pathological species will be transported intracellularly to the site of release. Interestingly, studies using microfluidic chambers have shown that all pathogenic forms of tau can be transported along axons in primary neuronal cultures. Both anterograde and retrograde transport of these proteins was observed [147].

Following release, the final step in the process of tau propagation is the uptake of tau aggregates by recipient cells and consequent induction of intracellular tau aggregation. This process than is repeated in the other healthy neurons to induce further spreading. It is still unclear how this happens and what species are released and spread from cell-to-cell, but multiple hypotheses have been established by several studies [148,149].

***Release*:** The molecular mechanisms underpinning the secretion of tau have been investigated in multiple studies. Tau aggregates can be secreted into the extracellular space naked or within exosomes (*Fig 1.8*) via different mechanisms including: diffusion; classical secretion and unconventional secretion such as pore-mediated translocation; ABC transporter-based secretion; membrane-bound organelle-based secretion; and the Golgi bypass pathway [148]. The most studied pathway is exosome-based secretion. Exosomes are membrane-bound extracellular vesicles that are released from cells upon fusion of an intermediate endocytic multivesicular body (MVB) with the plasma membrane. Exosomes from CSF of AD patients contain aggregated and hyperphosphorylated tau as a result of tau release [150,151].

Moreover, it has been demonstrated using microfluidic devices that synaptic connectivity is required for exosomes to mediate the transfer of tau [150].

As mentioned, tau can also be released into the extracellular space as free protein - as demonstrated by a study that used an anti-tau antibody [152]. There is the possibility that, after cell death, pathological seeds are released into the extracellular space and diffuse throughout the local parenchyma; however, there is no direct evidence of this hypothesis in diseased brains [153].

Furthermore, other cell types, namely microglia (MG), might play a role in the local propagation of tau by taking up and ejecting bioactive seeds. The role of MG in tau clearance and spreading is quite controversial. On one hand, MG can clear the CNS by phagocytosing

extracellular aggregated and hyperphosphorylated tau as well as synapses or entire neurons that contain NFTs. On the other hand, when MG are knocked out in an AD mouse model tau spreading was reduced [154]. Moreover, *in vitro* experiments showed that microglia derived from human tauopathy patients and from rTg4510 mouse can phagocytize seed-competent tau. However, rather than fully degrading it, they secreted tau back into the extracellular space indicating that a portion of tau spreading might be mediated via MG [155].

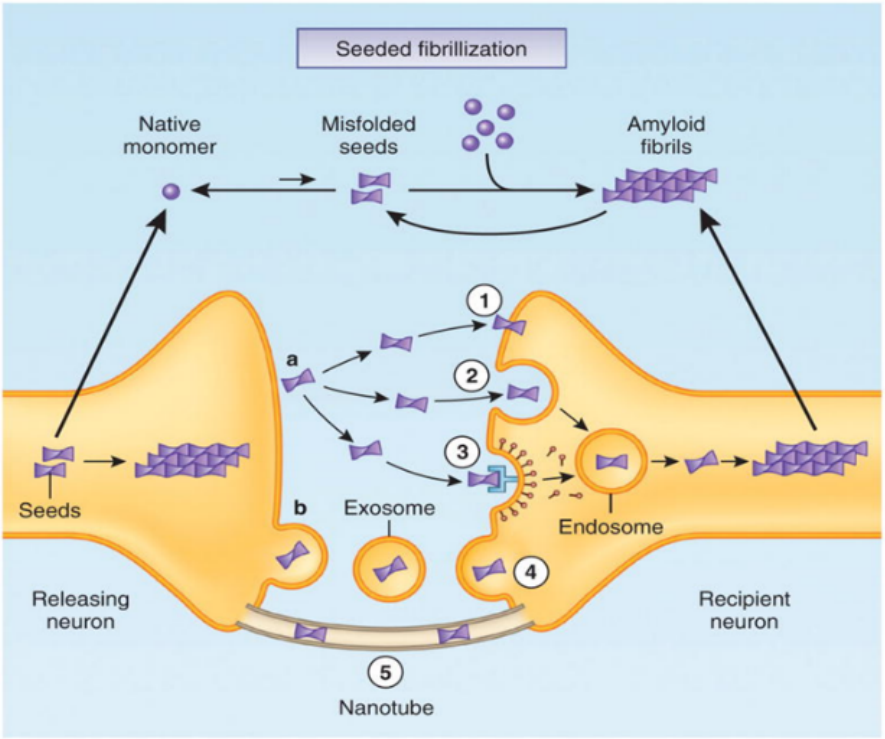


Figure 1.8: Potential mechanisms mediating cell-to-cell transmission of tau aggregates. *Misfolded tau seeds form in the cytoplasm of the donor neuron by seeded fibrillization and can be transferred to recipient neurons. A small amount of aggregates can be released into the extracellular space in the 'naked' form (a) or via membrane-bound vesicles such as exosomes (b). Multiple uptake mechanisms have been hypothesised: free-floating seeds may directly penetrate the plasma membrane of the recipient neuron (1). Seeds may enter by fluid-phase (2) or receptor-mediated endocytosis (3). Exosomes containing seeds may fuse with the membrane of the recipient neuron (4). Intercellular transfer of seeds may also occur by nanotubes that directly connect the cytoplasm of two cells (5). Finally, in the recipient cells, the seed can exit from the endosomes (by unknown mechanism) to then nucleate the fibrillization of native monomers in the cytoplasm of the recipient neuron. Adapted from* [137].

Uptake: Tau, present in the extracellular space, is then internalized by recipient cells through multiple mechanisms (*Fig 1.8*). Misfolded tau can be internalized at the axonal compartment but also at the somato-dendritic level [147].

A key mechanism identified for extracellular tau uptake is heparin sulphate proteoglycan-mediated macropinocytosis [156]. However, tau can also directly penetrate the plasma membrane or enter by fluid phase bulk endocytosis [147]. Exosomes containing tau can be taken up by endocytic pathways, in addition to direct membrane fusion with the recipient neuron [157].

Another hypothesis is that tau can be transported from cell-to-cell via tunnelling nanotubes, which are actin-enriched cytoplasmic protrusions bridging two cells by direct membrane fusion.

In support of this hypothesis, not only was misfolded tau observed in nanotube structures, but also the addition of tau fibrils to cell cultures increased the number of tunnelling nanotubes, which might facilitate the transmission process [158].

Finally, in the recipient cell, tau that is internalised by endocytosis and is now contained within endosomes, as well as tau that was internalised naked, can act, at a cytoplasmic level, as a nucleus for *de novo* fibrillization of the native tau monomer.

How tau can escape from endosomes is still not clear but recently it has been shown that the endolysosomal escape of tau seeds is a critical step in the propagation of tau. In particular, they have shown that defects in the endosomal sorting complexes, required for transport machinery, compromise endolysosomal integrity, and consequently promote the escape of tau seeds thereby accelerating the templating of tau in the cytosol [159].

In order to find targets to decrease tau propagation, the low-density lipoprotein receptor related protein 1 (LRP1) has been identified, as

this controls the endocytosis of tau and its subsequent spread. In particular, the knockdown of LRP1 in both H4 neuroglioma and induced pluripotent stem cell-derived neurons significantly reduced tau uptake, and the downregulation of LRP1 *in vivo* reduced the propagation of tau between neurons [160].

The direct transfer of tau between synaptically connected neurons is supported by the temporal and spatial pattern of spreading observed in tauopathies, which has been demonstrated *in vivo* and in culture models [161–163]. However, alternative mechanisms have been proposed: tau propagation could follow a pattern of selective neuronal vulnerability due to factors like poor myelination [164], high metabolic rates [165] and vulnerability to toxins [166]; or it could follow the progression of neuroinflammation, as MG have been implicated in tau propagation through phagocytosis and exosome secretion [167,168].

Many factors could influence the transmission of pathological seeds. Neuronal activity has been shown to promote the propagation of various pathological proteins [150,169–172]. In particular, an increase in neuronal activity can increase the level of extracellular tau in the brain [170]. Vice versa, overexpressing human tau in primary neurons and mice lead to an elevation of neuronal activity, which caused an increase in tau secretion *in vitro* and an increase in tau propagation *in vivo* [172].
The increased secretion of tau induced by neuronal activity could be mediated by increased Golgi dynamics [173].

Furthermore, chronic sleep deprivation causes an increase in neuronal activity and therefore can facilitate the secretion and propagation of tau [174]. It is not surprising that AD and PD patients have shown abnormal neuronal activity, such as the seizure-like and sleep disorders, that likely facilitate the spreading of pathological seeds [175,176].

1.2.3.2 Animal and cellular models of tau spreading

The pathophysiological mechanisms of Alzheimer's disease are multifactorial, and this underlies one of the main problems in AD research, which has been to establish of robust *in vitro* and *in vivo* models that fully recapitulate the pathology.

Cellular and animal models of tauopathies are useful tools for investigating the causes and consequences of tau aggregation. As mentioned before, multiple studies have shown that pathological seeds generated from recombinant proteins, animal models, or hAD brains can induce tau aggregation and pathology both *in vitro* and in animal models (*Table 1.1*).

Cell-to-cell transmission of tau was first demonstrated in the ALZ17 transgenic mouse model, which expresses human wild-type tau but does not naturally develop aggregates. Tau aggregates were extracted from transgenic mouse brains that express the P301S tau and then injected in the ALZ17 model where they induced the slow assembly of wild-type tau into silver-positive, filamentous and hyperphosphorylated tau species several months post-injection. These were detectable at the injection site and in closely connected

brain regions, suggesting that tau may have been released at the synapses [177].
A similar mechanism was also observed after the injection of TgP301S tau extracts from the hindbrain of symptomatic mice into the hippocampus and overlying cerebral cortex of non-symptomatic mice transgenic for human P301S tau. Tau inclusions form in the hippocampus, which then spread rapidly (2-4 weeks) to synaptically connected brain regions, demonstrating the transmissibility of tau pathology [162].

Interestingly, it has been shown *in vivo* that not all the pathological tau species seed in the same way; in fact, synthetic tau fibrils can induce tau aggregation in transgenic mice that express the P301L mutant form of human tau, but not in wild-type mice [123]. However, when treated with hAD seed derived from AD brains, even WT mice can develop aggregates [125,142].
This again demonstrates that tau seeds derived from human Alzheimer's disease brains have unique conformations that are not readily recapitulated by their recombinant protein counterparts [146].
The stereotypical transmission pathway of pathological tau has been demonstrated in a mouse model that specifically expresses P301L mutant tau in layer II of the entorhinal cortex [178]. In these mice, the mutant form of tau spreads to neighbouring cells in the entorhinal cortex, and to connected brain regions including the hippocampus and cingulate cortex. However, tau pathology has also been detected in

cortical regions outside of layer II of the entorhinal cortex, complicating the interpretation of the results [179].

Another strategy to initiate tau pathology in a defined brain area is using lentiviruses (LVs) for local overexpression without diffusion: one study that used LVs demonstrated that wild-type tau protein is transferred long distances through a trans-synaptic mechanism *in vivo* [180], and another study used the microinjection of plasmids in giant anterior bulbar neurons to induce the overexpression of WT or mutated human tau [181].

In vivo mouse models demonstrated that distinct pathological conformers (strains) of assembled tau exist, which are specific for each tauopathy. An example is the work of Mark Diamond's group, where they injected various clones of truncated recombinant tau aggregates from HEK293 cells into hippocampus of young TgP301S mouse brains and observed that the resulting brain depositions were reminiscent of the injected clone [182]. They propagated these same tau species through multiple generations in a prion-like fashion, showing that the pathology observed in subsequent generations was due to endogenous tau templated with the seed of the parental line [183].

Finally, they homogenised brains from these animals and seeded HEK cells expressing 4R tau that, consequently, formed identical inclusions to those present in the original cells in agreement with the prion hypothesis.

The same group also showed that different tau strains may explain the diversity of human tauopathies, as they isolated different tau clones from HEK293 cells, injected these into TgP301S (PS19) mouse brains and observed strain-specific patterns of tau pathology [184].

In concert, these studies have begun to explain the complex pathophysiology of tauopathies, but many questions remain to be answered. Nevertheless, cell-based models, remain an invaluable tool to dissect tau aggregation mechanisms in a complex cellular system.

Many cellular studies attempted to further characterize tau propagation and its associated mechanisms. Diamond's group, for example, used a Fluorescence Resonance Energy Transfer (FRET) technique to demonstrate trans-cellular propagation of tau aggregates [152]. During FRET, one protein of interest is tagged with a donor fluorophore (CFP), and another protein of interest is tagged with an acceptor fluorophore (YFP). The excitation of the donor fluorophore leads to the transfer of energy to acceptor fluorophore only when the tagged proteins in are close proximity (typically 2–6 nm), resulting in a fluorescent signal. This allows the discrimination of aggregated species from non-aggregated species in living cells.

In this work [152], two truncated tau constructs – K18(ΔK280)-CFP and K18(ΔK280)-YFP – were expressed in separate cell populations, which were then combined. Trans-cellular movement and co-aggregation of tau aggregates moving between cells was observed,

as confirmed by a positive FRET signal. More recently, the group improved the FRET assay and engineered a monoclonal FRET biosensor HEK293T cell line (“tau biosensor cells”), which stably express the tau repeat domain (RD) with the P301S mutation fused to either CFP or YFP.
After application of exogenous seeds, the nucleated aggregation of the tau FRET reporter proteins was detected by flow cytometry with a reported sensitivity in the femtomolar range [185].

One of the drawbacks of this particular FRET approach is that the addition of a large fluorescence tag to tau might alter its propensity to accumulate and aggregate and interfere with the interaction between the proteins of interest.
Another technique often used to study tau propagation is the bimolecular fluorescence complementation (BiFC). In this methodology, the fluorescence reporter is split into two non-fluorescent fragments and tagged to the proteins of interest. Only when those proteins of interest are associated together can fluorescence be emitted, due to the reconstitution of the fragmented fluorophore [186]. There are two BiFC approaches: the first one is the “turn-off”, which is used to detect early processes of tau aggregation, such as soluble tau intermediates. For example, FL tau was fused to a small GFP fragment (GFP11) and co-expressed in cells expressing a larger GFP fragment (GFP1–10). Only tau monomers, or small aggregates, allow the large GFP fragment to access the small fragment fused to tau, leading to the reconstitution of the fluorescently

active GFP. However, as tau aggregates, this reconstitution of active GFP is impaired, leading to reduced GFP fluorescence in cells [187].
The second approach employs Venus-based “turn-on” BiFC systems. The Venus fluorescence protein is split into two non-fluorescent N- and C-terminal fragments (VN173 and VC155), which are used to label tau. When tau assembles together and aggregates, the GFP is reconstituted and a dramatic increase in fluorescence is produced [188].

1.2.3.3 The role of glial cells in tau spreading

Neuroinflammation is a common characteristic of most neurodegenerative diseases. The role of the inflammatory mechanism is to respond to the presence of pathogenic species and to restore the physiological situation.
However, once activated, the inflammatory process can become deleterious sometimes, exerting a harmful influence within the parenchyma, causing cellular dysfunction, and ultimately leading to the elimination of, otherwise, healthy cells. Glial cells such as microglia and astrocytes have been extensively studied in relation to tau spreading and clearance [189]. Some evidence suggests that glial cells can facilitate the removal of pathological species from the extracellular space, thereby inhibiting the spreading of pathological seeds. In fact, microglial cells can phagocytose soluble and insoluble tau [190] and astrocytes can take up tau fibrils *in vitro* and reduce tau pathology in mutant tau transgenic mice [191]. However, other studies have suggested that microglia and astrocytes could also facilitate tau

spreading and promote disease progression. Pharmacological depletion of microglia suppressed the propagation of tau pathology in a transgenic mouse model. Inhibiting exosome secretion by microglia also reduced tau spreading both *in vitro* and *in vivo* [168].
However, even though many studies confirm this particular phenomenon [192], others have shown the opposite effect [193], indicating how timing and dosage are important in designing a study and suggesting that we must continue exploring into these mechanisms to understand when we can intervene on both microglia and astrocyte functions to achieve a beneficial effect.

Moreover, it has been shown in PSP human brains that tau aggregates develop in astrocytes and oligodendrocytes [78,194], suggesting that tau can be transmitted between neurons and glial cells, or among glial cells [195].
Overall, the role of microglia and astrocytes must be fully elucidated in order for the neuroinflammatory system to become a potential pharmaceutical target.

1.3 Microfluidic Devices

Microfluidic devices (MFDs) are platforms that have been widely used as an *in vitro* model to investigate the propagation of different aggregated proteins in multiple cellular models. There are many types of MFDs containing between two to seven chambers [196], but they all share the same characteristics: the chambers in which the cell cultures are plated are physically separated by microgrooves, and fluidically isolated via the maintenance of a media gradient between the chambers. This spatial separation of cell populations is very useful for the study of signalling, protein transfer, and cell growth [197]. The length of microgrooves are also variable, ranging from 150um to 900um, depending on the purpose [150,180,198].

Due to the versatility of MFD platforms, the last decade has seen several studies published from various fields using this technique. For example, MFDs have been used to study the extravasation of cancer cells by creating a bone-like environment [199]; the transport of nanometre organelles such as mitochondria [200] and to investigate the effect of amyloid-beta applied in either somatic or axonal positions [201].

Focusing on the study of tau propagation, MFDs are becoming a common platform to study neuron-to-neuron transmission, especially using two- and three-chamber devices (*Figure 1.9*) [150,163,180].
The beauty and the advantage of this model in the study of propagation mechanisms between two or more cell populations, is that

it provides isolation between the compartments where cells are plated. For example, neuronal cultures are separated by the microgrooves that, irrespective of the length, are only big enough to allow axons to pass through, providing spatial separation from the soma and dendrites [163,202]. The compartments are hydrostatically isolated, due to their structure, and a barrier to diffusion can be created by adding a higher volume of media in one side of the device.

The result of this set up is that, when studying propagation of a protein from one side to the other, the protein of interest can only reach the ‘recipient compartment’ by being transported through axons, as the fluidic isolation ensures that material cannot pass by passive diffusion.

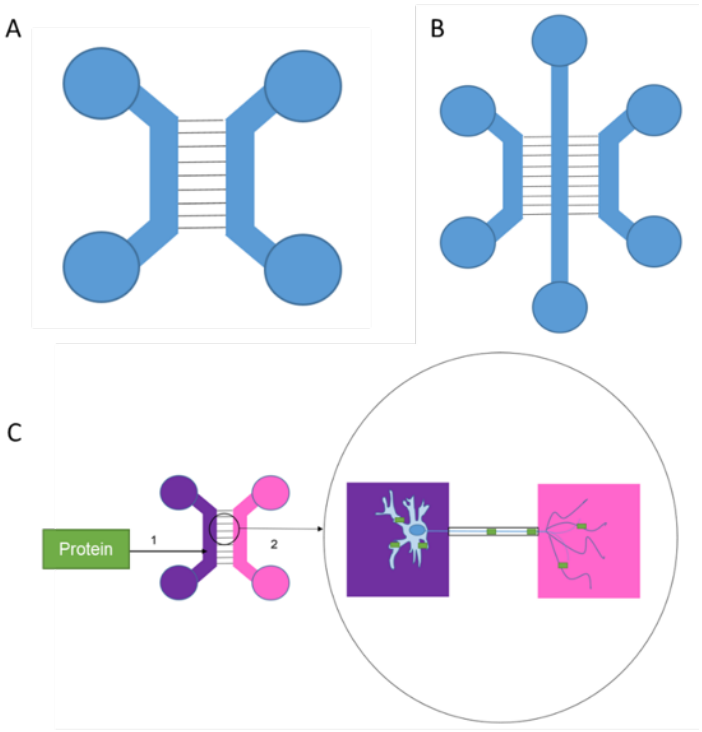


Figure 1.9: Representation of 2 and 3 chamber microfluidic devices, and their use in tau propagation. *A 2-chamber microfluidic device where the two chambers are joined together by microgrooves. Each chamber is attached to two reservoirs (circular ends) which is where the media is kept and exchanged during the protocol. Having a higher volume of media in one side (left or right) of the device prevents passive diffusion into the chamber with the high volume and generates fluidic isolation (A). Three chamber microfluidic device, where the first chamber is joined to the middle chamber by microgrooves and the middle chamber is joined to a third chamber by microgrooves. Each chamber has two reservoirs (B). Example of neurons plated in 2-chamber MFDs to study protein propagation. In this case the neurons are plated in the first chamber (purple) and the axons project through the microgrooves into the second chamber (pink). The protein of interest (green) present in the first chamber, can only be transported though the axons in the microgrooves to reach the second chamber, where it will be detected (C).*

1.3.1 Trans-neuronal tau propagation

As discussed above, disease-specific tau spreading follows a stereotypical route when it spreads through different brain regions, which is primarily determined by axonal connections between these anatomical regions, indicating a trans-synaptic spread. To better understand how tau is internalised and transferred, multiple studies have investigated different experimental designs including different types of neurons and different species of tau seeds to induce aggregation in microfluidic devices.

One of the first studies investigated WT tau propagation in 2-chamber devices. Rat cortical neurons were plated in the devices and the donor side was transduced with a lentivirus that would overexpress fluorescently tagged WT tau (V5 epitope). After 48h, the tagged tau was found not only in the donor cells but also in the microgrooves and in the recipient cells indicating that propagation, but not aggregation, had occurred [180].

In another study, rTg4510 neurons were plated in the donor side of the MFD, and MAPT-/- neurons were plated in the recipient side of a two-chamber device. Human P301L tau from the rTg4510 neuronal culture was shown to be transferred between axons, and present in neurons of the second chamber as well as the media, providing strong evidence for the neuron-to-neuron transfer of tau, as the recipient neurons did not express any endogenous forms of tau [169].

Another way to induce and study tau aggregation is to add a seed species that can trigger tau misfolding and oligomer formation. Many different forms of seed have been used in MFDs: in one study tau aggregation and propagation were observed when lysate from a biosensor cell line was added to neurons expressing mutant tau, not only in the donor side but also in the microgrooves and propagation side [169].

Primary neurons in MFDs have also been seeded with different sized tau aggregates demonstrating that both short fibrils (both straight and helical twist structures) and low molecular weight (small spherical oligomers with diameters ranging from 10 to 30 nm) human tau are present in the neurons as well as axons in the microgrooves, whereas long tau fibrils are bound to the neuronal membrane but are not internalized [147].

MFDs have been used to study the direction in which tau is transported through the axon, either from the cell body toward the axon terminals in an anterograde manner, or in the opposite direction in retrograde manner [203]. Results show that the propagation can occur in both directions within the axon and that tau aggregates colocalised initially with dextran, a marker for endocytosis and at later stages with lysosomal markers [147].

Since it has been shown that retrograde transfer of tau is possible, it is probable that when using 2-chamber devices, neurons from the recipient chamber can project their axons into the donor chamber and pick-up aggregates. In order to evaluate this mechanism, three-

chamber devices have been used to provide further spatial separation. Indeed, after addition of tau aggregates derived from a biosensor cell line to the first chamber, tagged-inclusions from the donor chamber were seen at DIV15-18 in neurons of the third chamber, providing further support for the anterograde propagation of tau aggregates from chamber one to three [169].

Another approach used to strengthen the evidence that the results are due to true neuron-to-neuron transfer, is to plate neurons in 2- or 3-chamber devices on different days. This allows the population plated first to project its axons through to the second chamber and to physically occlude the microgrooves, before plating the neurons in the second chamber [198].

1.3.2 The role of synapses in tau propagation

Neuron-to-neuron propagation of tau has been widely demonstrated and it highlights the importance of synapses in this mechanism. Numerous studies have focused their attention on demonstrating how synapses are fundamental in tau spreading, some of them employing the use of MFDs.

One study has demonstrated the importance of synapsis in tau propagation via exosomes, which is one of the main hypothesised mechanisms of transcellular tau propagation. Exosomes containing GFP-tagged tau can move from one chamber to another via axons and are released from synaptic compartments. Interestingly, this happens

only if neurons are mature enough and if the synapses are fully developed, otherwise transfer does not occur [150]. Moreover, when the same experiment was done in 3-chamber devices where the cellular population in the central chamber was absent, exosomes from chamber 1 could not be found in chamber 3, indicating not only that synaptic connection is really fundamental for tau propagation but also that the operational distance of exosomal spreading is quite short. This is also in line with the results of another paper demonstrating that using shRNA for synaptic adhesion molecules – Neuroligin-1, -2 and -3 – impaired the formation of synapses, which significantly decreased the amount of aggregated tau in the recipient compartment, relative to neurons treated with an shRNA control [163].

Finally, neuronal activity can affect tau propagation; increased neuronal activity increases tau release. This was demonstrated in 3-chamber MFDs where cells in the first chamber were treated with tau fibrils and the cells in the second chamber were treated with tetrodotoxin, a sodium channel blocker which prevents neuronal activity. The result was a reduced number of tau aggregates in the third chamber with respect to the control, suggesting that the reduction in synaptic transmission elicited by tetrodotoxin impaired the transneuronal propagation of tau aggregates [163].

1.3.3 MFDs to develop tau targeted therapeutics

One of the principal reasons for needing to understand the mechanism of tau propagation is to develop therapies that could act on it. One strategy is to use small molecules or antibodies that can target tau in the extracellular space and prevent its uptake by the recipient cells [204]. For example, a paper published in 2018 used shiga-Y5, a curcumin derivative that was shown to prevent tau pathology in a Tg4510 tau mouse model [205] and another group used a PHF1 anti-tau antibody in TgP301S mice that showed a reduction in neuronal atrophy in the brain region of treated mice [206]. These studies give a significant indication as to whether a treatment may work in humans. However, before the *in vivo* stages of drug development, compound screening occurs *in vitro,* which is where MFDs can be employed for medium- to high-throughput screening assays of preclinical portfolio molecules.

For example, one paper has studied the most effective antibodies, for preventing the neuron-to-neuron transfer of tau. Primary neurons were plated in 3-chambers MFDs (Fig 1.8); neurons in chamber 2, were transduced with tau RD-P301L-CFP and tau RD-P301S-YFP that can be used in a FRET assay. Chamber 1 was treated with brain extract of rTg4510 mice and, after 6 days, the neurons in chamber 2 were treated with either the 6C5 antibody or an IgG control. Aggregates from chamber 1 that were propagated into chamber 2 induced the templated misfolding, and subsequent aggregation, of the fluorescently tagged tau, which emitted a fluorescent signal upon

aggregation. Quantification of the fluorescent tau aggregates exhibited a reduction in the number of tau-positive neurons with the 6C5 treatment, relative to the control (*Figure 1.10*). The antibody was further shown to slow progression of tau pathology in larger *in vitro* studies [207].

This study highlights a very useful application of the microfluidic device system. Not only is this a method for early-phase screening but it also specifically looks at transneuronal tau propagation. However, the complexity of this particular format renders it inappropriate as a high-throughput assay, especially because of the inherent variation involved in the transfection of primary neurons. It is plausible that in the near future this technique could become one of the key methods to produce hit molecules for further testing *in vivo* before the transition to clinical trials, but more work is required to develop and optimise a valid and reproducible assay.

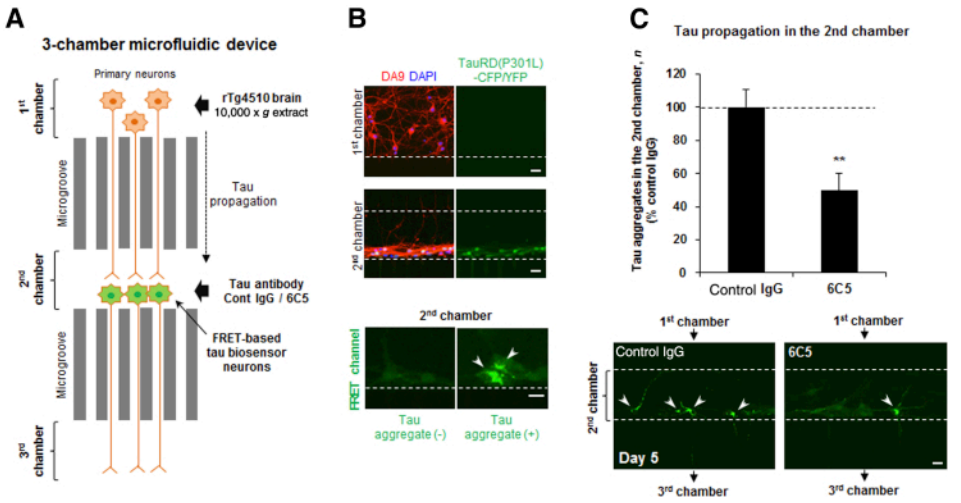


Figure 1.10: 3-chamber microfluidic devices shows 6C5 antibody blocks neuron-to-neuron spreading of tau pathology. Diagrammatic representation of the 3-chamber device system. Neurons were plated in the first and second chamber, with the second chamber neurons being transduced with a lentivirus construct containing two P301L tau repeat domains tagged with either CFP and YFP. Brain extract from rTg4510 mouse model was added to the first chamber and the number of aggregates in the second chamber was quantified after five days (A). Images of neurons from the first two chambers in the microfluidic device stained for both total tau (DA9, red) and for the nuclei (DAPI, blue). Both lentiviral-induced tau proteins are shown in green in the second chamber. FRET images show aggregated tau (arrows) in the second chamber five days post-seeding (B). The number of aggregates in the second chamber was quantified as a way to view tau propagation (C). Confocal images in the FRET channel of tau uptake in the second chamber neurons are also shown in the bottom row (C). The arrows indicate intracellular tau aggregates. 10 or 11 devices were used per group. **P < 0.01 versus control IgG in a two-tailed t-test. Scale bars – 20 um. Image and figure legend taken or based on [207].

1.4 Tau modulators and related Clinical Trials

There is an urgent need for a disease modifying drug for Alzheimer's disease. In fact, after 114 years since this pathology has been first described, there is still no treatment able to block the onset or to slow down the progression of this neurodegenerative disease. No significant new drug for AD has been approved in the last 14 years, despite extensive clinical trials that showed significant failures [208].

For many years pharmaceutical companies have largely focused with very limited success on developing Alzheimer's drugs against β-amyloid peptides mostly because of the β-amyloid cascade hypothesis that indicated this protein as the primary cause of the pathology. However, with the new discoveries in the development of AD, drug discovery has shifted to drugs against tau.
On Alzforum.org is possible to review all the current therapies that are being studied for AD. In particular, of the 265 therapeutics listed, only 24 have tau as target. Of these, 10 are small molecules, 1 is DNA/RNA based, 12 are immunotherapies and 1 is a neuropeptide (*Table 1.2*).

Therapy	Synonyms	FDA Status	Company	Therapy Type
AADvac1	Axon peptide 108 conjugated to KLH	Alzheimer's Disease (Phase 2), Progressive Nonfluent Aphasia (Phase 1)	Axon Neuroscience SE	Immunotherapy (active)
ACI-3024	Tau MorphomerTM	Alzheimer's Disease (Phase 1), Other Tauopathy (Phase 1)	AC Immune SA	Small Molecule
ACI-35		Alzheimer's Disease (Phase 1)	AC Immune SA, Janssen	Immunotherapy (active)
ASN120290	ASN-561	Progressive Supranuclear Palsy (Phase 1)	Asceneuron SA	Small Molecule
AZP2006	AZP-2006	Progressive Supranuclear Palsy (Phase 2), Alzheimer's Disease (Phase 1)	AlzProtect	Small Molecule
Anle138b		Multiple System Atrophy (Phase 1)	MODAG GmbH	Small Molecule
BIIB076	NI-105, 6C5 huIgG1/l	Alzheimer's Disease (Phase 1)	Biogen, Eisai Co., Ltd., Neurimmune	Immunotherapy (passive)
BIIB080	IONIS-MAPTRx, ISIS 814907	Alzheimer's Disease (Phase 1)	Biogen, IONIS Pharmaceuticals	DNA/RNA-based
Bepranemab	UCB0107 , UCB 0107 , Antibody D	Progressive Supranuclear Palsy (Phase 1), Alzheimer's Disease (Phase 1)	Hoffmann-La Roche, UCB S.A.	Immunotherapy (passive)
Davunetide	NAP, AL-108	Mild Cognitive Impairment (Discontinued), Progressive Supranuclear Palsy (Discontinued), Schizophrenia (Discontinued), Frontotemporal Dementia (Inactive)	Allon Therapeutics Inc., Paladin Labs Inc.	Other
Epothilone D	BMS-241027	Alzheimer's Disease (Discontinued)	Bristol-Myers Squibb	Small Molecule
Gosuranemab	BIIB092, BMS-986168, IPN007	Progressive Supranuclear Palsy (Discontinued), Alzheimer's Disease (Phase 2)	Biogen, Bristol-Myers Squibb	Immunotherapy (passive)
JNJ-63733657		Mild AD (Phase 1)	Janssen	Immunotherapy (passive)
LMTM	TRx0237, LMT-X, Methylene Blue, Tau aggregation inhibitor (TAI)	Alzheimer's Disease (Phase 3), Frontotemporal Dementia (Phase 3)	TauRx Therapeutics Ltd	Small Molecule
LY3372689		Alzheimer's Disease (Phase 1)		Small Molecule
Lu AF87908		Alzheimer's Disease (Phase 1)	H. Lundbeck	Immunotherapy (passive)
PNT001		Alzheimer's Disease (Phase 1), Traumatic Brain Injury (Phase 1)	Pinteon Therapeutics	Immunotherapy (passive)
RG7345	RO6926496	Alzheimer's Disease (Discontinued)		Immunotherapy (passive)
Rember TM	Methylene Blue , methylthioninium (MT), TRx-0014, Tau aggregation inhibitor (TAI)	Alzheimer's Disease (Discontinued)	TauRx Therapeutics Ltd	Small Molecule
Semorinemab	RO7105705 , MTAU9937A, RG6100	Alzheimer's Disease (Phase 2)	AC Immune SA, Genentech, Hoffmann-La Roche	Immunotherapy (passive)
TPI 287		Alzheimer's Disease (Inactive), Corticobasal Degeneration (Inactive), Progressive Supranuclear Palsy (Phase 1)	Cortice Biosciences	Small Molecule
Tideglusib	NP031112, Nypta® , Zentylor™ , Glycogen synthase kinase 3 inhibitor, NP12	Alzheimer's Disease (Discontinued), Progressive Supranuclear Palsy (Discontinued)	Zeltia Group	Small Molecule
Tilavonemab	ABBV-8E12, C2N 8E12, HJ9.3	Progressive Supranuclear Palsy (Discontinued), Alzheimer's Disease (Phase 2)	AbbVie, C2N Diagnostics, LLC	Immunotherapy (passive)
Zagotenemab	LY3303560	Alzheimer's Disease (Phase 2)	Eli Lilly & Co.	Immunotherapy (passive)

Table 1.2: Current therapeutics studied in Clinical Trials for Alzheimer's Disease. *There are currently 24 therapeutics that target tau for AD pathology (December 2020). Most of them are immunotherapy agents (orange) or small molecules (white) and they are either in Phase 1, Phase 2 or are discontinued (info taken from Alzforum.org).*

There are different approaches that can be taken to act on tau pathology as modulating tau phosphorylation or other post translational modifications (PTMs), stabilizing microtubules, inhibiting tau aggregation and targeting tau with antibodies (immunotherapies) [209].

1.4.1 Modulating tau post translational modifications

Tau hyperphosphorylation is one of the hallmarks of neurodegeneration and it is the result of multiple protein kinase activity. It has been hypothesized that kinases as GSK-3β, Fyn or CDK5 could be potential therapeutic targets however, due to the large number proteins that these kinases have an effect on, the drugs developed are not very specific and, consequently, it has been observed several toxicity and side effects [210]. An example is Tideglusib (NP031112, NP-12), an orally available GSK-3β inhibitor [211].

Even though in preclinical studies it reduced tau phosphorylation, neuronal loss, and gliosis, and reversed a spatial memory deficit in transgenic mice [212], in the clinical trial it missed its primary endpoint and some of the secondary endpoints, thus showing no significant clinical benefit [213].

Another example is Saracatinib (AZD0530), a Fyn inhibitor shown to reduce memory deficits in transgenic mice and reported to be safe and

well tolerated in a Phase 1 clinical trial (NCT01864655) [214] but discontinued in Phase 2 for lack of efficacy [215].

Tau is not only phosphorylated but can undergo to other PTMs as lysine acetylation or glycosylation that may lead to an increase of tau phosphorylation and to impaired tau function thus promoting pathological aggregation [216,217].

Salsalate, has been shown to inhibit acetyltransferase p300-induced tau acetylation and to improve tau-mediated behavioural impairments and neurodegeneration in a FTD mouse model [218]. This compound completed both a pilot futility Phase 1 clinical trial (NCT02422485) and a Phase 1b clinical trial (NCT02460731). Unfortunately, there was no detectable effect on disease progression.

LY3372689 and ASN120290, previously known as ASN-561, are inhibitors of O-GlcNAcase (glycoside hydrolase enzyme that removes O-linked N-acetylglucosamine (N-GlcNAc) from proteins) and are both in Phase 1 Clinical Trials.
ASN120290 in P301L human tau mouse model induced a reduction in insoluble PHF and in NFTs but clinical studies are not yet listed in Clinicaltrials.gov. LY3372689 trial will run through October 2020 [219].

1.4.2 Stabilising microtubules

The role of tau protein is to stabilize microtubules and, when it is phosphorylated, as shown in AD, it loses this ability resulting in axonal transport defects and synaptic dysfunction.
One of the therapeutic strategies is to enhance microtubules stabilisation using small molecules.

Epothilone D (BMS-241027) is a small-molecule that has been described as able to restore the spatial memory deficits by reducing tau pathology and hippocampal neuronal loss in transgenic animals [220]. It was tested in 2013 in a Phase 1 clinical study (NCT01492374) but no results have been published.

Davunetide (also known as NAP or AL-108) has produced promising effects on memory and behaviour in tau transgenic mice [221] and even though it was shown as safe and tolerable in mild cognitive impaired subjects [222], a later Phase 2/3 clinical trial (NCT01110720) missed all the endpoints [223].

1.4.3 Tau aggregation inhibitors

Tau aggregation is one of the most studied mechanism for the development of AD treatments. This mechanism has been modelled in different *in vitro* assays that lead to the identification of several molecules [224]. Despite most of them showed efficacy *in vitro*, they often didn't show the same outcomes *in vivo*.

One of the molecules that can inhibit tau aggregation is Methylene Blue, also known as Rember or TRx0014. It has been shown that it prevents tau aggregation *in vitro* as well as in animal models [225]. A clinical trial (NCT00515333) reported signs of benefit in moderate, but not mild, AD [226].
A second-generation, more stable replacement formulation of Methilene Blue known as LMTM or TRx0237, has reached Phase 3 clinical trials (NCT01689246 and NCT01689233) but it showed no signs of efficacy on the primary endpoints [227,228]. Moreover, one of the limitations of this molecule is that not only findings are mixed with some works reporting no inhibition of tau and neurotoxicity *in vivo* [229], but it also has pleiotropic effects, so it is activity is difficult to characterise.

Anle138b, also known as 3-(1,3-Benzodioxol-5-yl)-5-(3-bromophenyl)-1H-pyrazole, is an oral, brain-penetrant, general inhibitor of protein aggregation. It has been shown to suppress oligomer formation *in vitro* and *in vivo* inhibiting protein accumulation and neurodegeneration [230]. Preclinical studies in mouse models of tau pathology, showed a decrease in neuronal loss, tau deposition and an improvement in cognitive functions [231,232]. An *in vitro* study showed that this compound inhibited tau aggregation in cell culture models [233].
A Phase 1 clinical trial (NCT04208152) described this drug as safe.

ACI-3024, also known as Tau Morphomer, is a small-molecule inhibitor of tau aggregation. Even if no preclinical information on ACI-

3024 is formally published, according to data presented at conferences, the compound disrupts tau aggregates *in vitro* and it disaggregates tau NFTs in human brain sections *ex vivo*. *In vivo* studies on Tg4510 mice, showed a reduction of brain aggregated and insoluble tau as well as microglia activation.
Phase 1 safety and tolerability study in healthy volunteers is now complete and data release is exprected soon.

1.4.4 Tau immunotherapy

Tau immunotherapy is a promising approach for tau clearance and various anti-tau strategies have shown good results in animal models [234].
This method can be divided in active immunotherapy (vaccination), that aim to stimulate production of specific antibody against tau, or passive immunotherapy that is based on the use of synthetic anti tau antibodies. Both approaches are capable of clearing tau pathological species that could eventually result in neuronal function improvement. Therefore, it is important to choose the right epitope (abnormally phosphorylated or pathologically relevant conformational epitopes) in order to stimulate an effective immunity response against the toxic tau species.

Two active immunotherapy agents are now in Phase 1 clinical trial: AADvac1 and ACI-35.

AADvac1is a vaccine consisting of a synthetic peptide derived from amino acids 294 to 305 of the tau sequence (KDNIKHVPGGGS). After that preclinical studies reported meeting safety requirements and a reduction in tau pathology in animal models [235], clinical trials have started in order to show the efficacy in human patients.
Two Phase 1 clinical trials (NCT01850238 and NCT02031198) showed no treatment-related adverse events and reported a trend toward lower hippocampal atrophy and an improvement of cognitive impairment [236].
The following Phase 2 clinical trial (NCT02579252) showed that 80% of immunized patients developed high-affinity tau antibodies, which bound aggregated tau in autopsy brain tissue. Even if this study showed also a reduction of CSF pTau181 and pTau217, the treatment produced no cognitive benefit.
Currently this vaccine is in Phase 1 pilot trial in nonfluent/agrammatic variant primary progressive aphasia (PPA) patients.

ACI-35 is a liposome-based vaccine that contains 16 copies of a synthetic tau fragment phosphorylated in S396 and S404.
Preclinical studies in both wild-type C57BL/6 and P301L mutant tau transgenic mice, showed a rapid generation of high titres of polyclonal IgG antibodies specifically directed against phosphorylated tau that reduced soluble and insoluble tau in brain extracts [237].

A Phase 1b/2a to evaluate the safety, tolerability and immunogenicity of this vaccine in early AD patients started in June 2020 (NCT04445831).

Passive immunotherapy agents are much more common than the active ones in fact, there are now ten agents in clinical trials, five in Phase 1, four in Phase 2 and one was discontinued.

Zagotenemab (LY3303560) is an anti-tau antibody against an early pathological conformation of tau.
In vitro data showed that selectivity binds N-terminal region of aggregated tau. *In vivo* data showed that in P301S mice, it blocked pathology induced by injected tau seeds [238,239].
Based on these results, two Phase 1 clinical trial (NCT02754830 and NCT03019536) of Zagotenemab started to assess the therapy's safety and tolerability in participants. Recruitment has been completed but the trial is still active with an estimated completion date of June 2020.
Meanwhile, a Phase 2 clinical trial (NCT03518073) in patients with early symptomatic Alzheimer's disease has begun. The trial is expected to be completed in October 2021.

Semorinemab, also known as Abbv8E12, is an anti-tau IgG4 antibody that target only extracellular tau. It binds the N-terminus of all six isoforms of human tau, both monomeric and oligomeric, regardless of their phosphorylation status. In preclinical studies in P301L mice it reduced tau pathology in a dose dependent way [240].
After a Phase 1 study that assessed the safety of this antibody, a Phase 2 named TAURIE (NCT028208960) started in people with prodromal or probable AD. Even if this study missed its primary efficacy endpoint of reducing cognitive decline, in February 2019

another Phase 2 study, LAURIET (NCT03828747), started in people with a diagnosis of probable AD. It is set to run until May 2021.

Tilavonemab is a humanized IgG4 antibody that recognizes the N-terminus of aggregated, extracellular tau. Its characteristic is that, differently from the other therapies, its mechanism of action doesn't require tau uptake into neurons.
Preclinical studies in P301S tau-transgenic mice, showed a reduction in brain atrophy, NTFs pathology and insoluble tau levels [241].
After a Phase 1, a Phase 2 and a Phase 2 PSP trials (NCT02880956), in July 2019, an interim analysis of the latter study found no benefit of antibody over placebo, and AbbVie stopped the study.

AIMS OF THE STUDY

Alzheimer's disease (AD) and, in general, sporadic tauopathies are a class of pathologies that are characterized by the presence of intracellular hyperphosphorylated and aggregated tau. For these neurodegenerative diseases, there is currently no disease-modifying treatment, but new interventional approaches are being evaluated. In particular, some early-phase clinical trials are testing compounds and antibodies that can mitigate the transcellular spread of tau, on the basis of the observation that tau undergoes predictable spatiotemporal spreading during the clinical manifestation of tauopathies, which is underpinned by synaptically connected networks.

Microfluidic device-based assays have previously been utilized to recapitulate this mechanism of tau propagation *in vitro*, as a platform to test potential therapies; however, these methods often rely upon experimental parameters that may compromise the reliability of these systems such as tau overexpression, fluorescent tags, or MAPT mutations.

The main purpose of this research project has been to establish a new microfluidic method that could improve upon existing assays in order to help the screening of efficient and effective treatments. In particular, the aim was to develop a humanized, *in vitro* neuronal microfluidic platform to recapitulate and study tau propagation and aggregation in a qualitative and quantitative way.

In order to achieve this outcome, the workflow was structured with several experimental aims, which follow:

- To establish and validate a rat cortical neuron (RCN) aggregation assay that uses seeding-competent material from human AD brains (hAD seed) to induce endogenous aggregation.
- To establish a propagation assay using commercially available microfluidic devices (MFDs) and high-content imaging (HCI) techniques.
- Statistically optimize the MFD propagation assay, evaluate different concentrations of hAD seed, and perform proof-of-concept inhibition experiments with active molecules/antibodies as well as exploratory experiment, such as calcium imaging.
- Convert the MFD assay into a smaller, medium-throughput format that allows the user to handle 16 two-chamber devices simultaneously in the footprint of a standard 96 well plate.
- Utilize this new assay format for both tau propagation experiments, and for exploratory experiments.
- Humanize the assay using hTau mouse cortical neurons instead of RCNs to improve physiological relevance of the platform, and to study the aggregation and propagation of human tau instead of the murine homolog.

.

2. MATERIALS AND METHODS

2.1 hAD Seed Preparation: sarkosyl extraction of tau aggregates from human AD brains

Post-mortem human brain tissue was provided by the King's College London Brain Bank after confirmation of consent and histological confirmation of tau pathology. The pool of cortical tissues used were obtained from ~20 patients with Alzheimer's disease, modified Braak (Brain Net Europe) stage 6 with moderate amyloid angiography. The average age was 71 years, and the gender was mixed male and female. The samples chosen for the preparation were those with the highest levels of AT8-positive Tau (0.5 µg/ml) as determined by AlphaScreen. All human tissue was handled in compliance with the regulations set by the HTA Human Tissue Act 2004. Upon receipt, the tissue was analysed for both total tau and pathological tau (AT8-positive) content by AlphaScreen.

2.1.1 Standard Preparation

Method summarized in *Figure 2.1*. The brain tissue was weighed, and the tissue was homogenized for 10 minutes in DPBS supplemented with protease inhibitor cocktail using an Ultra Turrax homogenizer at 25,000 rpm; a final volume of 10 mL of DPBS was used for each gram of brain tissue. The homogenate was then centrifuged at 10,000 RCF for 10 minutes at 4°C, and the supernatant was isolated by decanting this into a beaker through a filter. The pellets were resuspended, and the process of homogenization and centrifugation was repeated a further two times, pooling the supernatants from each cycle. The

pooled supernatant volume was measured, and a suitable volume of 30% sarkosyl was added to reach a final concentration of 1% sarkosyl. The resulting solution was placed on a shaker at room temperature for 1 hour. Afterwards the sarkosyl solution was centrifuged at 100,000 RCF for 1 hour at 4°C. The resultant supernatant was discarded into 1 M NaOH for decontamination. The pellet was washed carefully with DPBS supplemented with protease inhibitors, and then resuspended in 50mM Tris pH 7.4, with complete protease inhibitor cocktail. The resuspended pellet was then homogenised using a QSonica hand-held sonicator probe at 40% amplitude for approximately 10 pulses. The resulting suspension is the standard preparation hAD seed, which contains tau aggregates capable of inducing endogenous aggregation, and will be used throughout most of this study. hAD seed concentration was determined using the AlphaScreen protocol.

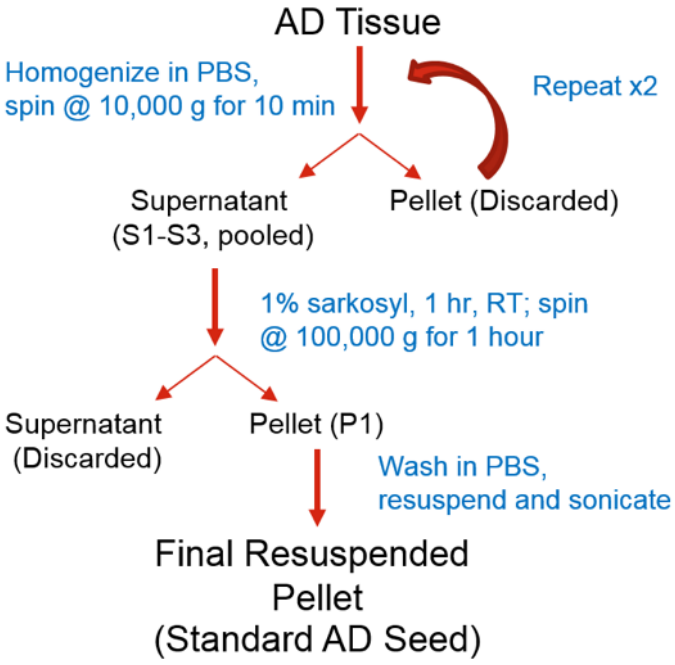


Figure 2.1: Summarized protocols for the standard preparation of human Alzheimer's disease derived tau aggregates*. Image adapted from [97].*

2.1.2 AlphaScreen protocol for determining the concentration of tau

AlphaScreen assay (Perkin Elmer) was used to determine the concentration of total tau in hAD seed using tau specific antibodies in the manner described previously [242]. The assay is a sandwich assay that has higher specificity than an ELISA, due to its use of two antibodies specific for the target of interest. The first anti-analyte antibody is biotinylated and binds streptavidin donor beads, and the other anti-analyte antibody is bound to an acceptor bead. When the two antibodies bind the target, they are brought in proximity to one another. Following excitation with a laser, the donor bead releases a

singlet oxygen molecule which further activates a fluorophore on the acceptor bead and causes light emission. The AlphaScreen assay used in this study was optimized for the detection of total tau, using the total tau-specific antibodies DA9 and TG5 (originally from P. Davies, now produced in-house) (*Tab 2.7*). Before incubation with the antibodies, the samples were incubated with either guanidine hydrochloride (GuHCl) or AlphaScreen assay buffer (DPBS with 0.1% casein) for 1 hour, where the GuHCl is used to disaggregate tau to get an accurate read of the concentration.

10 µL/well of both the biotinylated antibody (50 µg/mL, 10 µg/mL final concentration in each well) and acceptor-conjugated antibodies was added to a 384-well plate (#784075, Greiner), followed by 5 µL/well of hAD seed samples, with and without GuHCl. Two standards of known tau concentration were also diluted in assay buffer (0.1% casein in DPBS) and added to this plate, for subsequent interpolation of hAD seed tau concentration. Following overnight incubation at 4C, 5 µL/well of streptavidin-coated donor beads at 80 µg/mL prepared under subdued light conditions (40 µg/mL final concentration in each well) diluted in assay buffer was added to the 384-well plate. The plate was then sealed and gently agitated at room temperature in the dark for 4 hours. Following incubation, the plate was read using the EnSpire plate reader (Perkin Elmer) with excitation at 680 nm and emission at 520-620 nm. Data from the AlphaScreen was plotted in GraphPad.

2.1.3 Sarkosyl extraction of intracellular tau aggregates and Western blotting

Rat cortical neurons (RCNs) were plated in 2 mL of media at $1.7x10^6$ cells/well in 6-well plates (#354413, Corning). At DIV7 cells were seeded with 18 nM of hAD seed that was first sonicated for 1 minute at 20% amplitude, with 1-second pulses (QSonica Probe), and then filter sterilized with a 0.22 µM filter and syringe (PN4602, Pal Acrodisc). At DIV14 half of the existing media was removed and exchanged for fresh media. At DIV21 the media was fully aspirated, and the cells were washed twice with DPBS. The neurons were then incubated with gentle rocking for 15 minutes at -4°C in 300 µL/well of lysis buffer (RIPA buffer (#R0278, Sigma) supplemented with 0.5 mM Phenylmethylsulphonyl fluoride (PMSF), 2 mM Sodium ortho-vanadate, Phosphatase Inhibitor Cocktail 3 (#P0044, Sigma), Phosphatase Inhibitor Cocktail 2 (#P5726, Sigma) and Complete Mini Protease Inhibitor Cocktail Tablet (#11836153001, Roche)). After incubation, the cells were harvested by physical dissociation with a cell scraper, and the lysates were then collected in Eppendorf tubes. The lysates were centrifuged at 13,000 RCF for 10 minutes at 4°C to pellet the cell debris (*Fig 2.2*). A BCA assay was then run to determine the concentration of protein in the sample supernatants, which were then normalized to the lowest sample concentration. These normalized supernatants – referred to as Total Lysates (TLs) – were then supplemented with a suitable volume of 30% sarkosyl to produce a final concentration of 1% sarkosyl (#61747, Sigma), and incubated for 1 hour at room temperature with agitation. TLs were then centrifuged

for 60 minutes at 100,000 RCF at 4°C in an Optima TLX 55 ultracentrifuge.

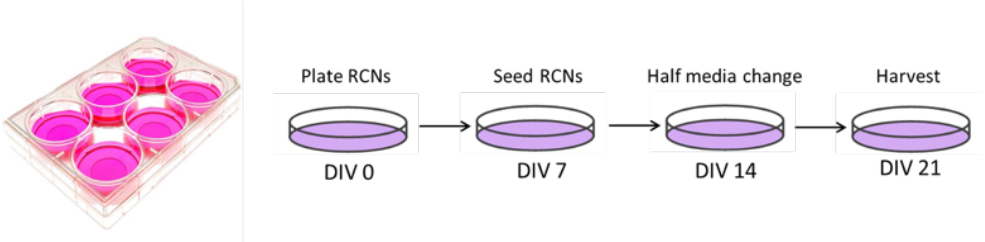


Figure 2.2: Summary of 6-well RCN assay*: cells are plated at DIV0, seeded at DIV7 and half media change is done at DIV14. Cells are then harvested at DIV21 and lysates are collected and analysed via Western Blot.*

Pellets were washed twice with 0.5 mL RIPA buffer, centrifuged for 5 mins at 13,000 RCF and then resuspended at 1/10th of the original sample volume in a solution of 50 mM Tris pH7.4 supplemented with Complete tablet (Roche) and 1 mM PMSF. The resuspended pellets were then sonicated with approximately twenty 1-second pulses, at 40% amplitude, until completely dispersed, and frozen at -80°C.

For Western Blotting, the samples were prepared with 4x SDS NuPAGE Sample Buffer containing 5% β-mercaptoethanol and heated to 95ºC for 10 minutes. The denatured samples were then run in 8% Bis-Tris NuPAGE midi gels, at 200V, using 1x NuPAGE MOPS SDS Running Buffer. Tau Protein Ladder (rPeptide, t-1007-2) was loaded as control for the identification of the tau isoforms.

The separated proteins were transferred to Amersham Hybond nitrocellulose membranes using semi-dry blotting, with NuPAGE transfer buffer 2x plus 10% MeOH, at 25V for 90 minutes. Membranes

were then incubated in blocking buffer (5% non-fat dried skimmed milk plus 0.05% Tween20 (Sigma) in DPBS) for 1 hour, before incubation with primary antibodies, diluted in the same blocking buffer, overnight at 4ºC with shaking. Primary antibodies used were T49 (#MABN827, Millipore) and AT8 (in-house) and secondary antibodies were anti-mouse IgG HRP (#7076, Cell Signalling). All membranes were incubated in West-Femto (#34094, Thermo Fisher) detection reagent. Images were acquired using ImageQuant LAS 4000 Mini.

2.2 Rat primary Cortical Neuron cultures, 96-well assay

2.2.1 RCN dissociation and plating protocols

Note: Protocol for Cortices from an average of 10 - 14 embryos.

The RCN growth medium was prepared under a BSC (biosafety cabinet), in accordance with the above recipe and filter sterilised through a Corning 500 mL vacuum filtration system. 90 mL of RCN media from a previous RCN preparation was supplemented with 10 mL of Foetal Bovine Serum (Gibco, 10500-064) – once prepared, the mixture was filter sterilised through a Corning 250 mL vacuum filtration system. A 3 mL plastic Pasteur was used to carefully transfer the cortical tissues in a 15 mL conical tube. Once the tissue had settled, a stripette was used to aspirate as much media as possible without taking up tissue. 5 mL of Trypsin/EDTA Pink (Gibco, 25300-054) was added to the tissue to wash – this was then carefully aspirated, without taking up tissue. Another 5 mL of Trypsin/EDTA Pink was added to the tissue and the Falcon tubes were incubated in water bath for 15 minutes – every 5 minutes, the Falcon tubes were gently rocked to mix the tissue and ensure complete digestion. After the 15-minute incubation, the Trypsin was aspirated from the Falcon tubes, and the tissue was washed 3x with 5 mL of FBS-supplemented RCN media. The final wash of FBS-RCN Media was aspirated, and the tissue was washed once with 5 mL of the HBSS-DNase solution (Sigma, D4263). This wash was aspirated, and further 3 mL of HBSS-DNase was added before trituration. The tissue was then triturated in three stages of increasing resistance: first, a Pasteur pipette was used to triturate the tissue and begin dissociation of the tissue (15 times); this was then

repeated with a 10 mL stripette (5 times); and finally, with a 1000 µL Gilson pipette (15-20 times). A 15 mL Falcon tube with the tissue homogenate was topped to 10 mL by adding HBSS-DNase solution and then placed into a Sigma Zentrifugen 4K15 bench-top centrifuge (200g; 5 minutes; RT). After the centrifugation, the supernatant was aspirated with a 10 mL stripette, and care was taken to avoid disruption of the pelleted cells. The pellet was resuspended in 5 mL of HBSS-DNase solution with a 10 mL stripette and the content was split across 2 new conical tubes, 2.5 mL each. Another 2.5mL of HBSS-DNAse was added to each tube and mixed using 1ml Gilson (20 times down inside of tube). With a 10 mL stripette the content of the tubes was pooled together, and it was centrifuged for 5 min at 200g (RCF). (Note: two spins release more neurons from Prep). The pellet was resuspended in 3 mL of fresh RCN media using the 1mL Gilson pipette than topped up to 7mL. The cell suspension was filtered through a 100um filter, into a sterile falcon tube and additional 5mL was used to wash the tube through the filter. In a cryovial, a 1:5 cell aliquot was taken for cell counting: 100 µL aliquot of cell suspension was mixed with 100 µL Trypan blue 0.4% (Sigma, T8154), and 300 µL of RNC media – this solution was then mixed and loaded into a disposable haemocytometer. Cell counts were acquired through a light microscope, and used to determine manually the concentration of cell suspension required to plate at a concentration of 40000 cells/well (4 x105cells/ml, adding 100 µL per well)

$a)$ $(Cell\ count\ in\ 4x4\ grid)x\ 5 = Cells\ x\ 10^4/mL$

$b)$ $$\frac{Required\ cell\ density}{Output\ of\ (a)}\ x\ volume\ needed$$
$$= volume\ of\ cell\ suspension\ required\ for\ dilution$$

Automated cell counts were acquired through Olympus, R1 cell counter automated. Cells were stained with neat Trypan-Blue (100 µL of TB and 100 µL of cell suspension). The suspension was mixed and loaded into a disposable cell counting slide (Olympus, R1-SLI).
Live cell counts were used to determine the concentration of cell suspension to plate at the desired concentration.

2.2.2 Plating and treating RCN in 96-well plates

Primary rat cortical neuronal cultures were prepared from E18 embryos harvested from time-mated CD® Sprague-Dawley (Charles River) rats. The dissociated neurons were plated on poly-D-lysine-coated (PDL) 96-well plates (#354640, Corning). The growth media (RCN media) was made with Neurobasal media (21101-049, Invitrogen) supplemented with MACS Neurobrew-21 (130-093-566, Miltenyl Biotech), 0.4mM L-glutamine (25030-024, Life Technologies) and antibiotics and antimycotics (A5955, Sigma).
In brief, the paradigm for the 96-well assay consists of seeding at DIV7, a half media change at DIV14, and fixation at DIV21 (*Fig 2.3*). In detail, RCN plates were incubated for 7 days (37°C and 5% CO_2) before seeding. On DIV7 50 µL of media was removed from the wells using an Integra Viaflo 96/384 robot using a custom program that was designed to leave 50 µL of media in each well. hAD seed was then

prepared at 2x final desired concentration (48 nM) in fresh growth media, and this mixture was added back to the 96-well plates at 50 µL/well; plates were covered with Breathe Easy sealing membranes before being returned to the incubator. At DIV14 half of the existing media was replenished again using the Integra Viaflo 96/384 robot to leave 50 µL of media in each well and adding back 50 µL/well of fresh RCN media. At DIV21 cells were fixed with 100% methanol to extract soluble proteins, as described previously (Guo, J.L. et al. 2016). In brief, the growth media was completely aspirated, and cells were washed twice with 100 µL/well of DPBS. This was followed by the addition of 100 µL/well of ice-cold 100% methanol, and a 15 minutes incubation at -20°C. Subsequently, the cells were washed three times with 100 µL/well of DPBS, with the final wash being left on for storage. Plates were kept at 4C° until immunocytochemistry (ICC) was performed.

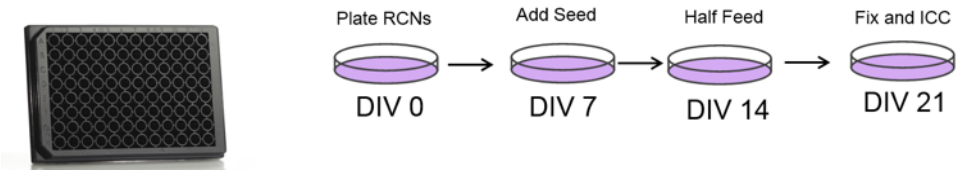


Figure 2.3: Assay timeline of the 96-well assay. *In the 96-well assay the cells were plated at day in vitro 0 (DIV0) into 96-well plates (Corning Biocoat 96-well poly-D lysine coated, Fisher Scientific), human derived tau aggregates "seed" was added at DIV7, followed by a change of half of the media at DIV14 and fixing the cells at DIV21.*

2.2.3 Immunocytochemistry and imaging

The DPBS previously added to the cells was tipped off, and the cells were blocked with 100 µL/well of Intercept Blocking Buffer (LI-COR) containing 0.1% Triton for one hour at room temperature. The primary antibody used for this assay was tau clone T49 (#MABN827, Millipore), which was prepared at a 1:1000 concentration using Intercept blocking buffer as a diluent and adding 100 µL/well. The cells were then incubated with the primary antibody overnight at 4°C with gentle agitation.

On the following day, the primary antibody was tipped off, and the cells were washed three times with 100 µL/well of DPBS. The secondary antibody used for this assay was Goat anti-mouse IgG1 647 Alexa Flour-conjugated antibody, as well as Hoechst 33342 (Invitrogen) to stain for nuclei, which were both prepared at 1:1000 concentration using Intercept blocking buffer as a diluent. The secondary antibody solution was added to the cells at 100 µL/ well and left for 1 hour at room temperature. The plates were then washed three times with 100 µL/well of DPBS, before being left in 100 µL/well DPBS at 4°C until high-content imaging using the Operetta (Perkin Elmer). Images were typically taken using the 20X water objective, with 9 fields of view per well, and a Z-stack of 5-7 slices. The images were analysed using Perkin Elmer software Harmony (*more details in 2.4.8*); the final readouts were “T49 inclusion count normalized to the total nuclei count” and “live nuclei count” (determined by a nuclei area threshold). Data was plotted in GraphPad.

2.3 Microfluidic Xona Assay

2.3.1 Plasma bonding of MFDs to glass-bottom plates

The 6-well glass-bottom plates (#P061.5HN, CellVis) and the Xona microfluidic devices (#SND450, Xona) were plasma bonded using the plasma cleaning oven (Henniker, HPT-200) using the following settings: 45 seconds at 50% power, gas flow (air) set at 7 sccm.

Devices were inserted in the 6-well plates using a 3D printed holder (*Fig 2.4*) in order to position them roughly at the same position in each well.



Figure 2.4: 3D printed holder. *It is attached at the bottom of the plate making it more stable. The inner black squares delimit the area in which the microfluidic devices should be attached, thereby improving the consistency between wells; this is important for the high-content imaging systems. In collaboration with Brendan Hampshire.*

2.3.2 Poly-D-Lysine coating of Xona MFDs

A PDL solution was prepared at 0.5 mg/mL using sterile DPBS (#P6407-5MG, Sigma) and 100 µL of solution was added in all the chambers and kept for 90 minutes at 37°C. The solution was aspirated,

and the devices were washed 3 times with 150 µL of DPBS that was let flow from the left chambers into the channels. Subsequently 150 µL of RCN media was added to each chamber and plates were kept in the incubator until cellular suspension from the embryos dissociation was made.

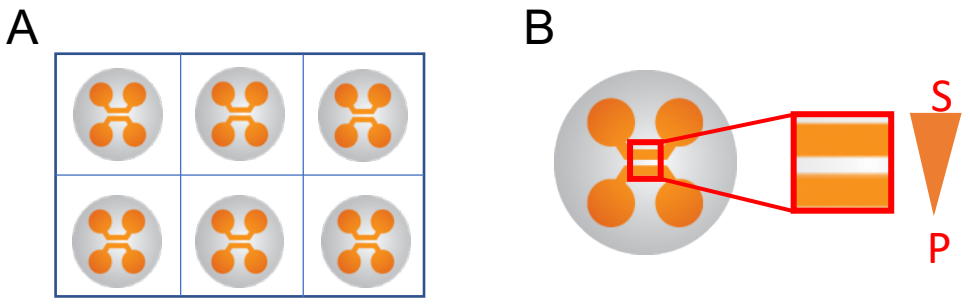
2.3.3 Plating Rat Cortical Neurons in Xona MFDs

Primary rat cortical neuronal cultures were prepared from EC18 embryos from time-mated CD rats. The dissociated neurons were spun and resuspended in order to have a density of 40000 cells/µL and plated in Xona 2-compartment (SND450) silicon devices, pipetting in each channel 20 µL of cellular suspension. Plates were then put in the incubator for 10 minutes to let cells adhere before adding 150 µL of RCN media in each chamber. Plates were sealed with membrane Breath Easy.

2.3.4 Treating neurons in Xona MFDs

Neurons were washed at DIV3 to remove the dead cells that had not adhered during cell plating. These devices are composed by two different compartments, a top one also called “seeding” side and a bottom one defined “propagation” side. This definition is related to the treatments that neurons undergo, in fact, at DIV7 the media in the chambers was completely aspirated and cells in the seeding side (*Fig 2.5*) were seeded with the appropriate amount of hAD seed and cells in the propagation side were treated with the specific treatment (compound or antibody). In order to fluidically isolate the two compartments, a gradient of media was created between the two

channels adding 80 µL of hAD seed (18 nM) at the seeding side and 200 µL of antibody (100 µg/mL) or compound (10 µM) at the propagation side. At DIV10 and 17 the media was completely aspirated and replenished with media only at the seeding side (80 µL) and with the treatment at the propagation side (200 µL). at DIV 21 cells were fixed removing all the media from the chambers and adding 100 µL in each chamber of ice-cold methanol; plates were kept at -20°C for 15 minutes to allow fixation. Subsequently 3 washes with DPBS were performed adding 150 µL of DPBS only in the left chambers and letting the DPBS flow and wash the channels. Plates were then kept at 4°C until ICC was performed.



*F**igure 2.5: Microfluidic plate set up.** Schematic of a 6-well plate set up (A) where each well contains a microfluidic unit. The area of biological interest in a typical two-compartment microfluidic device is highlighted within the red box (B). Each device is composed by a Seeding side (S) where neurons are seeded at DIV7 and a Propagation side (P) where aggregates formed in the Seeding side can propagate and induce endogenous aggregation. A hydrostatic gradient is maintained using different media volumes in the two sides in order to fluidically isolate them. More specifically, the propagation side received almost 2-fold higher media volume compared to the seeded side.*

2.3.5 Immunocytochemistry and imaging

The immunocytochemistry protocol was done as described in 2.2.3 with the only difference being how cells were washed. In this case the DPBS was aspirated and the devices were washed 3 times with 150 µL of DPBS that was let flow from the left chambers into the channels. Moreover, the imaging was performed using the Opera Phenix (Perkin Elmer), a more advanced high content imaging system than the Operetta. In particular, a total of 153 image fields were captured using a 3% field overlap using 10 Z-stacks of 20X AIR objective.

2.3.6 Image analysis of Xona MFDs

Once the images were acquired with the Opera Phenix, Harmony Software was used to quantify the number of T49 positive aggregates and to count the number of total and live nuclei. First, stacks of each image were maximum projected and filtered using the sliding parabola feature to smoothen the background and get rid of the fluorescent noise (*Fig 3.13*). Subsequently, machine learning was used to define two areas, (tau positive area and the background area) and then, within the positive area, the software was trained to identify the T49 positive threads. Total and live nuclei (area threshold at 50 μm^2) were also detected and analyzed. At the end of the analysis results were exported in an Excel file divided by object (total nuclei, thresholded nuclei, T49 positive aggregates) and well.

Harmony Software recognizes the whole image area as region of interest (ROI) and is not able to detect and separate the seeding and propagation side. In order to do that we have developed a Java software called Cell Counter. This program can display the objects

identified in Harmony (nuclei and threads) using the x-y coordinates in a simple x-y plot that can be used to manually define by the user the “top” and “bottom” areas also known as “seeding” and “propagation” sides (*Fig 3.13*). In these areas the software can count the objects and produce an Excel file that contains all the information stratified by well position, treatment condition and location for further analysis.

2.3.7 Xona MFDs assay: characterization of tau aggregates released in the propagation side

In order to characterize released tau by the neurons plated in the MFDs, an experiment was set up as described: seven 6-well bottom-glass plates were plasma bonded with Xona devices for a total of 42 devices. At DIV0 RCNs were plated with a density of 40000 cells/µL and plated in Xona 2-compartment (SND450) silicon devices pipetting only in the seeding side 20 µL of cellular suspension. Plates were then put in the incubator for 10 minutes to let cells adhere before adding 150 µL of RCN media in each chamber.

Neurons were washed at DIV3 to remove the dead cells that had not adhered during cell plating. At DIV7 the media in the chambers was completely aspirated and replenished: cells in the seeding side were seeded with 80 µL of hAD seed (18 nM) at the seeding side. 200 µL of RCNs media was added at the propagation side in order to fluidically isolate the two compartments. At DIV10 and 17 the media was completely aspirated and replenished maintaining the gradient. Each time the media was replenished, the media from the propagation side was collected, supplemented with protease inhibitor (Complete Mini

Protease Inhibitor Cocktail Tablet (#11836153001, Roche)) and snap-frozen before being stored at -80°C. At DIV 21 media was collected and cells were fixed removing all the media from the chambers and adding 100 µL in each chamber of ice-cold methanol; plates were kept at -20°C for 15 minutes to allow fixation. Subsequently 3 washes with DPBS were performed adding 150 µL of DPBS only in the left chambers and letting the DPBS flow and wash the channels. Plates were then kept at 4°C until ICC was performed.

In order to sarkosyl extract tau that was released in the media, all the aliquots of media from DIV10,17 and 21 were pulled together and supplemented with a suitable volume of 30% sarkosyl to produce a final concentration of 1% sarkosyl (#61747, Sigma), and incubated for 1 hour at room temperature with agitation. Samples were then centrifuged for 60 minutes at 100,000 RCF at 4°C in an Optima TLX 55 ultracentrifuge. Pellets were washed twice with 0.5 ml RIPA buffer (#R0278, Sigma), centrifuged for 5 mins at 13,000 RCF and then resuspended at 1/10th of the original sample volume in a solution of 50 mM Tris pH7.4 supplemented with Complete tablet (Roche) and 1 mM PMSF. The resuspended pellets were then sonicated with approximately twenty 1-second pulses, at 40% amplitude, until completely dispersed, and frozen at -80°C.

For Western Blotting, the samples were prepared with 4x SDS NuPAGE Sample Buffer containing 5% β-mercaptoethanol, and heated to 95ºC for 10 minutes. The denatured samples were then run in Novex™ 8-16% Tris-Glycine Plus Midi Gels (Invitrogen,

Cat#WXP81612BOX), at 200V, using 1x Novex™ Tris-Glycine SDS Running Buffer (10X) (Invitrogen Cat#LC26754) and BioRad Precision Plus Protein Dual Color Standards (Biorad, Cat#1610374). The separated proteins were transferred to Amersham Hybond nitrocellulose membranes using semi-dry blotting, with NuPAGE transfer buffer 2x plus 10% MeOH, at 25V for 90 minutes. Membranes were then incubated in blocking buffer (5% non-fat dried skimmed milk plus 0.05% Tween20 (Sigma) in DPBS) for 1 hour, before incubation with primary antibodies, diluted in the same blocking buffer, overnight at 4ºC with shaking. Primary antibodies used were T49 (#MABN827, Millipore) and CP27 (in-house) and the secondary antibody used was the anti-mouse IgG HRP (#7076, Cell Signalling). All membranes were incubated in West-Femto (#34094, Thermo Fisher) detection reagent. Images were acquired using ImageQuant LAS 4000 Mini.

2.3.8 Calcium imaging in Xona devices

Rat cortical neurons plated and seeded as usual (*2.3.3 and 2.3.4*) and they were kept in an incubator at 37ºC for a total of 21 days.

Cells were then washed twice with PBS and they were incubated in the dark for 1h in HBTS (Hepes buffered Tyrode solution, Gibco) with 4μM Fluo-4 AM / 0.005% Pluronic F127. The solution was then replaced with HBTS immediately before running the assay. Xona plates were imaged with the microscope Zeiss Axioscope setting the fluorescence signals recording at 2 s intervals with a 0.4 s exposure time and using as center of the image the microgrooves. For the initial experiments after the baseline record (1-2 minutes circa), 50μM KCl

was added only at the seeding side and for the second set of experiments 10μM Gabazine was added after the baseline only at the seeding side.

Using a customized software (Cell Profiler) cells were detected as ROI and florescence was analysed for each region. Successively the analysis was run separating the seeding and propagation sides. Data were then plotted in Graphpad Prism.

2.4 High Throughput (HT) microfluidic assay

2.4.1 Plasma bonding of HT devices on glass surfaces

HT devices are made by Michele Zagnoni at Strathclyde University using PDMS and a 96-well-like mask that allows to make a plate with 8 microfluidic units. These devices were plasma bonded on large cover glasses (thickness 0.15 mm) (#260462, Tedpella) made of an optical grade borosilicate glass using oxygen in the plasma cleaning oven (Henniker, HPT-200) with the following settings: 60 seconds, oxygen flow set at 4 sccm and power at 30%. After 10 minutes from the bonding, devices were coated with Poly-Ornithine at 0.01 mg/ml (Sigma, P4957). All the wells (making sure that evaporation in the microgrooves does not occur) were aspirated and 50 µL of coating solution was injected and let flow from the left chambers into the channels (*Fig 2.6*), before filling up the right wells. Devices were left to incubate in the hood with the coating solution for 90 minutes. Coating solution was washed out 3 times with sterile media, by emptying and refilling the device wells as previously done. Coated devices were stored in an incubator until ready for cell plating.

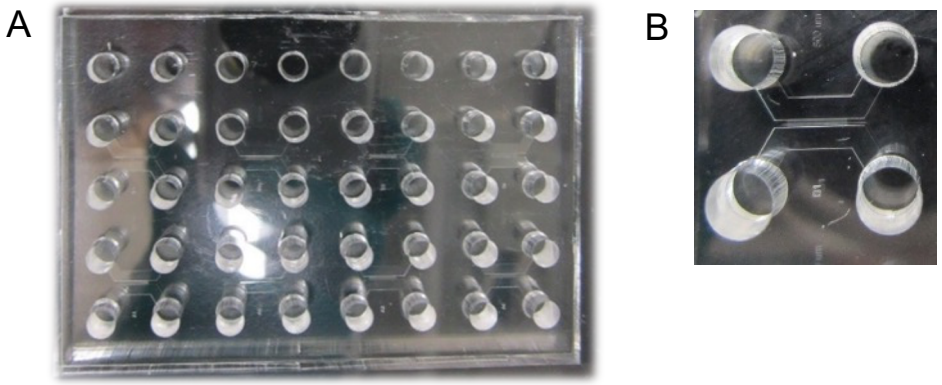


Figure 2.6: HT microfluidic devices: *HT devices are made of PDMS and composed by 8 microfluidic units (A). Each unit is structured as the Xona devices and it is composed by a Seeding side (top channel) and a Propagation side (bottom channel) (B).*

2.4.2 Plating Rat Cortical Neurons in HT devices

Primary rat cortical neuronal cultures were prepared from EC18 embryos from time-mated CD rats. The dissociated neurons were spun and resuspended in order to have a density of 25000 cells/µL and plated in HT devices pipetting in each channel 5 µL of cellular suspension. Plates were then put in the incubator for 10 minutes to let cells adhere before adding 50 µL of RCN media in each chamber.

2.4.3 Treating neurons in HT devices

The treatment protocol used for HT plates is the same of Xona devices with the only difference of the volumes used. In order to fluidically isolate the two compartments a gradient of media was created between the two channels adding 30 µL of hAD seed (18 nM) at the seeding side and 60 µL of antibody (100 µg/ml) or compound (10 µM) at the propagation side. When cells are fixed, 60 µL of DPBS was used to wash and 50 µL of ice-cold methanol to fix them.

2.4.4 Immunocytochemistry, imaging and image analysis

The immunofluorescence protocol used for HT plates is the same of the Xona devices (*2.3.5*) but in this case an aluminium insert was made and used to adapt the HT plate in the Opera Phenix plate reader. In fact, because the plate is 96-well like, this insert can be used to fit 2 plates in a “96-well shaped” plate (*Fig 2.7*). The images were then acquired with both 20X AIR objective, N/A 0.8 µM, and 40x water objective 10 z planes, and 2 fluorescent channels (Hoechst, Alexa 647) using a 3% field overlap using 10 Z-stacks. Once the images were acquired with the Opera Phenix, Harmony Software and Cell counter were used to quantify the number of T49 positive aggregates and to count the number of total and live nuclei in both seeding and propagation sides (more details *2.3.6*).

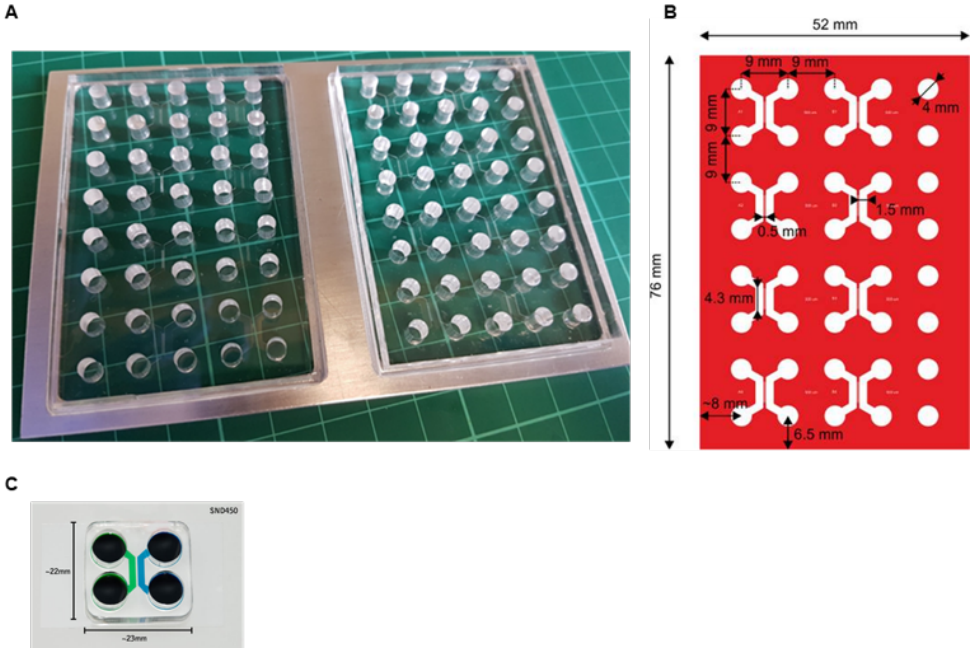


Figure 2.7: Microfluidic platform devices for enabling transformation of microfluidic assay model to a higher throughput assay format by increasing the number of experimental replicates*. The higher throughput platform microfluidic devices (A) have significantly smaller dimensions (B) when compared to the commercially available devices from Xona (C). In particular, the new plate can accommodate two smaller devices that contain 8 units each so the throughput of the MFD assay went from 6-unit/plate to 16-unit/plate.*

2.5 Humanized High Throughput microfluidic assay

2.5.1 Genotyping

In order to separate Tau +ve and -ve embryos, tails from embryos were genotyped using REDExtract-N-Amp-Tissue PCR Kit (Sigma, XNAT-100RXN) (*Fig 2.8*).

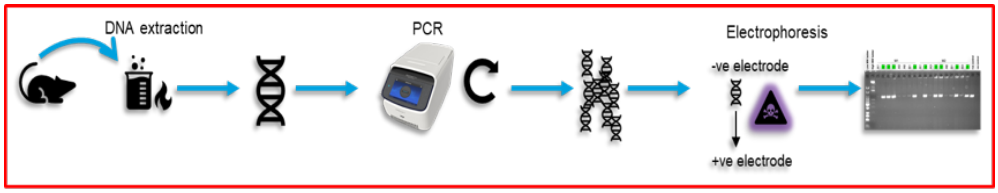


Figure 2.8: Schematic of the Genotyping protocol*. Genomic DNA is extracted from embryo tails using a specific kit. PCR is performed in order to amplify the number of hTau gene copies. Gel electrophoresis is run with EtBr in order to visualise the amplification bands.*

The genes that we looked at were human Tau and a mouse house-keeping gene as a positive control of the PCR protocol. Tails were kept in Hybernate buffer until the extraction was performed.

DNA extraction was performed following the supplier instructions: 100 µL of Extraction Solution was pipetted into a microcentrifuge tube and 25 µL of Tissue Preparation Solution was added to the tube and mixed pipetting up and down.

Using forceps rinsed in 70% ethanol, 0.5-1 cm piece of mouse tail tip (cut end down) was placed into the solution and mixed thoroughly by vortexing. Samples were incubated at room temperature for 10 minutes followed by 3 minutes at 95°C. 100 µL of Neutralization Solution B were added to sample and mixed by vortexing.

The REDExtract-N-Amp PCR Reaction Mix contains JumpStart Taq antibody for specific hot start amplification. Therefore, PCR reactions can be assembled at room temperature without premature Taq DNA polymerase activity.

The following reagents were added to a thin-walled PCR microcentrifuge tube for a final volume of 20 µL/tube (*Tab 2.1)*:

Reagent	**Volume for 1 reaction**
Water RNA free	2 µL
REDExtract-N-Amp PCR Reaction Mix	10 µL
Primer mix (2uM stock)	4 µL
Tissue extract	4 µL
Total	20 µL

Table 2.1: PCR Reagents.

To prepare the Primer mix, 2 µL of each primer (*Tab 2.2*) were added (100 µM starting concentration) in a final volume of 100 µL of water.

Gene target	Forward primer	Reverse primer
Human Tau	GCGGCCAACTGTTAGAGAG	CTGTGCATGGCTGTCCACTAACCTT
Mouse housekeeping gene	GAGACTCTGGCTACTCATCC	CCTTCAGCAAGAGCTGGGGAC

Table 2.2: PCR primers.

Master mix was prepared and split in PCR tubes (16 µL each) and 4 µL of tissue extract were added in each tube (PCR strips single lid (Eppendorf, 11858122)).

PCR was run following these parameters (*Tab 2.3*):

Step	Temperature	Time	Cycles
Hot Start	95°C	15 minutes	1
Denaturation	94°C	45 sec	30
Annealing	60 °C	1 min	
Extension	72 °C	1 min	
Final extension	73 °C	5 minutes	1
Hold	4 °C	Indefinitely	

Table 2.3: PCR protocol.

Once the PCR was run, the amplified products were run for 20 minutes at 150 V on a precast gel (3% TBE Wide Mini ReadyAgarose Precast

Gel, 15.6 x 10 cm, 32-well, with ethidium bromide #1613036) with TBE buffer (Thermo Scientific™ 10X TBE Buffer (Tris-borate-EDTA) #10130740) using a low molecular weight DNA marker (Quick-Load® Purple Low Molecular Weight DNA Ladder (N0557S)). The gel was then checked under U.V. light.

2.5.2 hTau neurons preparation protocol

The RCN growth medium was prepared under a BSC (biosafety cabinet), in accordance with the above recipe and filter sterilised through a Corning 500 mL vacuum filtration system. 90 mL of RCN media from a previous hTau preparation was supplemented with 10 mL of Foetal Bovine Serum (Gibco, 10500-064) – once prepared, the mixture was filter sterilised through a Corning 250 mL vacuum filtration system. 10% Virkon in water was used for decontamination. A Pasteur pipette was used to transfer the cortical tissue, and the media, from the 24-well plate to sterile 15 mL Falcon tubes – brains were pooled in accordance with genotyping results (e.g. Cortex only Tau-positive, or Cortex only Tau-negative). Once the tissue had settled, a stripette was used to aspirate as much media as possible without taking up tissue. 5 mL of Trypsin/EDTA Pink (Gibco, 25300-054) was added to the tissue to wash – this was then carefully aspirated, without taking up tissue. Another 5 mL of Trypsin/EDTA Pink was added to the tissue and the Falcon tubes were incubated in water bath for 15 minutes – every 5 minutes, the Falcon tubes were gently rocked to mix the tissue and ensure complete digestion. After the 15-minute incubation, the Trypsin was aspirated from the Falcon tubes, and the tissue was washed 3x with 5 mL of FBS-supplemented RCN media. The final

wash of FBS-RCN Media was aspirated, and the tissue was washed once with 5 mL of the HBSS-DNase solution (Sigma, D4263). This wash was aspirated, and further 3 mL of HBSS-DNase was added before trituration. The tissue was then triturated in three stages of increasing resistance: first, a Pasteur pipette was used to triturate the tissue and begin dissociation of the tissue; this was then repeated with a 5 mL stripette; and finally with a 1000 µL Gilson pipette. For each condition – Tau-positive or Tau-negative – the two Falcons of tissue homogenate were pooled into a single 15 mL Falcon tube, and topped to 10 mL by adding 4 mL of the HBSS-DNase solution. The two pooled Falcon tubes were placed into a Sigma Zentrifugen 4K15 bench-top centrifuge (200g; 5 minutes; RT). After the centrifugation, the supernatant was aspirated with a 10 mL stripette, and care was taken to avoid disruption of the pelleted cells. The pellet was first resuspended in 3 mL of fresh RCN media using the 1mL Gilson pipette than topped up to 7mL. The cell suspension was filtered through a 100um filter, into a sterile falcon tube and the remaining 3mL was used to wash through the filter. In a cryovial, a 1:5 cell aliquot was taken for cell counting: 10 µL aliquot of cell suspension was mixed with 10 µL Trypan blue 0.4% (Sigma, T8154), and 30 µL of RNC media – this solution was then mixed and loaded into a disposable haemocytometer. Cell counts were acquired through a light microscope and used to determine the concentration of cell suspension required to plate at a concentration of 28000 cells/µL.

$a)$ $(Cell\ count\ in\ 4x4\ grid)x\ 5 = Cells\ x\ 10^4/mL$

$b)$ $\frac{Required\ cell\ density}{Output\ of\ (a)}\ x\ volume\ needed$
$= volume\ of\ cell\ suspension\ required\ for\ dilution$

2.5.3 Humanized HT microfluidic assay

The settings of this assay are the same of the RCN version from the plasma bonding at the analysis so for the methods refer to *paragraph 2.4*. The only difference is in the imaging protocol since the antibody used to identify the aggregates now are targeting human Tau.

2.5.4 Immunocytochemistry and imaging

The cells were blocked in Intercept Blocking Buffer (LI-COR) containing 1% Triton for one hour at room temperature. The cells were then incubated with primary antibodies (*Tab 2.4*) overnight at 4°C with gentle agitation before being washed three times with DPBS as previously described. The cells were stained with the appropriate Alexa Flour-conjugated antibodies (*Tab 2.4*) as well as Hoechst 33342 (Invitrogen) to stain for nuclei, for 1 hour at room temperature. The plates were then washed three times in DPBS, before being left in DPBS at 4°C until high-content imaging using the Opera Phenix (Perkin Elmer) using both 20X AIR objective, N/A 0.8 µm, and 40x water objective 10 z planes, and 3 fluorescent channels (Hoechst, Alexa 647, Alexa 488 or 594). The images were acquired with the Opera Phenix using a 3% field overlap using 10 Z-stacks.

Antibody	Target	Host	Supplier	Cat. number	Dilution	Purpose
CP-27	Total Tau	Mouse IgG2b	In house	-	1:1000	Primary for IF and WB
AT-8	P-Tau at Thr 205, Ser 202	Mouse IgG1	In house	-	1:1000	Primary for IF and WB
MAPT	Total Tau	Mouse	In house	-	1:1000	Primary for IF
AT-100	P-Tau at Thr 212, Ser 214	Mouse IgG1	Thermo Fisher	MN1060	1:1000	Primary for IF
T 49	Total Tau-Rodent specific	Mouse IgG1	Millipore	MABN827	1:2000	Primary for IF and WB
Vimentin	Vimentin	Chicken polyclonal	Abcam	ab24525	1:500	Primary for IF
GFAP	Glial fibrillary acidic protein	Chicken	Abcam	ab4674	1:1000	Primary for IF
ALDOC	Aldolase C antibody	Mouse IgG	Neuromics	MO22135	1:500	Primary for IF

MAP-2	Dendrites	Rabbit	Millipore	AB5622	1:1000	Primary for IF
MAP1B	Neurons	Rabbit	Thermo Fisher	PA5--78052	1:1000	Primary for IF
Alexa Fluor 594	Anti-mouse IgG1	Goat	Invitrogen	A21125	1:1000	Secondary for IF
Alexa Fluor 647	Anti-mouse IgG2b	Goat	Invitrogen	A21240	1:1000	Secondary for IF
Alexa Fluor 488	Anti-mouse IgG1	Goat	Invitrogen	A11008	1:1000	Secondary for IF
DA9	Total Tau	Mouse	Produced in-house	-	-	AlphaScreen
TG5	Total Tau	Mouse	Produced in-house	-	-	AlphaScreen

Table 2.4: Description of the antibodies used for AlphaScreen, Western Blot and Immuno-Fluorescence.

2.6 Statistical Analysis

The Opera and Operetta results were plotted using GraphPad Prism 8.3.0 (San Diego, CA, USA). Results were represented as mean +/- SEM of independent experiments. Different number of repeats depending on the experiment. More information is provided in the legend of each result. One-way ANOVA with Dunnett's *post hoc* test was used.

3.1 hAD seed preparation

3.1.1 Sarkosyl extraction of human Alzheimer's disease seed generates concentrated tau extract which can cause endogenous tau aggregation

Alzheimer's pathology is one of the most severe neurodegenerative conditions and the most common cause of chronic dementia worldwide affecting more than 35 million people, that probably will duplicate by 2030 [243]. Therefore, it is urgent and fundamental to find a treatment and to develop the most physiologically relevant model system to study the pathology development and spread.

In this work we have used hAD tau enriched seed isolated from post-mortem brains of patients confirmed to have AD to seed rat cortical neurons (RCN) and hTau [244] cortical neurons to induce endogenous tau aggregation and propagation.

Phosphorylated, pathological tau was purified via sarkosyl extraction following cycles of centrifugation and resuspension as described in *Methods 2.1*. Following the purification an AlphaScreen was performed to identify the levels of total tau in the final resuspended pellet, which is the standard hAD seed used to induce aggregation in vitro. The AlphaScreen utilizes pairs of antibodies, in this case DA9-TG5, which identifies total tau levels within the sample compared to two standards; tau monomer which provides the concentration of PHF, and PHF from which the concentration of total tau in the samples can

be interpolated (*Fig 3.1*). The concentration of total tau in the newly purified hAD seed was 298.2 µg/mL, comparable to previous preparations. Further characterization of the seeding ability of the new hAD seed (named "new' in *Fig 3.2*) was done in the already established 96-well RCN assay (as described in *Results 3.2*) compared to that of the previous seed (named "old' in *Fig 3.2*). When diluted in media both produced a concentration response curve of aggregated endogenous tau (*Fig 3.2*).

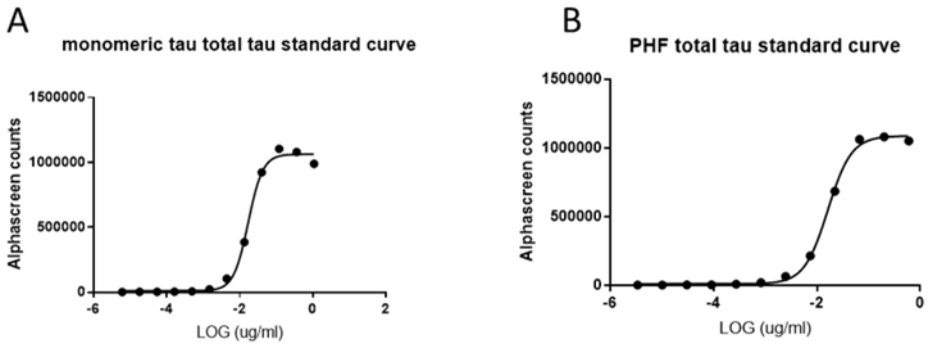


Figure 3.1: AlphaScreen standard curves from which the concentration of total tau can be interpolated. *Dilution curves were generated for monomeric tau, paired helical filament (PHF) aggregated tau and the sample which in this case was human derived, aggregated tau. These were incubated with guanidine used to disaggregate tau to get an accurate read of the concentration or DPBS before overnight incubation with antibodies and subsequently donor streptavidin before reading the plate. (A) Monomeric dilution curve of AlphaScreen counts against the log of the concentration, from this graph the concentration of PHF used is interpolated. (B) PHF standard curve shown in the form of AlphaScreen counts per concentration as determined from the monomer interpolation. Data was plotted in GraphPad.*

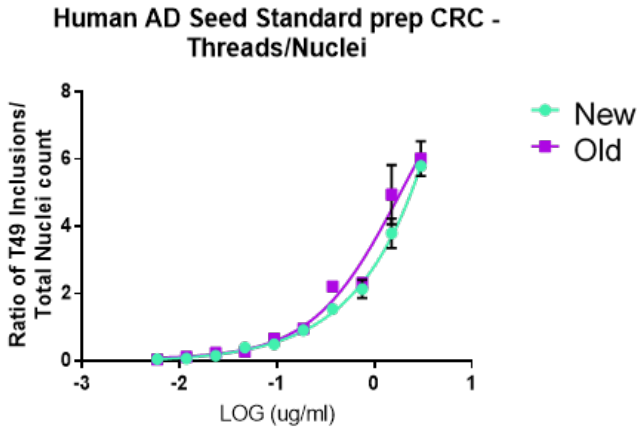


Figure 3.2: Comparison of seeding between the new Alzheimer's disease derived seed and previous preparation of seed. *Graph shows the number of T49 inclusions normalized to nuclei versus the log of concentration of seed added. Both New (purple) and Old seed (turquoise) show a similar pattern with increasing ratio as the amount of seed added increases. Data represents average of 2 replicates, plotted in GraphPad showing mean +/- SEM.*

3.1.2 Sarkosyl extracted human AD seed recruits rodent Tau to form insoluble aggregates

In the present study, we were able to replicate methods previously described [245], of sarkosyl extraction to prepare seeding-competent material extracted from human (h) AD brains (*Fig 3.3*). The hAD seed preparation previously quantified and characterized via AlphaScreen, was used to seed primary non-Tg RCNs at DIV7 that, at DIV21, were lysed and sarkosyl extracted in order to isolate insoluble tau.

Western blot (WB) analysis of the sarkosyl-extracted samples demonstrates that, when added to primary RCNs, the hAD seed recruits endogenous rodent tau and induces its aggregation as shown using the rodent specific antibody, T49 (*Fig.3.3, A*). Moreover, these

aggregates are not only T49 positive but also AT-8 positive (*Fig 3.3, B*) confirming their phosphorylation.

We have analysed 3R and 4R tau expression in a time course in RCN (*Fig 3.3, C*). To identify 3 and 4 R isoforms we used the tau protein ladder (rPeptide, t-1007-2) that contains all 6 tau isoforms. The expression of 3R and 4R Tau increased over time (mostly 0N3R and 1N3R as well as 0N4R and at a low level 1N4R), peaking at DIV15 and then start to decline. We hypothesise that the endogenous aggregates that would template from hAD seed (starting from DIV7) will contain both 3R and 4R Tau.

In summary, hAD seed extracted from AD patient brains can act as template for the misfolding of native tau that forms insoluble aggregates T49 and AT-8 positive consistent with findings in mouse cortical neurons [125].

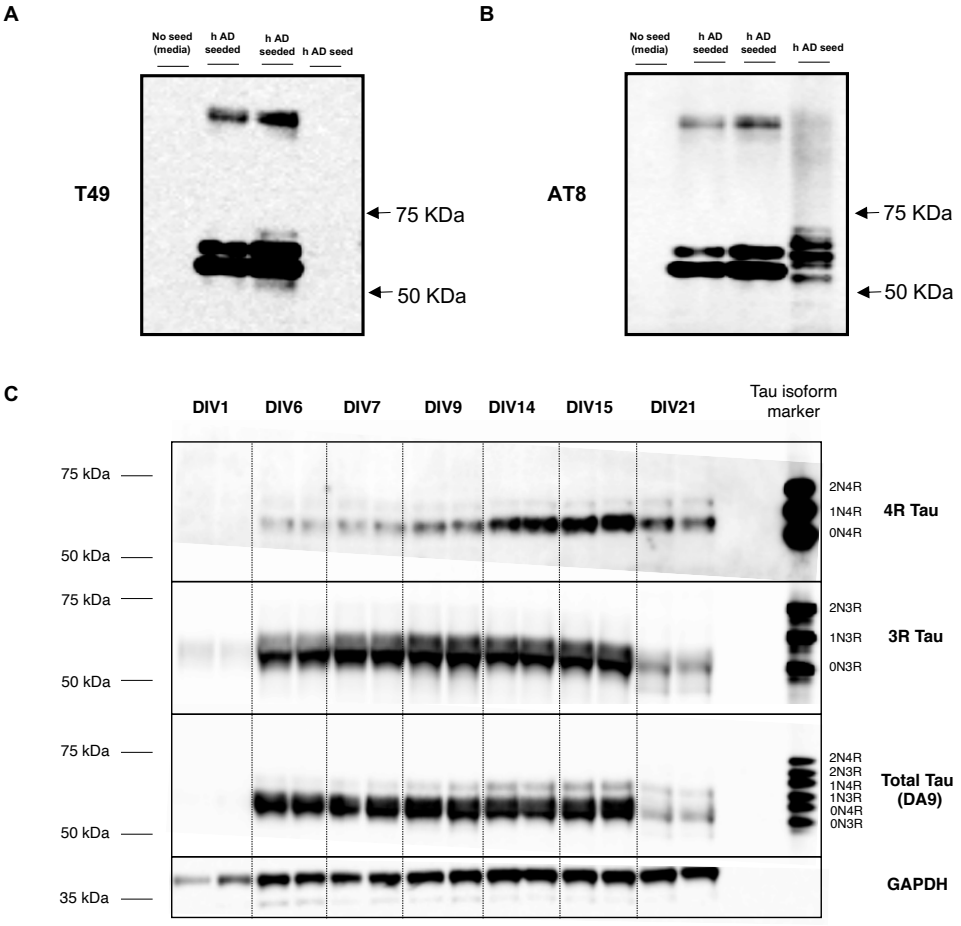


Figure 3.3: Purified hAD seed recruits rodent tau to form AT8 insoluble aggregates in RCN neurons that express both 3 and 4R tau. *Western blot of sarkosyl extracted material from RCNs treated with h AD seeds (from 2 separate seeding extractions) and probed with rodent specific antibody, T49 (A) or pS202/205 Tau, AT8 (B). Western blot experiments show that total tau expression, as well as 3R tau expression, increases after a week and stays stable until it decreases at DIV21. 4R tau expression increases over time and peaks at DIV15 before it starts decreasing. These results show that at the time of seeding (DIV7) both 3 and 4R tau isoforms are expressed by RCN (C).*

3.2 RCN Tau aggregation assay

3.2.1 RCNs assay characterization: seeding neurons with hAD seed

Primary rat cortical neurons were plated in 96-well plates at 40,000 cells/well in 100 µL of media. Cells were kept in culture for a week and, at DIV7, neurons were seeded with different concentrations of hAD seed starting from 3 µg/mL (72 nM) following an 8-point concentration curve, 1:3 dilutions. Each dose was repeated 6 times in the plate. After a media change at DIV14, cells were methanol fixed at DIV21 and ICC and image analysis were performed as previously described in methods (*Methods, 2.2.3*). We have also demonstrated that methanol fixation is crucial in order to wash away soluble proteins and to visualize only aggregated tau as shown in *Fig 3.4*.

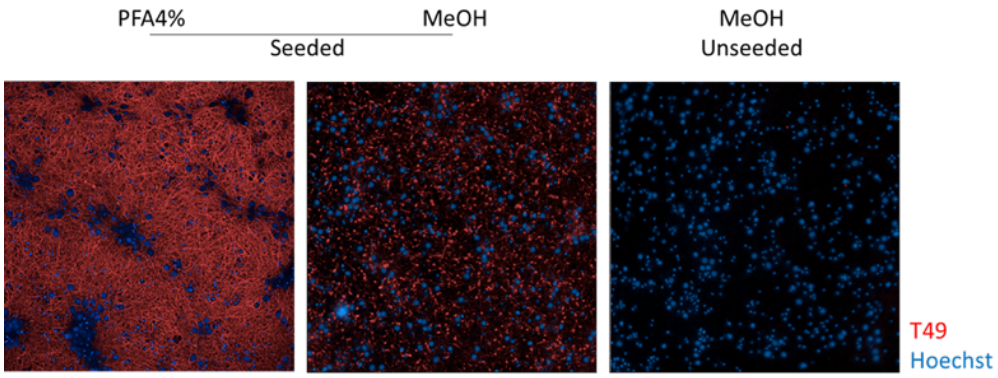


Figure 3.4: Importance of MeOH fixation method*. RCN were treated with hAD seed in DIV7 and fixed at DIV21 with either PFA 4% or iced cold MeOH before staining with T49 (rodent total tau antibody) and Hoechst.*

We can observe in *Fig 3.5* a dose dependent increase of T49 positive aggregates that, at the highest dose induces cell toxicity; for this reason, the 3 µg/mL (72nM) data point was excluded from the GraphPad plot in order to run a more accurate analysis.
Since we stained with T49 antibody, which is specific for rodent tau, we could exclude that the effect was due to the hAD seed added at DIV7.
The analysis software computed the EC80 as 0.75 µg/mL (18 nM) of hAD seed and, since there was no cell toxicity and we could observe a good aggregate formation, we decided to use this concentration in our subsequent experiments.

In conclusion, similarly to the western blot results (*Results 3.1.2*), we can see that the h AD seed can seed the neurons and induce neuritic thread-like inclusions that are positive for T49 antibody consistent with findings in mouse cultures [125].

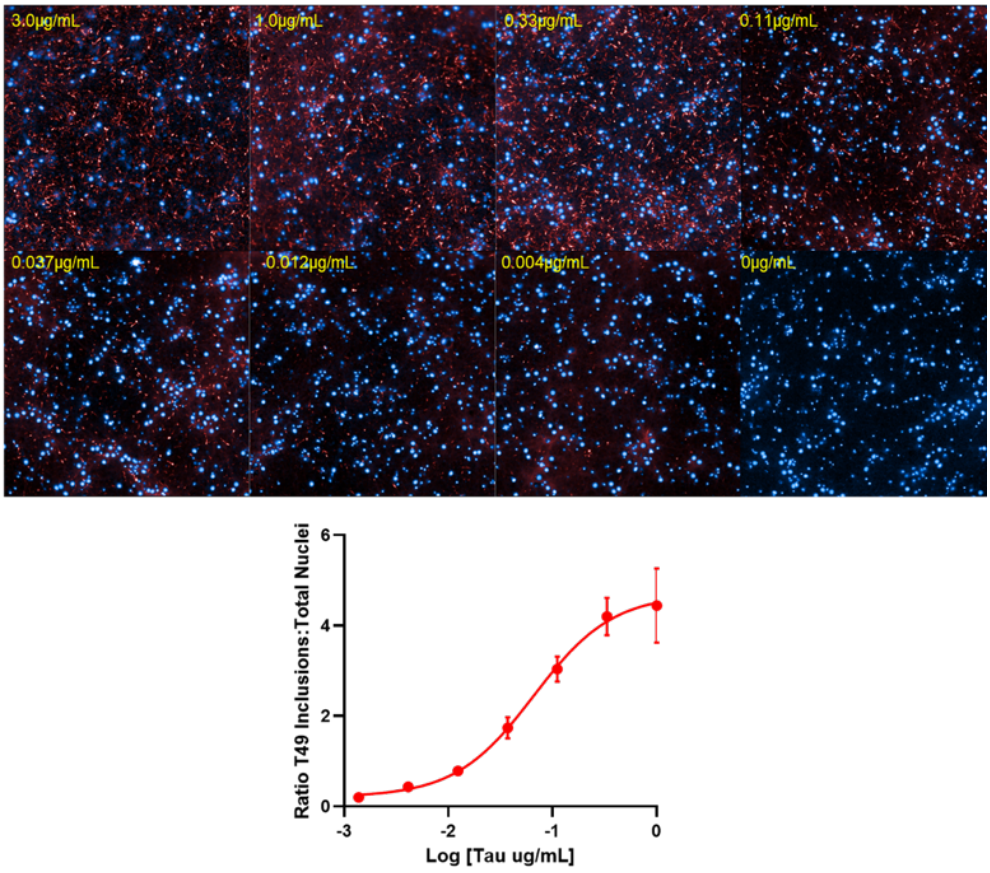


Figure 3.5: h AD seed concentration response curve in RCNs in a 96-well assay format. *High content imaging reveals a concentration-dependent increase in the number of T49-positive neuritic thread-like inclusions resulting from addition of increasing concentrations of h AD seed. Image acquisition with Operetta, 8 replicates for each condition.*

3.2.2 RCN assay characterization: the effect of hAD seed on endogenous rodent tau

After having determined the optimal concentration of hAD seed to use in this cell model, we wanted to demonstrate how hAD seed could induce endogenous tau aggregation over time.

For this experiment RCNs were plated in 4 x 96-well plates at 40,000 cells/well in 100 µL of media; one plate for each time point (DIV7, DIV10, DIV14 and DIV21). Cells were kept in culture for a week and at DIV7 neurons were seeded with 18 nM of hAD seed or with 2.4nM of hAD seed as quality control (QC). Plates were fixed for every time point as previously described in Methods (*Methods 2.2.2*) and T49/Hoechst ICC was performed.

As we can see from *Fig 3.6* there is a time dependent increase of T49 inclusions from DIV7 to DIV21.

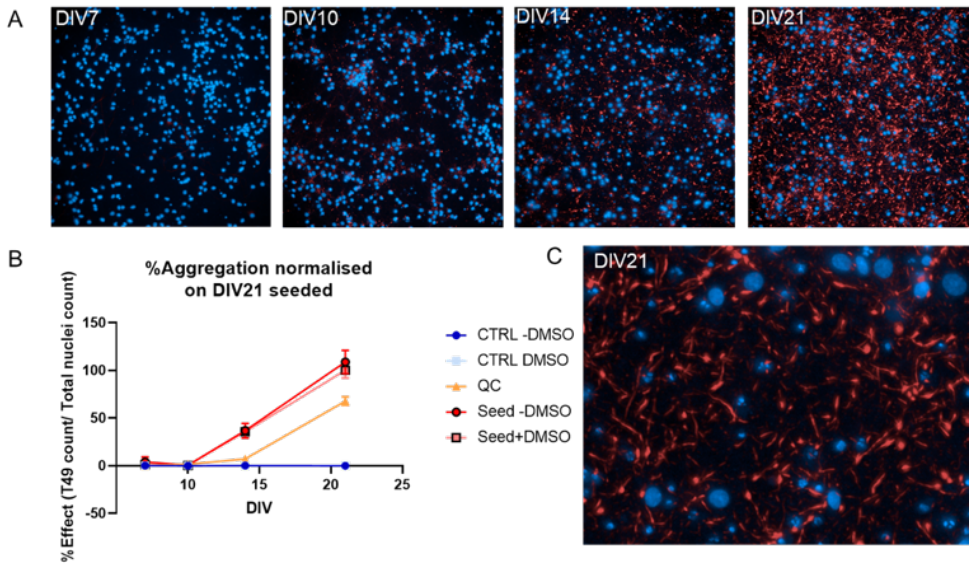


Figure 3.6: Aggregation course in RCNs in a 96-well assay format. *High content imaging shows how aggregates form over time (A). The percentage of effect expressed as T49 positive aggregates normalised to total nuclei count has been normalised to the number of aggregates at DIV21. CTRL condition is unseeded, and QC (quality control) is 2.4nM seed that we use as an internal control (B). T49 positive aggregates have a neuritic thread-like morphology at DIV21 (C).*

For the first few days the aggregation is slow, possibly because the hAD seed requires time to enter the neurons and template the endogenous tau, but then the aggregation increases exponentially (*Fig 3.6 B*). At DIV21 we can observe T49 positive, thread-like inclusions that cover most of the well area that are very similar to the threads observed previously [125].

3.2.3 RCN tau aggregation assay: effect of Anle138b on tau aggregation

Having determined the effectiveness of hAD tau seed on RCNs and the timeline to run this assay, we decided to test a small molecule inhibitor to prove the importance of this assay for performing small molecule screening.

The molecule that we decided to test is the di-phenyl-pyrazole Anle138b that has been previously reported to inhibit protein aggregation in *in vitro* and *in vivo* systems [231].

Following the previously described protocol, at DIV7 RCNs were seeded and treated with a concentration response curve (CRC) of Anle138b starting from 30 µM (0.3 %DMSO). At DIV14 a half media change was performed, and the compound was replenished. Each concentration had 5 repeats.

As we can observe from *Fig 3.7*, there is a dose dependent effect of Anle138b to reduce the number of neuritic thread-like aggregates after h AD seeding.

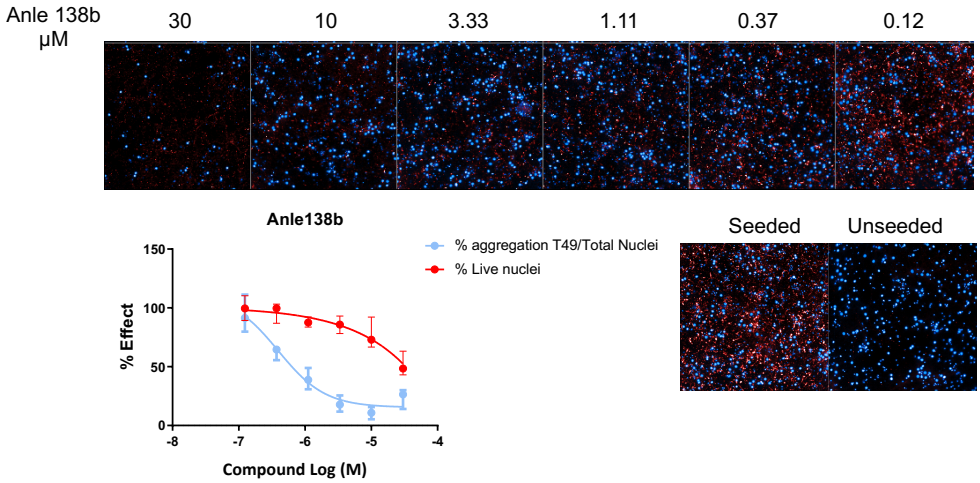


Figure 3.7: Anle138b effect on tau aggregation in a 96-well assay format. *High content imaging reveals a concentration-dependent decrease in the number of T49-positive neuritic thread-like inclusions resulting from the treatment with increasing concentrations of Anle138b. This compound, despite being very effective in decreasing tau aggregation, is also toxic at high concentrations as we can observe from the count of live nuclei. Image acquisition with Operetta, 5 replicates for each condition.*

Even though this compound is very potent (IC50= 1.99E-05 M), it's also toxic at 30 µM, so the concentration that demonstrated the best inhibitory effect and no cytotoxicity was 10 µM despite a small effect on cell viability.

3.3 Xona microfluidic devices, RCN tau propagation assay

The aim of this work was to develop, based on the RCN aggregation assay previously described a propagation assay that could be used not only to study tau propagation but also to test compounds that could inhibit the seeding ability of propagated tau.

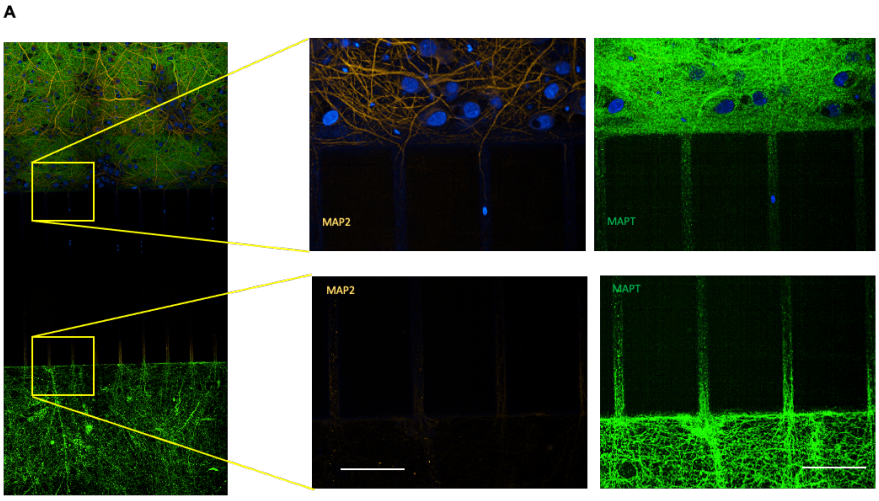
3.3.1 Using microfluidic devices to study propagation of h AD templated rodent Tau

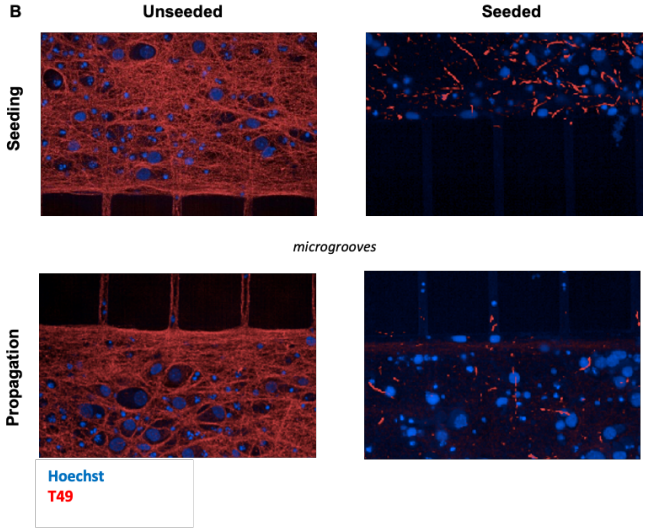
We started using commercial two-compartment microfluidic devices that have been previously used as an *in vitro* model system to study propagation of insoluble protein aggregates [207,246]. This platform allows the separation of two cellular population not only physically by microgrooves barriers but also fluidically using a media gradient between the two compartments. This ensures that the eventual transmission of aggregates is due to cellular mechanisms and not passive diffusion. Due to the dimensions of the microgrooves of 3 μm height and 450 μm length, only axons can pass into the microgrooves. As confirmed in our optimisation process staining RCNs for MAPT, a total tau antibody that stains both axons and dendrites, and MAP2, that stains only dendrites (*Fig 3.8 A*). For our experimental set up we have optimised the use of Xona polydimethylsiloxane (PDSM)-made 2 compartment microfluidic devices that were plasma bonded on glass surface wells of 6-well imaging plates (*Fig 2.5*). Since this assay recapitulates the 96-well assay, we assessed the health and morphology of primary non-Tg RCNs over three weeks and they demonstrated healthy neuronal morphology and network connectivity over time (*Fig 3.8 C*).

Once we demonstrated that the neurons were healthy, we experimented if this platform could actually reflect tau propagation after seeding with hAD seed.

As described in *Methods*, the seeding compartment of Xona devices were seeded with 18 nM of hAD seed as established with the 96-well assay and cells were kept in culture for a total of 21 days before being fixed with methanol to remove soluble proteins and imaged with an Opera Phenix.

Fig 3.8 B shows that when RCNs were not seeded T49 signal was diffuse and stained the whole cytoskeleton of neurons, but when hAD seed was added it was possible to detect, both in the seeding and propagation sides, endogenous neuritic thread-like inclusions very similar to the ones we observed both in the 96-well assay and previously [125].


A
MAP2
MAPT
MAP2
MAPT


B
Unseeded
Seeded
Seeding
microgrooves
Propagation
Hoechst
T49

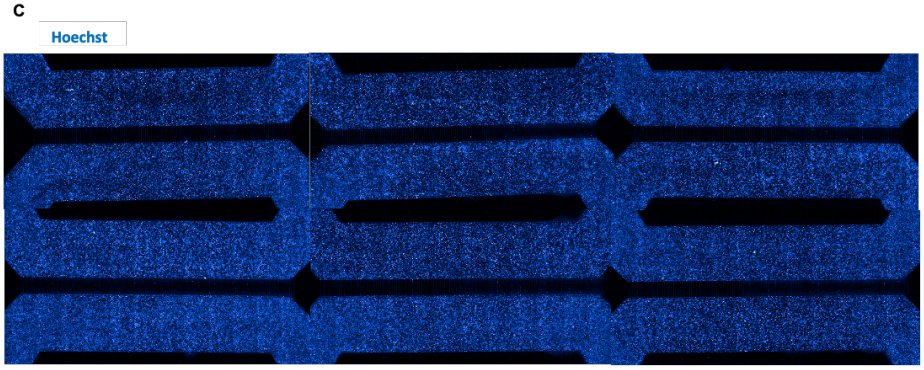

C
Hoechst

Figure 3.8: RCNs were cultured in two-compartment microfluidic devices in a 6-well plate assay format to study trans neuronal aggregated tau. *Immunocytochemistry demonstrated that in RCNs cultured for three weeks in two-compartment microfluidic devices only the axons (MAPT) can grow through the 450 µm long microgrooves rather than the dendrites (MAP2). Bar, 50 µm (A). RCNs cultured in 2-compartment microfluidic devices template the hAD seed and propagate. The control unseeded neurons represent a diffuse T49 staining whereas in the presence of the hAD seed the neurons demonstrate neuritic thread-like inclusion morphology. The results have been reproduced in two independent experiments (B). Mosaic of the 6 single microfluidic units composing the 6-well plate used to culture RCN (C).*

For the first time we have demonstrated that non-Tg RCN can be seeded with hAD seed and that the endogenous aggregates can propagate through axons and induce pathology in another, physically separated cell culture. We have also demonstrated that the characteristic neuritic thread-like aggregates are mostly axonal and somatic since they do not co-localise with MAP2. We tried different cytoskeleton and specific axonal markers such as B-III Tubulin, MAP1B and Neurofilament H but, possibly because of MeOH fixation and the age of the neurons when they are fixed, the staining was not optimal; nevertheless, we could see co-localisation of T49 aggregates with MAP1B (*Fig 3.9*).

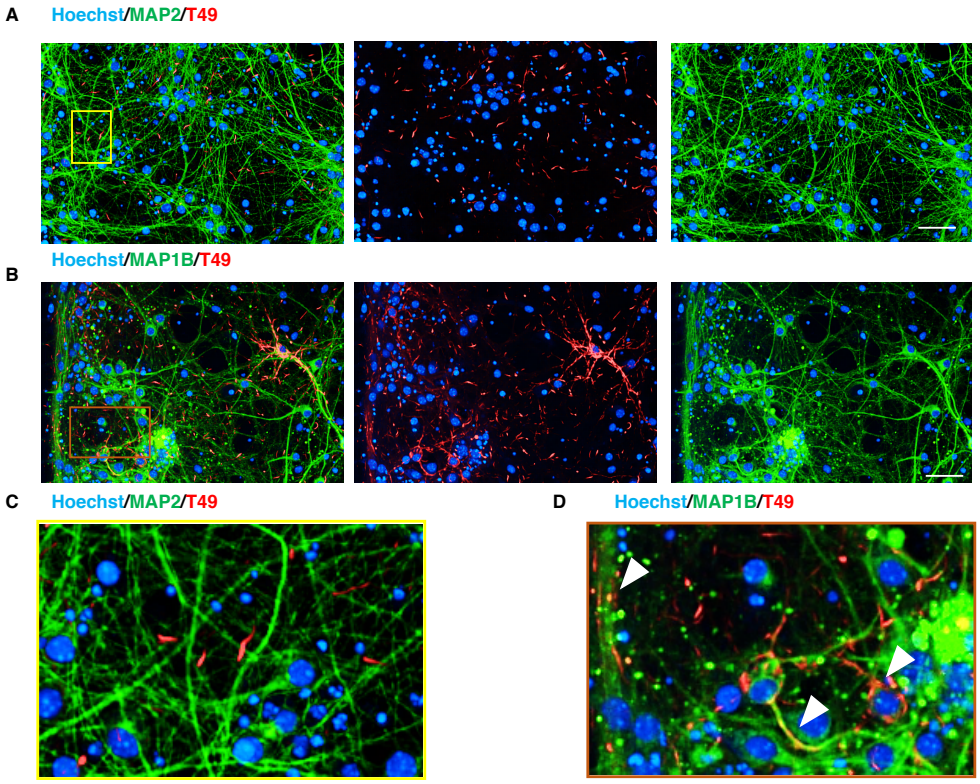


Figure 3.9: T49 positive inclusions are localised in the axons and soma of RCNs *Sparce co-localisation between the T49 neuritic thread-like inclusions in RCNs and MAP2, a specific dendritic marker (A and zoomed image in C), but good co-localisation with MAP1B, a neuronal cytoskeleton marker (B and zoomed image in D), indicating that the inclusions observed after seeding with hAD seed are not dendritic but somatic and axonal. Arrow heads in the bottom panel indicate co- localisation between MAP1B and T49. Image acquired with Opera Phenix and 20x Objective. Bar, 50 µm (D).*

3.3.2 Propagation of endogenously aggregated rodent tau is a real effect and not a device artefact.

We have demonstrated that seeding RCN with hAD seed induced tau propagation and endogenous aggregation in the propagation compartment. To demonstrate that this is a real effect and not a device artefact, we have used Xona 3-chamber devices. Indeed, since cells in the 2-chamber devices are plated in the seeding and propagation sides at the same time at DIV0, we could hypothesize that axons from the propagation side can take up the seed from the seeding side and, consequently, that the aggregation in the propagation compartment is not principally due to endogenous aggregation and propagation of tau in the seeding side.

The 3-chamber Xona devices are made with PDSM exactly as the 2-chamber units and allow 3 cell populations to be physically and fluidically separated when a gradient of media is applied. To demonstrate that the appearance of tau aggregates is really due to propagation, RCNs were plated at DIV0 either in all the 3 compartments or only in C1 and C3 with no cell population in the middle chamber C2 (*Fig 3.10*).

At DIV7 cells in C1 were seeded with 18 nM of hAD seed and a media gradient was made in order to contain the seed only in C1. Exactly as described for the 2-chambers, at DIV21 cells were fixed and imaged as in the 2-compartment devices.

As described in Fig *3.10 A*, when RCNs in C1 are seeded, their endogenous tau can aggregate and propagate in C3 via C2 neurons that, with their synapses, link C1 and C3 populations. However, when in C2 there are no neurons (*Fig 3.10 B*), C1 and C3 are not synaptically connected so the tau released in C2 cannot be taken up from C3 axons. Therefore, it cannot induce any aggregation as we can see from the lack of T49 inclusions in C3, suggesting indeed that there is no axonal growth overlap between the two neuronal populations.

We can then conclude that the propagation observed in the 2-chamber devices is real and that it is due to a cellular mechanism that requires well-formed synapses and neuronal populations synaptically connected.

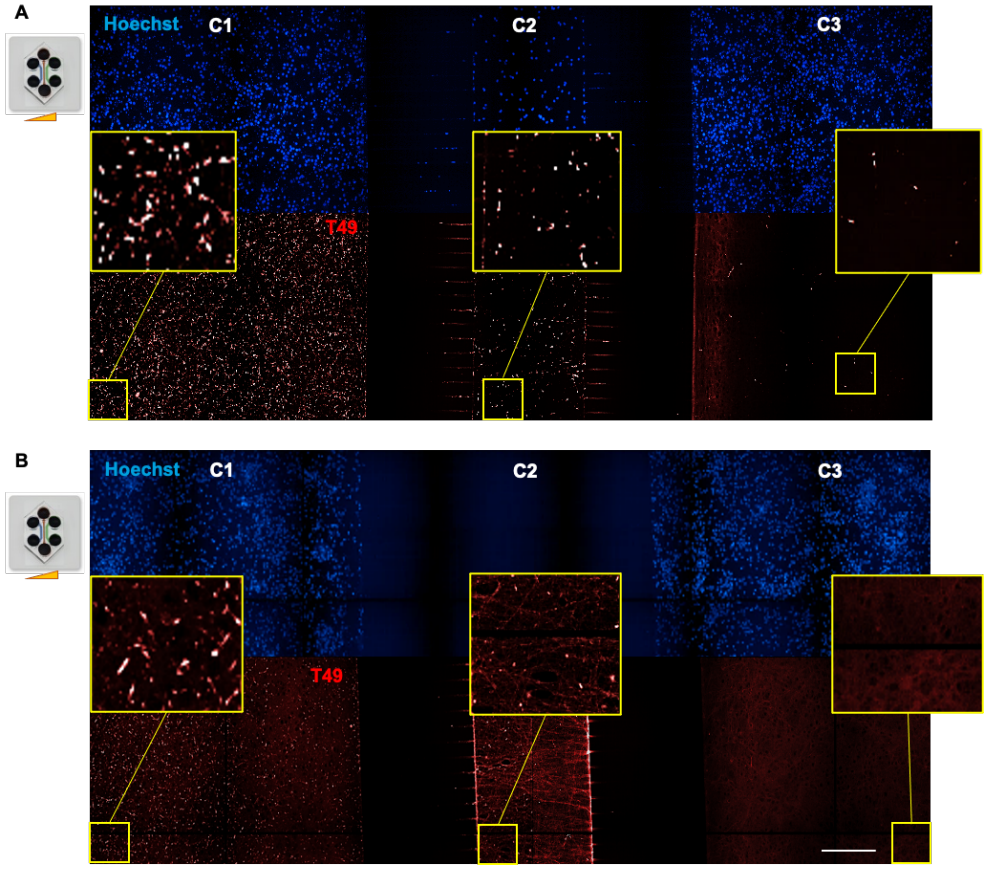


Figure 3.10: Propagation of endogenously aggregated rodent tau is a real effect and not a device artefact in three-chamber microfluidic devices. *RCNs were plated at DIV0 in compartments C1, C2 and C3 of a three-compartment microfluidic device and the neurons of C1 were seeded with 18nM of hAD seed at DIV7. Cells were fixed two weeks later following the timelines of the 2-compartment microfluidic devices, and stained for rodent specific tau, T49. T49 positive inclusions were detected in C3 (A). When no RCNs were plated in C2, there were no T49 positive inclusions detected in compartment C3, suggesting that there was no axonal growth overlap between the two neuronal populations (B). Image acquisition with Opera Phenix 20x Magnification, image tiled montages with zooms for each compartment in the yellow square, Bar 50 µm.*

Having shown that the propagation is real and that synapses are needed to see propagation, we wanted to demonstrate that the propagated tau was mainly axonal. Since axons from both compartments can pass the microgrooves it can be assumed that neurons from the propagation side can capture the hAD seed with their axons and retrogradely transport it into their cell bodies where it would induce aggregation. We hypothesised that both of these mechanisms were causing the presence of rodent aggregated tau in the seeding side, but we wanted to make sure that the main component was anterograde axonal transport from cells in the seeding side to the propagation side.

We proceeded with two different approaches; the first one was to use 3-chamber devices and plate cells in the middle chamber at DIV0 and in the external chambers with a week difference at DIV7 when neurons in the middle chamber were seeded with hAD seed. In this way, we were sure that cells in the propagation sides (external chambers) couldn't project their axons and capture hAD seed and we could also compare the propension of the seed to be propagated in the two different compartments. As show in F*ig 3.11*, we could see propagation both in the left and right compartments and we could count a similar amount of T49 inclusions in the left and right chambers indicating that there is no preferential direction for axons. Unfortunately, at DIV7 axons from the middle chamber that had already invaded the external chambers affected the uniformity of the neuron plating in DIV7 which resulted in neurons clumped together.

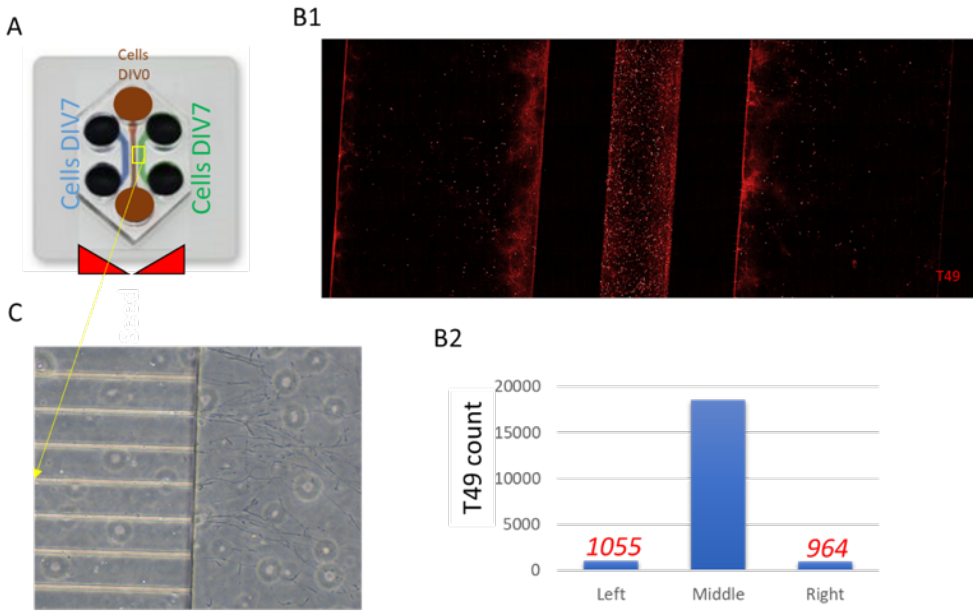


Figure 3.11: Testing real tau propagation*. 3-chamber devices (A) were used to demonstrate that when RCN are plated at DIV0 and seeded at DIV7, they can intake hAD seed, form endogenous rat aggregates and equally propagate to the external chambers (B1-2) that were plated with neurons only after a week so that they couldn't project their axons in the seeding side, and they couldn't intake seed actively. RCNs plated in the middle compartment at DIV0 projected their axons to the propagation side very early on so the plating of RCNs at DIV7 in the propagation side was affected (C).*

In order to confirm these results and to solve the plating problem, we used a second approach: unidirectional devices with round gap grooves *(Fig 3.12, A)* whose particular structure only allows axons from one side to pass to the other compartment [247].

For this preliminary experiment three devices were used and seeded with different concentrations of hAD seed, 48, 24 and 12 nM to see a dose response effect on tau propagation. Media was refreshed at DIV 14 and cells were fixed at DIV 21 with ice-cold methanol and stained for T49 and Hoechst.

In *Fig 3.12 B,* the signal window is very small since even 48 nM of hAD seed induced very little seeding. This could be related to the high cell death that we can observe from the Hoechst staining, probably due to too many cells plated. As observed before, the number of aggregates that we can detect is highly dependent on the number of cells plated and their health.

Nevertheless, we can still see a dose dependent increase in tau aggregation in the seeding side of these devices and a subsequent propagation.

Due to these results, we can then be confident with the findings observed in the Xona devices and can continue using a simpler and more economical assay as the classic MFD platform.

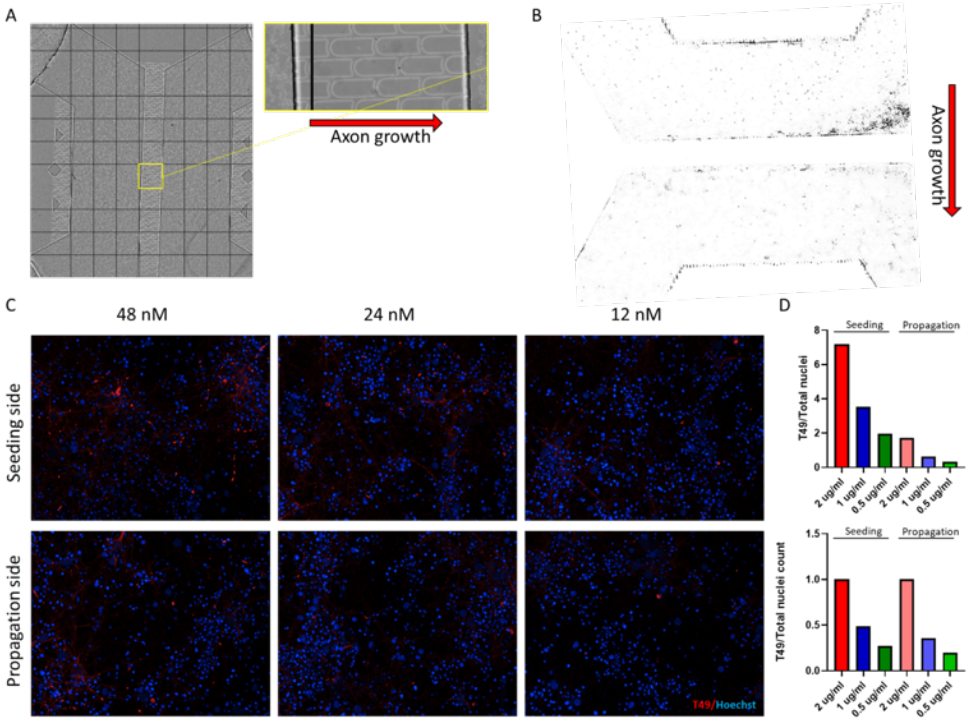


Figure 3.12: Unidirectional devices experiment supports the strength of the MFD assay*. RCNs were plated in unidirectional devices with round gap grooves (A) that were seeded with increasing concentrations of hAD seed (C). The device seeded with 48 nM of hAD seed was used to show that the signal window is not optimal (T49 aggregates in black, B). Quantification of T49 count normalised on the total nuclei count show a seed dependent propagation of rodent tau in the propagation side (D). Preliminary results, N=1.*

3.3.3 Xona MFDs assay: image analysis and quantification method of T49 propagated thread-like inclusions

We have demonstrated that hAD seed can induce tau aggregation in the seeding side of the 2-chamber microfluidic devices and that endogenous aggregated tau can propagate to the propagation side and seed another population of neurons. To demonstrate the robustness of our platform and to develop not only a qualitative but

also a quantitative assay, we explored how we could quantify the T49 positive thread-like inclusions. As described in the methods section, the images generated with the high content image screening system Opera Phenix (Perkin Elmer), were first analysed with the Harmony software. Using the machine learning function, we trained the software to recognise T49 thread-like inclusions and applied a software pipeline to count nuclei, total and live. The results were exported to an Excel file which was processed by the Cell Counter software.

This app was developed in our laboratory and it was used to quantify and separate our results between seeded and propagation compartments. *Figure 3.13* summarises the main steps followed when using both Harmony and the Cell Counter. This specific computer software enabled us to automate and quantify for the first time Tau pathology in a non-Tg neuronal microfluidic model.

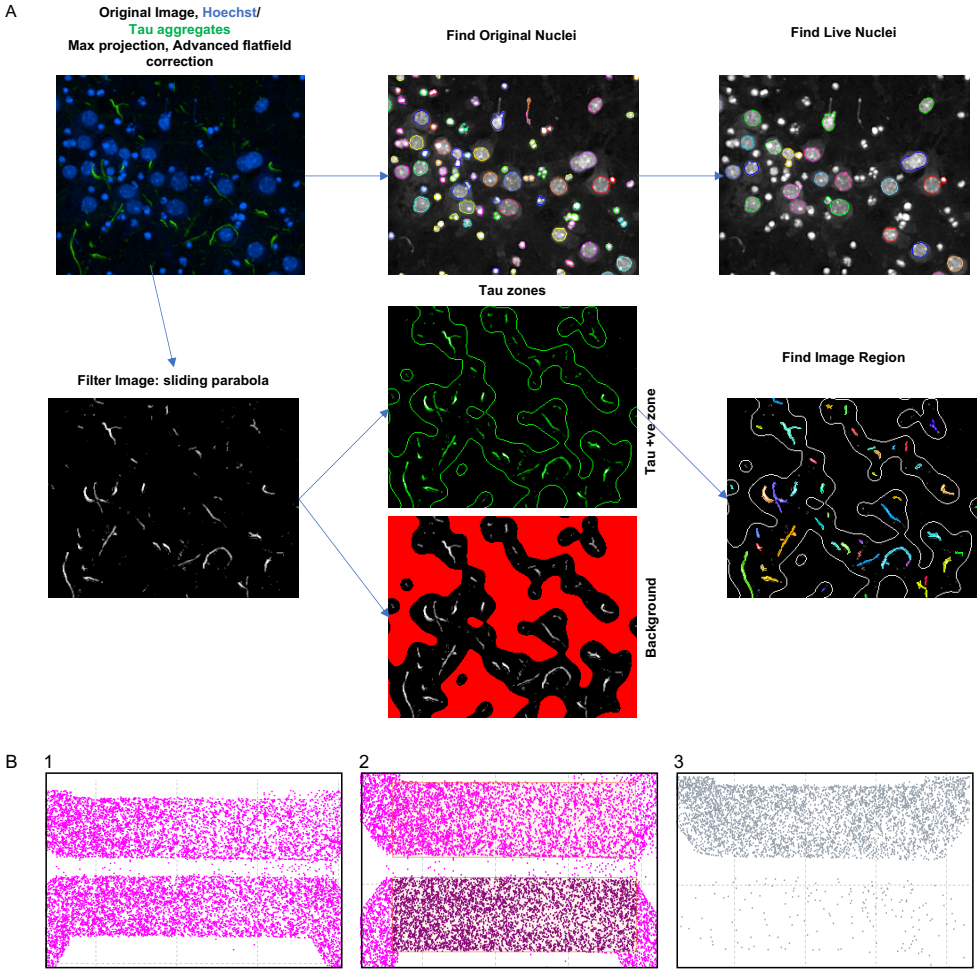


Figure 3.13: High Content Image Analysis pipeline and the Java program used to quantify the number of T49 neuritic-like threads in a tau-positive zone. *The original merged image undergoes maximum projection and flatfield correction using the Harmony software (A) before being filtered to eliminate and smoothen the fluorescent background for the T49 staining. The total number of nuclei is counted with Hoechst and from this population we define the live nuclei. The filtered T49 image undergoes machine learning in order to separate the background from the tau-positive zone where the T49 neuritic-like threads are counted. The results of this analysis is loaded into the Cell Counter computer program (B1) that allows the pixel visualisation of the nuclei (Hoechst staining) (B2) and the T49 neuritic-like threads in seeded (top) and propagation (bottom) compartments (B3). The ROIs in the top and bottom sides are manually selected and processed for the number of nuclei and T49 neuritic-like threads.*

3.3.4 Xona MFDs assay: optimization of experimental conditions

To optimize and validate the experimental and analysis conditions we ran a factorial experiment to assess the impact of seeding day, fixing day and plate uniformity on the seeding and propagation side. RCNs in Xona 6-well plates were seeded on DIV3, 7 or 10 (Seeding Day SD), and fixed on DIV 18, 21 and 24 (Final Day, FD). The standard condition was SD=7, FD=21 and this along with combinations (3, 17), (3, 24), (10, 17) and (10, 24) were tested on 5 plates. Each plate had unseeded wells to assess the effect of assay conditions on background conditions. The experiment was analysed by mixed models analysis of variance. The results showed that background levels varied substantially across plates (> 60 % of total variation) and between seeding and propagation sides, indicating on-plate controls for background levels are required for this technology, and estimates of background levels should be subtracted from all seeded wells. The results showed that total cell counts decreased as SD is postponed from DIV3 to DIV10, and as FD is postponed from DIV17 to DIV24, especially on the propagation side. Thread % (thread-like inclusion count / total nuclei) decreased as SD is postponed from DIV3 to DIV10 and increased as FD is postponed from DIV17 to DIV21, and strikingly the propagation side was a constant proportion of the seeded side (*Fig. 3.14 A*). The results indicate that the length of time post-seeding was the most important variable with SD=3 and FD=24 delivering the highest Thread %, however the risk of cell toxicity is elevated at FD=24, therefore SD=3 and FD=21 was deemed to be operationally the best combination (*Fig. 3.14 B*).

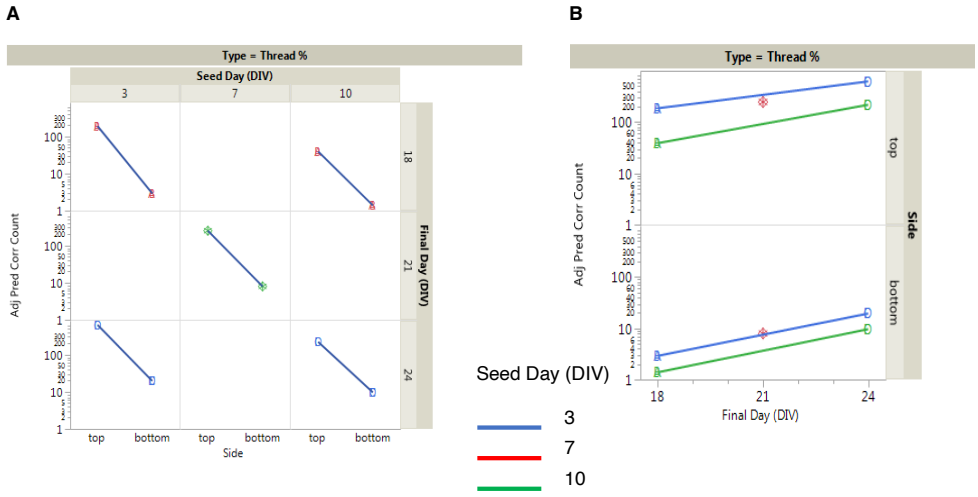


Figure 3.14: Optimization of experimental conditions. *Seeding side=top and Propagation side=bottom. Seeding-side thread percentage (Thread % = 100 x Thread count/cell count) decreases as Seeding day (SD) is postponed from DIV3 to DIV10 and increases as Final Day (FD) is postponed from DIV10 to DIV21 (A). Parallel lines between seeding and propagation side indicate propagation side results are proportional to seeding side results across these assay conditions. Thread % is maximized with the (SD, FD) = (3,24) combination, although the risk of cell death is elevated with such a late FD, and thus (SD,FD)=(3,21) is operationally the optimal combination (B).*

3.3.5 Xona MFDs assay: seeding and propagation of aggregated tau is hAD seed concentration-dependent

Since we had developed a platform that allowed us not only to induce tau aggregation and propagation but also to quantify neuritic thread-like inclusions, we wanted to test how well our microfluidic assay would respond to cell culture environmental changes. We seeded cells at DIV7 at the seeding side with increasing concentrations of hAD seed starting from 0 to 18 nM then fixed and imaged the cells at DIV21.

In *Fig 3.15*, there is a dose dependent increase of T49 thread-like inclusions both in the seeding and propagation side and a proportional correlation between the amount of thread-like inclusions in the two

compartments: the more thread-like inclusions in the seeding side the more propagation, and consequently aggregation, in the propagation side.

Moreover, we noticed that cells were healthy with each concentration of seed used in both compartments indicating that, at these concentrations, the hAD seed is not toxic and can be used for our purposes.

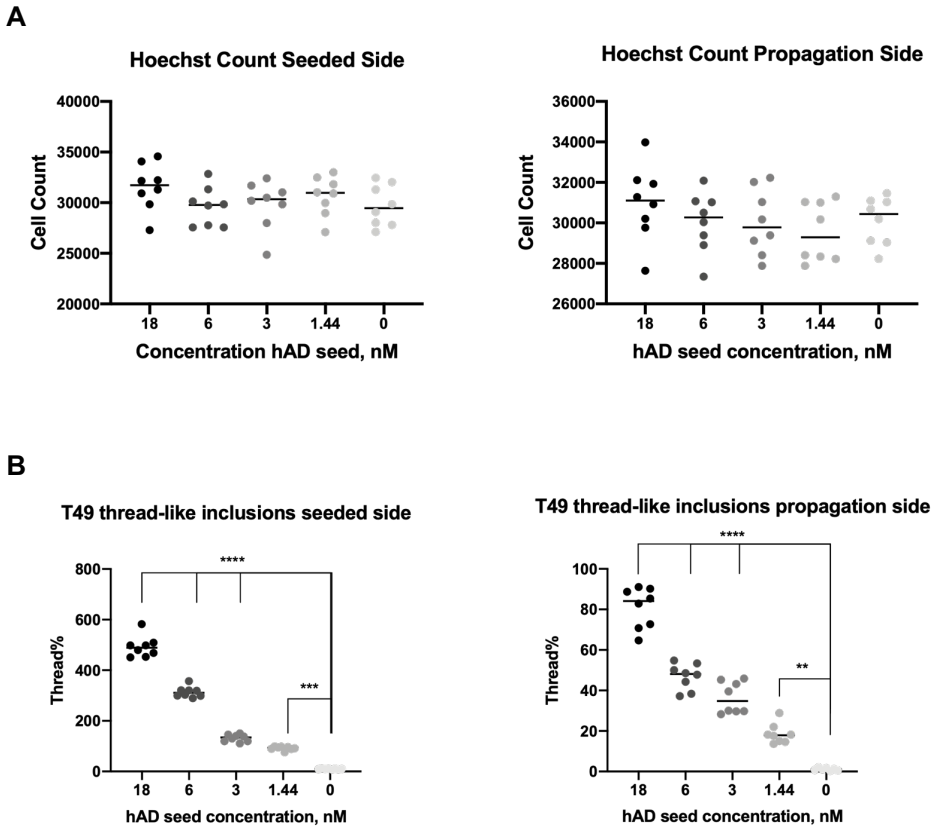


Figure 3.15: Quantification of the number of neuritic thread-like aggregates demonstrates that propagation of the pathology in RCNs is concentration dependent. *Quantification of the number of nuclei (Hoechst) (A) and neuritic thread-like aggregates (T49) (B) in both seeded and propagation compartments in a 4-point CRC of the hAD seed in RCNs starting from 18 nM. Statistical evaluation was performed using one way-ANOVA followed by Dunett's post-test, $p<0.05$, **, *** compared to the unseeded (0 nM) control. Results are represented as mean +/- SEM of 2 independent experiments with 8 replicates in total for each condition. (Thread % = 100 * Thread count/cell count).*

3.3.6 Xona MFDs assay: the aggregation and propagation of endogenous tau that result from hAD seeding can be pharmacologically inhibited

The microfluidic platform that we have developed is useful to study tau propagation and we have demonstrated that it is possible to manipulate the seeding and propagation levels. We decided to test whether a tool compound previously described in the literature could have an effect on the aggregation and propagation of tau [231]. The compound that we chose is Anle138b and we have demonstrated its efficacy in reducing tau aggregation in the 96-well RCN assay (*Results 3.2.3*). The concentration that demonstrated the best inhibitory effect and no cytotoxicity in the 96-well plate experiment was 10 μM. We decided to test Anle138b in MFDs following two experimental protocols; at DIV7, when cells were seeded, the compound was added in the first protocol both in the seeding and the propagation side (*Fig 3.16*, condition "seeded+propagation" and "S+P") and in the second one it was added only in the propagation side (*Fig 3.16*, condition "propagation" and "P"). Using these two approaches we wanted not only to demonstrate Anle138b efficacy in reducing tau aggregation in this model, but also its ability to reduce the number of neuritic thread-like inclusions that propagate as a consequence of seeding with h AD seed. *Fig 3.16* shows the ability of Anle138b to reduce tau aggregation. In fact, when the compound is applied to the seeding side along with the hAD seed, the reduction in the number of T49 thread-like inclusions observed in this compartment is 50% with respect to the DMSO control.

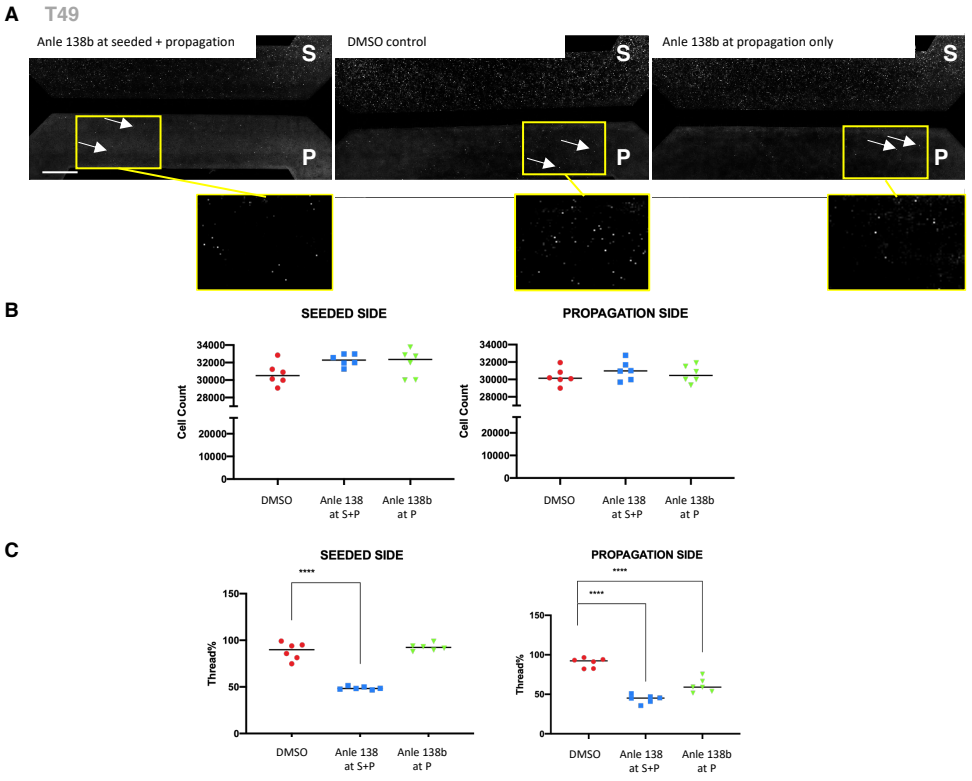


Figure 3.16: Addition of a small molecule aggregation inhibitor to RCNs in the microfluidic model results in inhibition of both aggregation and propagation. *Representative images of tiled montages of each 2-chamber microfluidic device for each tested condition: Anle138b added to the seeded and propagation compartment on the left, the DMSO hAD seeded control in the middle and the Anle138b added to the propagation compartment on the right, which demonstrates that the small molecule aggregation inhibitor, Anle138b had no effect on the number of Hoechst positive cells and inhibited both the aggregation and propagation of neuritic thread-like T49 inclusions. Bar, 500 µm (A). There were no changes in the cell numbers between the DMSO control and the Anle138b treatments when cells were counted for each microfluidic compartment (B). Quantification of these results demonstrates a decrease in the number of T49 positive neuritic thread-like aggregates as a result of the Anle138b treatment (C). Statistical evaluation was performed using one-way ANOVA followed by Dunnett's multiple comparison test $p<0.05$; results are represented as mean +/- SEM of 2 independent experiments with 3 replicates for each condition. (Thread % = 100 * Thread count/cell count). Zoomed images indicated by yellow square.*

This effect is reflected in the propagation side as well. There is a reduction in the number of T49 aggregates not only because of the direct effect of Anle138b that was added also to the propagation side, but because the endogenous aggregated tau in the seeding side that can propagate and induce aggregation in the second compartment is lower than in the control.

Conversely, when Anle138b was only added to the propagation side, it reduced the number of neuritic thread-like inclusions by 40% compared to the DMSO control.
Moreover, we can see from the nuclei count that none of these treatments are toxic so we can assume that the effects observed are not due to cytotoxicity.

As previously demonstrated in the 96-well RCN assay, Anle138b is a compound that can very efficiently inhibit the formation of tau aggregates induced by seeding with hAD seed. This compound also affects tau propagation as demonstrated in microfluidic devices. To our knowledge this is the first time that a tool compound has reportedly inhibited aggregation and propagation in non-Tg RCNs after seeding with purified seed extracted from human AD patients' brains.

3.3.7 Xona MFD assay: characterization of tau thread-like inclusions released in the propagation side

Having developed a microfluidic platform that can be used to study tau propagation, we wanted to study in more depth the nature of the thread-like inclusions that are released from the neurons in the seeding side and that induce tau aggregation in the propagation side. We plated RCNs in Xona devices only in the seeding side in DIV0 and then seeded them at DIV7 following the standard protocol with 18nM of hAD seed. At DIV 10, 17 and 21 media was collected from the propagation side and frozen at -80°C until further analysis.

We first tried to run both a Western blot and an AlphaScreen to study the levels of total tau and phosphorylated tau in the sample, but the protein level was below the detection capability.

We then decided to pool together all samples collected from all the time points and to perform a Sarkosil extraction in order to purify thread-like inclusions present in the media and to run these samples (P1) in a Western blot, staining for total tau (T49 rodent tau and CP-27 human tau).

Unfortunately, as we can see from *Fig 3.17*, this attempt did not work; possibly because the amount of aggregated tau released in the media is still below the detection limit and, in order to visualise inclusions, we should increase the sample number but the cost of these experiments didn't allow us to explore this further.

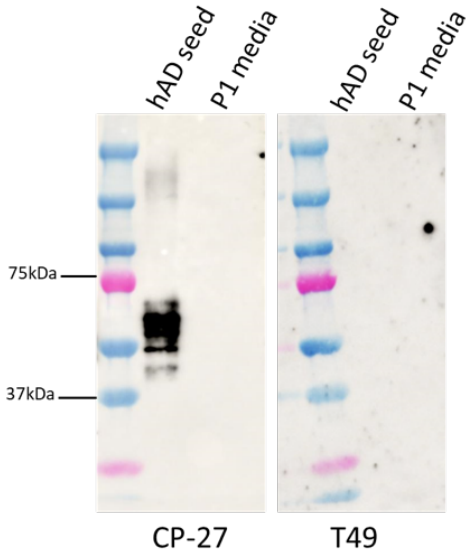


Figure 3.17: Western Blot of sarkosyl-extracted media collected from the propagation side*. RCN media collected for 11 days from the propagation side of Xona MFD plates was Sarkosyl-extracted and run in a Western blot to study tau release. The hAD seed used to seed the neurons is CP-27 positive but is not detected by T49, rodent specific tau. There is no signal for the P1 of the media indicating that the level of tau is too low to be detected by western blot.*

3.3.8 Xona MFD assay: functional studies can be run in this platform

To explore what kind of studies could be run in this platform we performed various functional studies that show how this assay can be used for more exploratory research. As an example, we studied the functional activity of neurons plated in the MFDs using calcium imaging. this technique allows to study not only spontaneous activity of neurons but also their synaptic communication.

At DIV 21 we loaded neurons seeded with hAD seed as well as unseeded controls with Fluo-4, a dynamic single-wavelength fluorescent calcium (Ca^{2+}) indicator that is widely used to monitor cytoplasmic Ca^{2+} levels. When there is an increase in neuronal activity and in cell firing, Ca^{2+} is released from intracellular stores, increasing its cytoplasmic concentration, and binds Fluo-4, causing its fluorescence intensity (at the emission wavelength of 525 nm) to rise dramatically which can be recorded.

Initially, we set up an experimental design to record from MFDs. For these experiments we used a ZEISS Axioscope microscope, and we centred the objective in the microgrooves area so that we could record from both seeding and propagation sides (*Fig 3.18, A*). During the first set of experiments, after approximately 2 minutes of baseline recording, we stimulated cells in the seeding side with 50 µM KCl, ensuring that the fluidic isolation between the two compartments were kept, so that the KCl couldn't move to the propagation side. We then recorded for another 5 minutes before stopping the recording and

analysed the data to study if the two populations were synaptically and electrically connected.

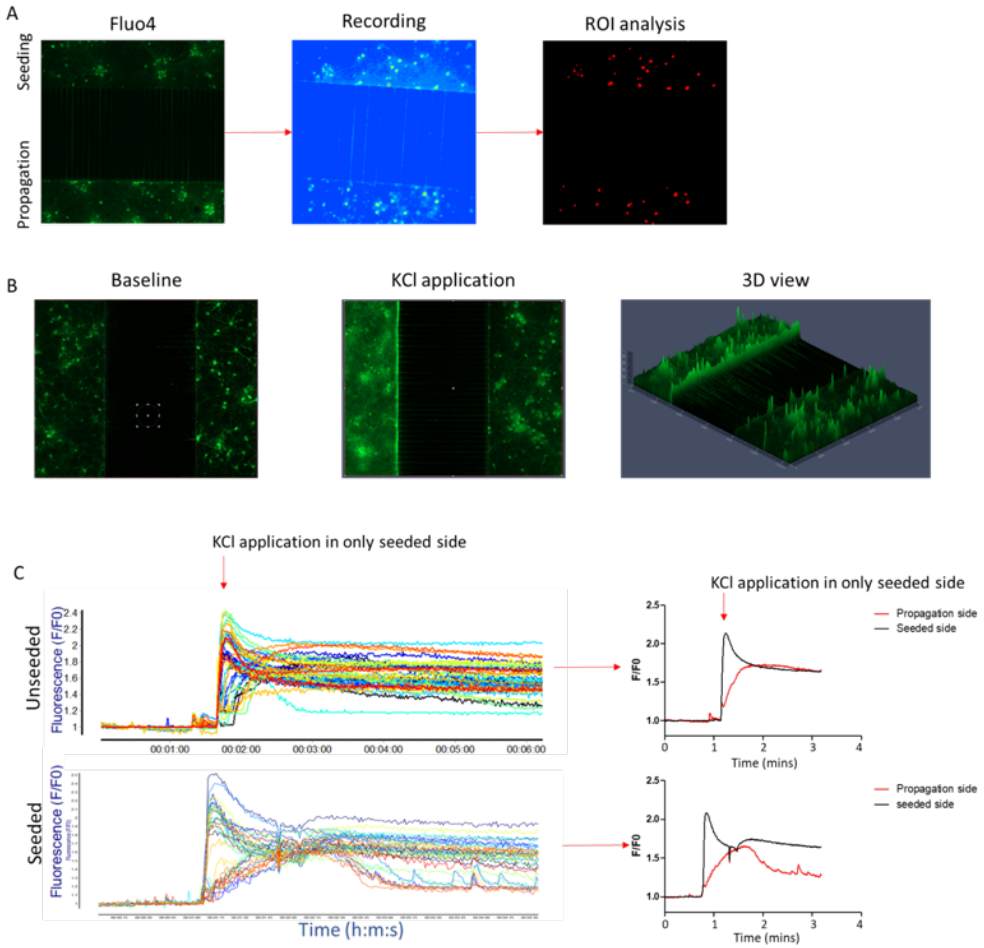


Figure 3.18: Calcium release experiments in microfluidic devices: *RCNs were loaded with Fluo-4 at DIV21 after being seeded at DIV 7. The microscope was focused at the centre of the microgrooves in order to record from both seeding and propagation sides (A). After 2 minutes of baseline cells in the seeding side were stimulated with 50 μM KCl. The software allows to visualise fluorescence peaks in 3D (B). The data from every cell was analysed and data were plotted both for seeding and propagation cell populations(C). Results from N=2 experiments with 4 devices each.*

As we can see from *Fig 3.18*, we can use the ZEISS ZEN imaging software to follow in real time the neuronal response. There is a very clear difference in fluorescence between the baseline and the addition of KCl. It is also possible to visualise the peaks in a 3D view that helps to understand the contribution of each cell (*Fig 3.18, B*).

As a result of these experiments, we can see that cells in the seeding side respond to the KCl stimulus immediately (*Fig 3.18, C*) inducing a depolarization and an increase in calcium fluorescence. We can also see a delayed response in the propagation side that indicates that the two populations are synaptically connected. The curve of the propagation side shows a much slower response of these cells highlighting a different kinetic profile for the propagation side.

When comparing seeded to unseeded cells, there was not much difference in the response to KCl in the seeded compartment. However, in the propagation side, cells from the seeded population were unable to sustain the Ca^{2+} response and 1 minute after KCl application, the signal started to decrease, with some small bursts of activity still present. While further experiments are required to determine the exact cause of these differences, these results indicate a decrease in synaptic connectivity in the propagation side. The response in the seeding side does not rely on synaptic connectivity, since KCl is directly applied directly here and not washed away, so its strong effect could mask any synaptic deficits.

For the second set of experiments, we stimulated neurons on the seeding side with 10 μM of gabazine in order to favour spontaneous firing of cells and study their response comparing seeded and unseeded cells. Gabazine is an allosteric inhibitor of GABA receptors; consequently, there will be a reduction of GABA-mediated synaptic inhibition or, in other words, an increase in neuronal activation.

As we can see from *Fig 3.19*, gabazine induced an increase in firing compared to the baseline in all the conditions. The cells in the propagation side responded to the gabazine with a delay with respect to the seeding side indicating that they were responding to the stimuli evoked by the neurons in the seeding side rather than directly to the gabazine. This confirms not only the synaptic connection between the two populations, but also the fluidic isolation between the two compartments.

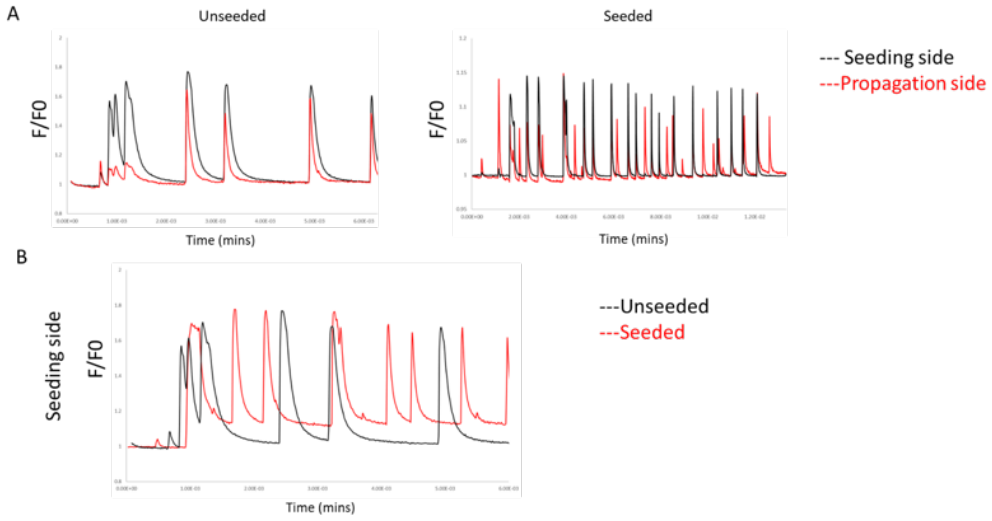


Figure 3.19: Gabazine stimulation of seeding side neurons*. RCN plated in microfluidic devices were treated with 10 μM gabazine and recorded from both seeding and propagation sides (A). Data from the seeding sides of the unseeded and seeded devices were plotted in the same graph to show the difference in the spontaneous firing of these neurons (B). Results from N=2 experiments with 4 devices each.*

Interestingly, when cells were seeded with hAD seed and treated with gabazine, they looked hyperactive and the frequency of their response was higher than the unseeded control (*Fig 3.19, B*) indicating that this is a seed related effect. This could be explained by hypothesising that the seed, applied for 14 days to the cells, induces either directly or indirectly, a change in the expression or in the activity of excitatory receptors such as glutamatergic AMPA or NMDA receptors, thereby leading to an increase in spontaneous firing.

This preliminary finding is in line with previous work that showed how in AD the excess of tau in dendrites upregulates NMDA receptor

activity, saturating the neurites with harmful levels of Ca^{2+}. Moreover, glutamate-induced excitotoxicity is inhibited by reducing tau levels [248,249] and exacerbated by overexpressing tau [250,251].

Over time, this increase in glutamatergic activity can lead to excitotoxicity that can damage postsynaptic sites and cause neuronal death, as is observed in AD brains [252]. In fact, *ex vivo* neuropathological studies, have shown that degeneration of glutamate-mediated pathways occurs early in the disease and in a pattern that corresponds with the distribution of plaques and tau tangles [253,254].

3.4 High throughput (HT) microfluidic assay as a miniaturized platform to study tau propagation

We have previously identified and developed a microfluidic assay that can be used to study tau aggregation and propagation and to test compounds that inhibit these processes. A limitation of this assay is its low throughput; in one plate we can fit only 6 MF devices which are not enough to plan a statistically relevant experiment when screening compounds or antibodies. To solve this issue, we collaborated with the University of Strathclyde that could manufacture a higher throughput MFD plate with format and dimensions similar to a 96-well plate (microgrooves are 500 μm long, 10 μm wide and 3 μm tall). Like the Xona devices, these plates are PSDM-made and can be plasma bonded to cover glasses. They contain eight 2-compartment MFD devices and two plates can fit in a 96-well like insert that can be imaged in the Opera Phenix. So, starting from a 6-unit format we progressed

to handling a 16-unit plate that, due to its small dimension, not only improved the throughput but also allowed us to save on reagents (*Fig 2.7*).

As a first step, we optimised the plasma bonding and the plating condition. Plasma treatment is useful to enhance functionality and biocompatibility of material surfaces. The plasma oven that we used can work both with normal air or with a specific gas such as oxygen to activate the top of devices and cover-glass surfaces, rendering them hydrophilic and promoting their attachment and adhesion. Oxygen plasma is recommended and used more frequently than air, so we decided to improve our protocol by adding oxygen.
After having established that the old oven conditions were not optimal with the addition of oxygen, we changed the variables to find the optimal plasma bonding protocol (60 seconds, 30% power).

Once the devices were ready to be used, we successfully optimised the neuronal density and coating material. We tested two densities, 20K and 25K cells/µL, and five coating conditions, PDL prepared in water 0.1% and 0.01%, PDL prepared in DPBS 0.01% and 1% and PLO 0.01%.

From *Fig 3.20,* it is evident that 25K cells/µL grow much better than 20K and that preparing PDL with water is not ideal for neuronal adhesion as shown by MAP2 staining. Moreover, PDL at 0.01% is not dense enough to favour cell viability. There was not much difference

between PDL at 0.1% and PLO at 0.01%, also confirmed by the nuclei count that was similar under both conditions. Therefore, we decided to use PLO which was also suggested by our collaborators at Strathclyde University.

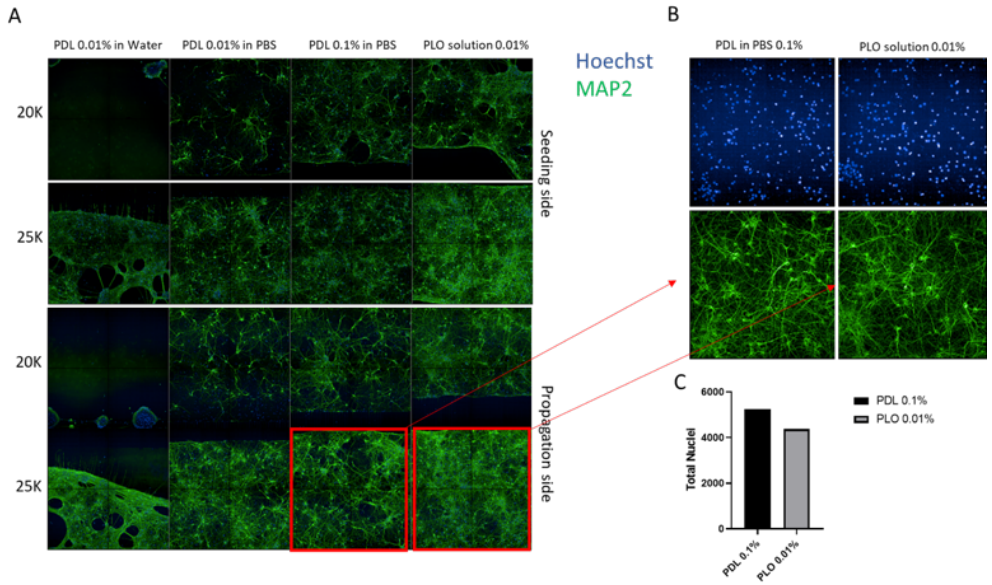


Figure 3.20: HT Optimization experiments: *RCNs were plated at different concentrations (20 or 25K/µl) in MFDs coated using multiple protocols and fixed after 3 weeks (A). Cells look healthy both using 0.1% PDL and 0.01% PLO (B) but nuclei count (C) reveals a preference for PLO.*

We then treated neurons with increasing concentrations of hAD seed to test whether we could see propagation in these devices and to determine the ideal hAD seed concentration, similar to what we did with the Xona devices. To find the ideal conditions to obtain a good signal window, we tried two different seeding days: DIV3 and DIV7 and kept the fixing day constant at DIV21.

The count of neuritic thread-like inclusions revealed that all the concentration of hAD seed tested both in DIV3 and DIV7 were able to induce tau aggregation and propagation in this model with a peak at 18nM in both cases. Even if the SD did not show statistical differences, there is a trend suggesting that, in line with the Xona results, seeding in DIV3, produces a higher T49 count in both seeded and propagation compartments with respect to DIV7. However, since cultured neurons at DIV3 are not fully mature and synapses form at DIV5-7 [255], DIV7 was chosen for seeding in the next experiments. As previously observed in Xona devices, irrespective of the seeding day, the amount of thread-like inclusions in the propagation side was proportional to the seeding concentration applied to the seeding side (*Fig 3.21*).

The nuclei count revealed that none of the hAD seed concentrations was toxic as seen from the Hoechst staining. Since the ratio between the number of inclusions in the seeding and propagation side of HT and Xona devices were very similar, we can conclude that this smaller format reproduces very closely the setting of the Xona devices but with the advantage of using less reagents and offering a higher throughput. This observation supports the use of this microfluidic platform as a higher throughput tool to study propagation of tau and develop therapeutic strategies.

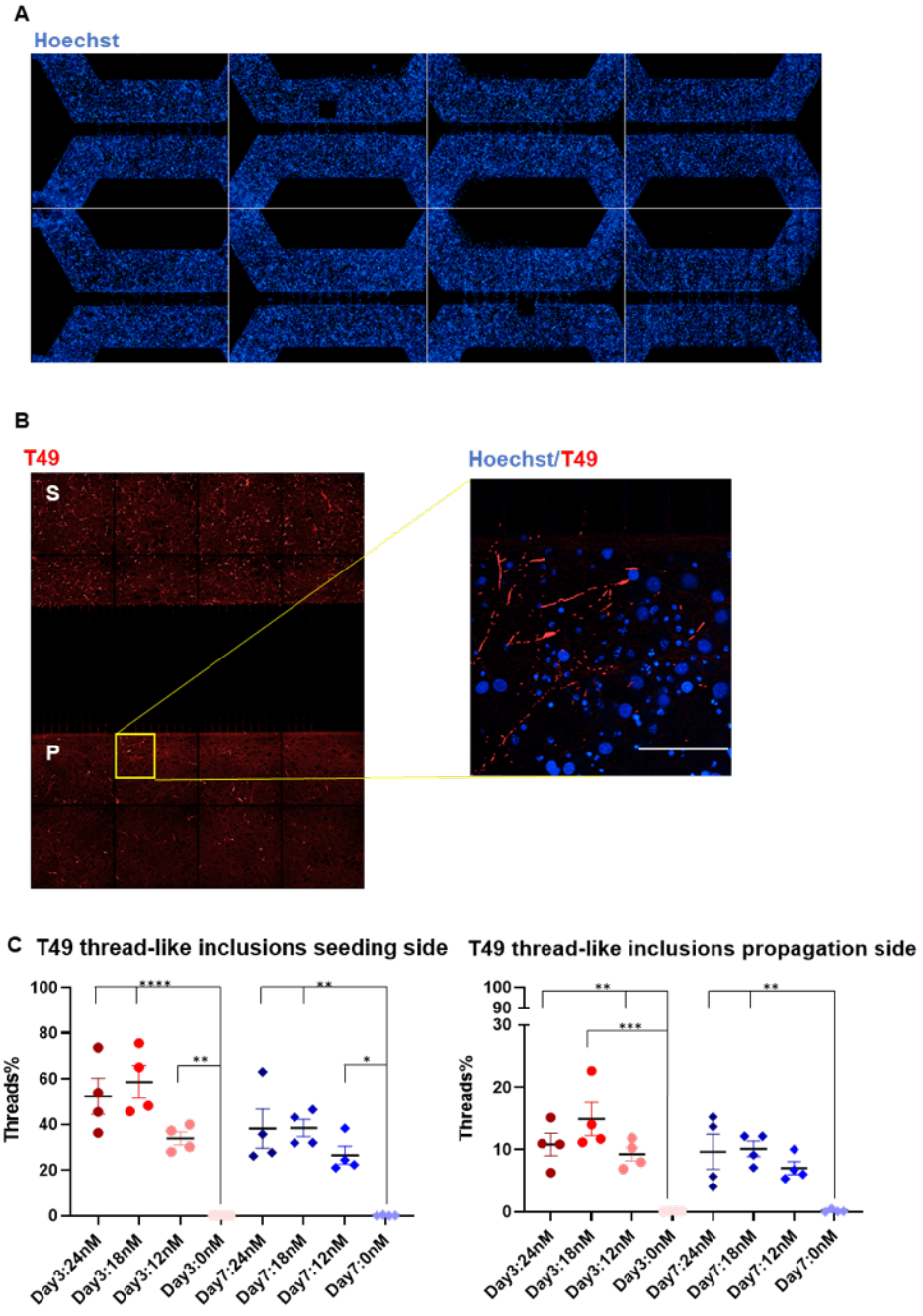

A
Hoechst
B
T49
S
P
Hoechst/T49
C
T49 thread-like inclusions seeding side
T49 thread-like inclusions propagation side
Threads%
100
80
60
40
20
0
****
**
*
Day3:24nM
Day3:18nM
Day3:12nM
Day3:0nM
Day7:24nM
Day7:18nM
Day7:12nM
Day7:0nM
90
30
***

Figure 3.21: Propagation of aggregated Tau in RCNs cultured in a novel higher throughput microfluidic platform. *A typical high throughput microfluidic device can support 8 small 2-compartment microfluidic devices where RCNs are cultured (image tiled montage) (A). When RCNs are seeded (B) with h AD seed they demonstrate the neuritic thread-like inclusion morphology and they propagate the templated seed as revealed by the T49 staining (B,). Quantification of the number of neuritic thread-like aggregates (T49) in both seeded and propagation compartments in a 3-point CRC of the h AD seed in RCNs starting from 24 nM. Statistical evaluation was performed for each time point using one way-ANOVA followed by Dunett's post-test, p<0.05, **, ***, **** compared to the unseeded (0 nM) control. No statistically significant differences between the single concentrations in DIV3 and 7 (D). Results are represented as +/- SEM of 2 independent experiments with 2 replicates for each condition. Bar, 50 µm. (Thread % = 100 * Thread count/cell count). Seeding on DIV 3 with 18 nM of h AD seed results in a higher count of inclusions in both seeded and propagation compartments compared to seeding on DIV 7 (C). Results are represented as +/- SEM of 2 independent experiments with 3 replicates for each condition.*

3.4.1 HT microfluidic assay: inhibiting tau propagation with a tool compound

The high throughput microfluidic platform that we have developed here is useful to study tau propagation using small amounts of reagent and a more functional experimental set up in comparison with the Xona platform. Next, we wanted to test this assay using the Anle138b compound to demonstrate that, in this platform, we can also affect the propagation of tau using a small molecule inhibitor. In this experiment, we used Anle at 10 µM so as not to induce cell toxicity. We only tested it in the propagation side since we already demonstrated both in the 96-well assay and in the Xona devices its ability to directly reduce tau aggregation. At DIV7, when cells were seeded, the compound was added to the propagation side and it was replenished at DIV10 and 17. Cells were fixed at DIV21 and imaged for T49 and Hoechst using the Opera Phenix. Images were analysed with Harmony software and Cell Counter app and plotted in Graphpad Prism.

As we can see from *Fig 3.22*, using this platform, Anle138b can decrease tau propagation by more than 50% compared to DMSO control (T-Test, $p<0.05$, results from 2 independent experiments with 6 replicates for each condition).

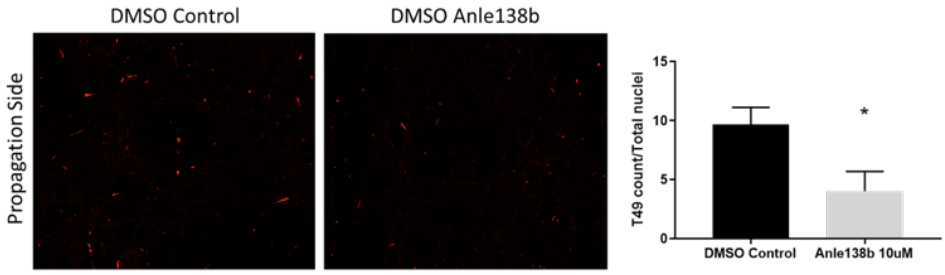


Figure 3.22: Testing the effect of Anle138b in the HT MFD assay. *Anle138b inhibited the aggregation and propagation of neuritic thread-like T49 inclusions. Quantification of these results demonstrates a decrease in the number of T49 positive neuritic thread-like inclusions as a result of the Anle138b treatment. Statistical evaluation was performed using multiple t-test with $p<0.05$; results are represented as mean +/- SEM of 2 independent experiments with 6 replicates for each condition.*

We can conclude that this second version of a tau propagation platform is as efficient as the commercial one but with the advantage of using less reagents (seed, compounds, antibodies…) and being higher throughput, allowing us to compare more conditions in a single plate.

3.4.2 HT microfluidic assay: inhibiting tau propagation by modulating neuronal mGluR receptors

Having established that we can use this HT platform to test compounds that we believe can have an effect on tau propagation, we

decided to test if modulating neuronal activity could affect tau release and propagation.

In particular, it has been previously shown that tau release, and consequently its propagation, is proportional to neuronal activity [246] so, we tried to modulate glutamate release acting on mGlu2/3 receptors. These proteins are present in the presynaptic membrane and they have an important role in vesicle release, by modulating both voltage-sensitive calcium channels and the fusion of the snare complex with the presynaptic membrane [256,257]. Therefore, acting on these receptors with an agonist, induces a decrease in intracellular Ca^{2+} levels and a consequent decrease in neuronal depolarisation and vesicle release.

RCNs were then plated as usual and seeded on DIV7; in the propagation side neurons were treated with 10 μM of mGluR agonist or antagonist (Lilly compounds) or a solution with agonist and antagonist. As per the original protocol on DIV21 cells were fixed, stained, imaged and analysed for T49 and Hoechst.

Fig 3.23 shows how treating neurons in the propagation side with the mGluR agonist induces a decrease in tau propagation with respect to the control. Indeed, the antagonist treatment didn't have any effect but, if applied in the presence of the agonist, it could reverse its effects.

This platform can then not only be used to test compounds but also to study biological events that could lead to a modulation of tau release and its consequent effect.

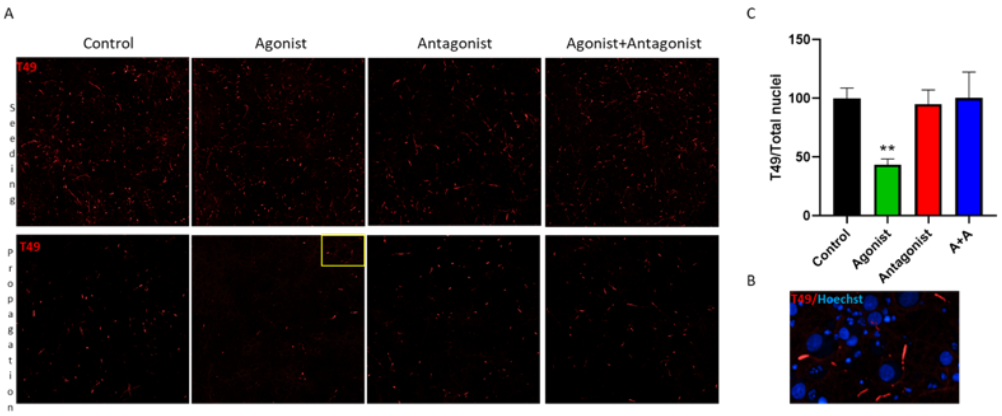


Figure 3.23: Effect of mGluR agonist and antagonist on tau propagation*. Microfluidic devices have been used to show the effect of mGluR regulation on tau propagation. (A) hAD seeded RCNs are stained for T49 (Alexa 647) and Hoechst both in seeding and propagation sides, zoomed image (B). Tau propagation was studied in the propagation side as a ration between T49 threads normalised on the number of cells (C). Statistical evaluation was performed using One-way ANOVA, Dunnett's test multiple comparison against the control. Results are represented as mean +/- SEM of 3 independent experiments with 6 replicates for each condition.*

3.5 Development of a humanized, high throughput, microfluidic assay platform

We have previously developed a microfluidic platform that can be used to study endogenous tau aggregation and propagation. The tau that is templating is human tau, extracted from AD patient brains and the tau that aggregates and propagates is rodent. It is well known that there are species differences in tau protein [258], which must be taken into account when compounds or antibodies are tested in non-human models. to have a more translational model of tau propagation we developed a hTau mouse cortical culture that we used in our HT MFD assay.

hTau mouse is a murine model that expresses only human tau in all its isoforms, including 3R and 4R isoforms [244] and that has replaced mouse tau with the reporter-protein GFP.

hTau mice are made by mating two existing lines of tau mice, 8c [259] and tau knock-out mice [260] that give 50% of tau positive embryos in the F2 generation (*Fig 3.24*). For this reason, in order to separate human tau positive and negative embryos, we have developed a protocol to genotype them.

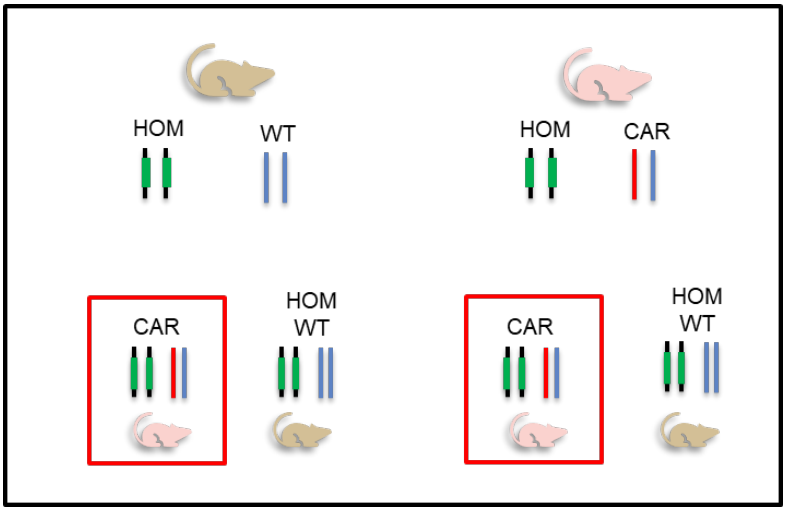
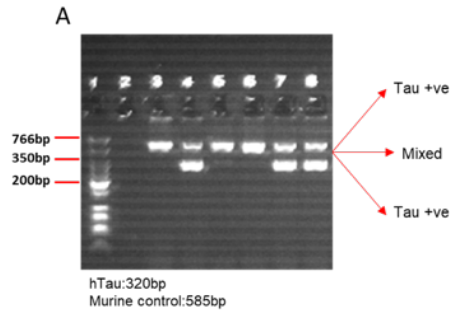


Figure 3.24: hTau genotyping scheme *describes how the breeding is done in order to have an F2 that is 50% expressing hTau and is not expressing mouse Tau. HOM= mouse tau KO, GFP has been put in place of mouse tau gene; CAR = human tau gene has been inserted into an independent locus; CAR are hemizygous (in red hTau, in blue the WT gene). Only 50% of the offspring is CAR; 50:50 mice are likely to express hTau.*

We used a kit to extract the genomic DNA from the embryos and run the PCR using human Tau primers as well as an internal murine control to confirm that the protocol itself worked.

Fig 3.25 shows that almost 50% of the embryos genotyped were tau positive, as expected from the Mendelian inheritance.



B

Seeded	**Tau+**	**Tau+**	**Tau-**	**Mixed**
Unseeded	Tau+	Tau -	Tau -	Mixed
Unseeded	Tau+	Tau+	Tau-	Mixed
Seeded	**Tau+**	**Tau -**	**Tau -**	**Mixed**

Figure 3.25: hTau embryos genotyping and plating in HT MF devices. *In order to distinguish between the hTau embryos expressing human tau and the others, they have to be genotyped. For the PCR two primers have been used, human tau and an internal mouse control (A). Once the genotype has been defined, neurons were prepared and plated in MFDs following a particular set up that allows to test all the conditions of seeding and of tau expression. Neurons were divided based on their expression of human tau, either tau positive, negative or mixed (manually mixing 50% of cells expressing htau and 50% of tau negative) (B).*

hTau cortical neurons were plated at DIV0 in HT MFDs based on their genotype either tau positive, negative or mixed (manually mixing 50% of cells expressing htau and 50% of tau negative). As previously established in RCN cultures, they were seeded at DIV7 with 18 nM of hAD seed, then methanol fixed at DIV21 to remove the soluble proteins. The staining of hTau differs from RCNs; since the tau here is human and the T49 antibody is rodent specific, the protocol was changed and 3 different antibodies were used: CP-27, for total tau, AT-8 and AT-100, for phosphorylated tau (different phosphorylated epitopes).

As shown in *Fig 3.26*, the three antibodies are all detecting endogenous, aggregated human tau. it is clear that the ratio of inclusions present in the tau mixed cultures is half of the tau positive

culture. This is expected since, to generate the mixed cultures, 1:1 of tau positive and negative embryos were combined to prepare and plate the neurons.

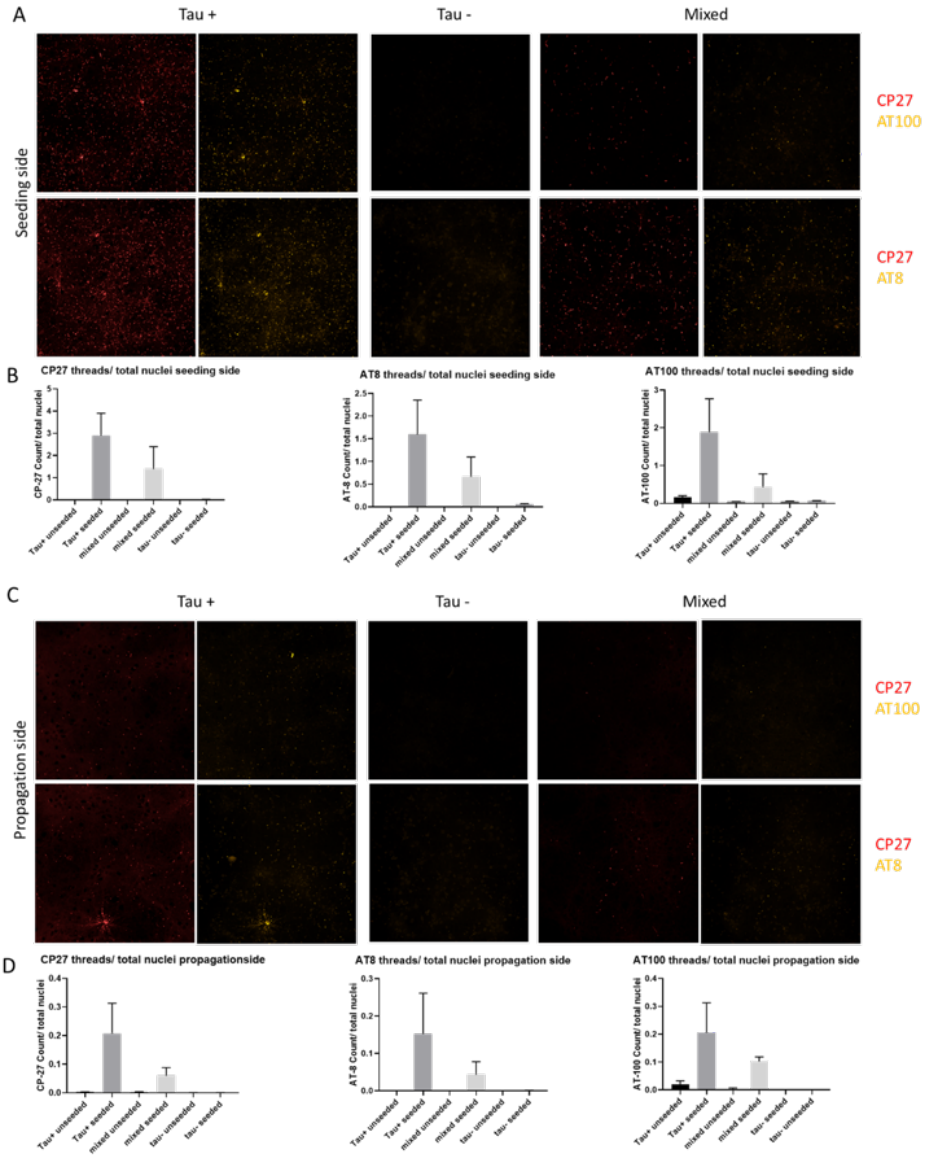


Figure 3.26: hTau antibody optimisation and correlation between tau expression and aggregate formation*. High content imaging with the Opera Phenix shows that both in the seeding (A) and in the propagation (C) side we can detect CP27, AT-8 and AT-100 positive inclusions. Their abundance is proportional to tau expression. As we can see in both B and D, tau +ve neurons have more inclusions than mixed and tau -ve neurons do not have any.*

An important feature of this assay is the presence of tau negative cells; these gave us the chance not only to detect any antibody-related background staining, but also to ensure that the signal we were detecting in tau positive cells was endogenous and not due to the hAD seed added at DIV7. As displayed in *Fig 3.26*, the signal in the tau negative cultures was very small for all the antibodies indicating that if tau is not expressed, the seed does not induce aggregation or propagation. Moreover, the seed was not detected after 14 days of incubation using the ICC protocol. This way we can analyse only the endogenous inclusions without using any other cell counterstain such as βIII-Tubulin.

To quantitively analyse these data, Harmony software was tuned and modified for every antibody and both the sliding parabola and the software training to separate tau positive and negative area were adapted.

The results of the two phospho-tau antibodies, AT-8 and AT-100, were very similar both in the seeding and propagation sides, but AT-8 results were more consistent and the signal was much cleaner, possibly due to the pipeline used. In fact, we can see from the graphs that there is a very little signal in the unseeded and in the tau negative cells with AT-100. Therefore, we decided to use AT-8 coupled with CP-27 for further experiments.
For the next experiments we also excluded the mixed cultures. Despite their usefulness to show that the more tau is expressed the more

aggregation and propagation, they were not required to test compounds in hTau cultures.

We then repeated this experiment three times excluding the mixed cultures and optimized the conditions for the secondary antibodies Alexa 647 for CP-27 and Alexa 488 for AT-8 (*Fig 3.27*).

Even though these cells expressed GFP, it was possible to use the 488 channel to detect clean inclusions. This is because the MeOH fixation washed away the soluble GFP proteins.

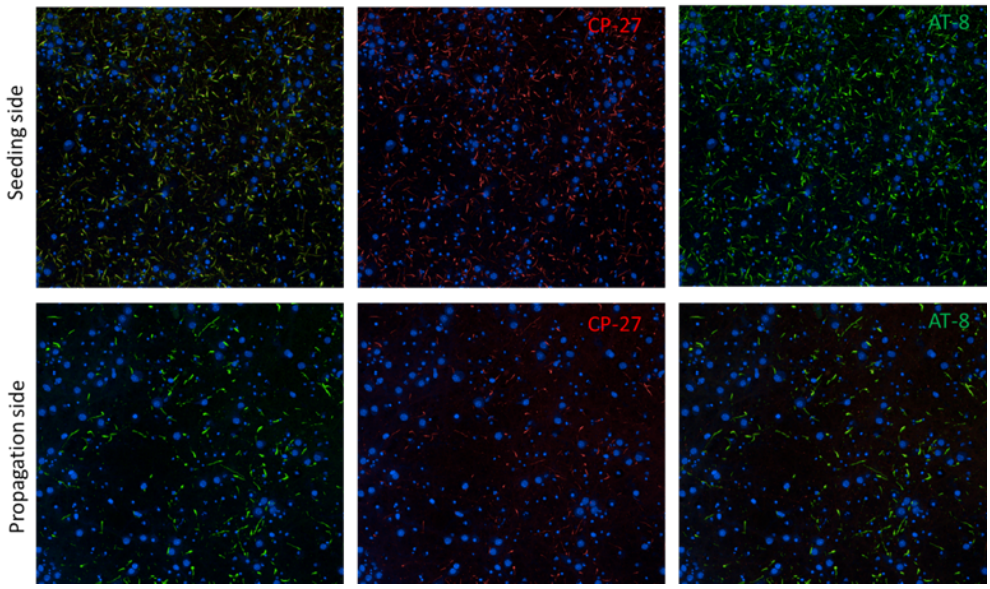


Figure 3.27: Optimisation of secondary antibodies for hTau cultures*. hTau neurons were cultured in MFDs, seeded at DIV7 and fixed at DIV21. ICC was performed using CP-27 and AT-8 as primary antibodies and Alexa 647 and Alexa 488 as secondary antibodies. As we can see these couples of primary-secondary antibodies gave a good signal and highlighted how we have more CP-27 and AT-8 positive aggregates in the seeding side than in the propagation side.*

As we can see form *Fig 3.27*, the signal window in the hTau cultures was much bigger than in RCNs possibly because, as previously demonstrated, like seeds like [139,146,184].

We can observe in some fields that CP-27 and AT-8 signals differ. It is clear that all the CP-27 positive inclusions are AT-8 positive but not vice versa *(Fig 3.28)*. We can speculate that initially, when aggregates form, they are not phosphorylated but that, over time this modification takes place and CP-27 inclusions start becoming AT-8 positive as well.

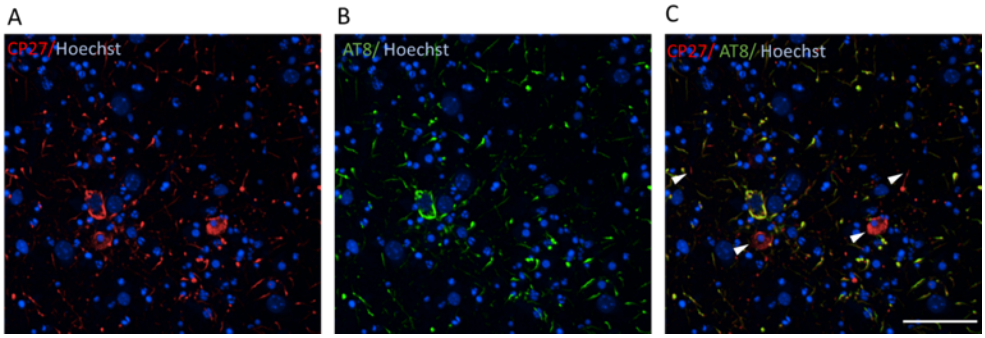


Figure 3.28: hTau MFD cultures show incomplete co-localization between CP-27 and AT-8 positive aggregates. Seeded *hTau neurons cultured for 21 days and imaged for CP-27 and AT-8 show endogenous tau aggregation and formation of both CP-27 (A) and AT-8 (B) positive threads. The two tau antibodies mostly co-localise but in some fields we can observe CP-27 formations that are not positive for AT-8 (C, arrows). 50um scale bar.*

Furthermore, as demonstrated for the RCNs, in this assay tau aggregates colocalise with MAP1B indicating that human tau aggregates are also mostly axonal and somatic (*Fig 3.29*).

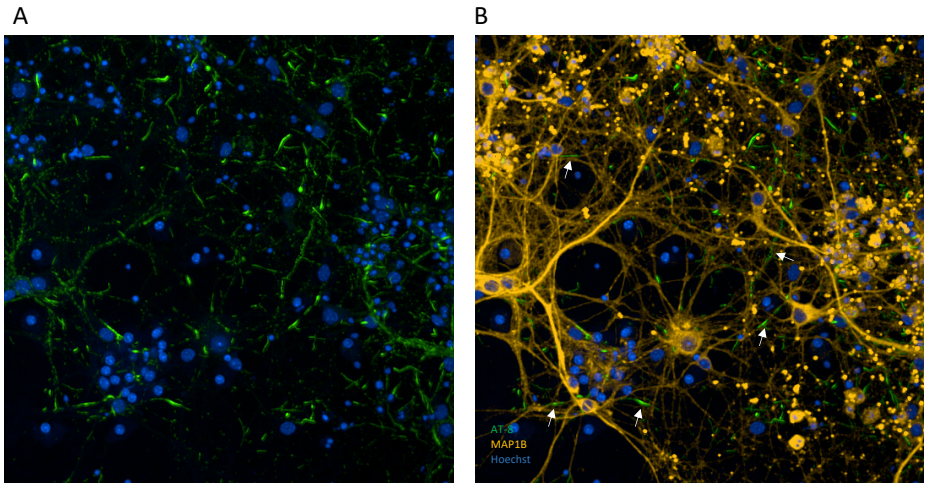


Figure 3.29: hTau aggregates co-localize with MAP1B. *Seeded hTau neurons cultured for 21 days and stained for AT-8 (A) and Map1B (B) show axonal and somatic localisation (B).*

3.5.1 hTau HT microfluidic assay: inhibiting tau propagation with a tool compound

Since we established a high throughput humanized microfluidic platform where endogenous human tau propagation can be studied, we decided to test Anle138b in this assay. hTau positive neurons were plated in MFDs at DIV0 and they were seeded with 18 nM of hAD seed at DIV7 in the seeding side. At the propagation side 10 µM of Anle138b or DMSO diluted in media was added. After a replenishment at DIV10 and 17, cells were fixed at DIV21 and imaged for CP-27, AT-8 and Hoechst using the Opera Phenix. Images were analysed with Harmony software and Cell Counter app and plotted in Graphpad Prism.

As we can see from *Fig 3.30*, Anle138b can decrease tau propagation by almost 80% compared to the DMSO control (T-Test, $p<0.01$, results from 2 independent experiments with 4 replicates for each condition). This compound seems to be more potent in this cell type compared to RCNs; since we do not know the exact mechanism of action (MOA) of Anle138b we can only speculate that it has higher affinity for the human version of tau than for the rat one.

To conclude, we have established a humanized version of the previous propagation assay that is a useful tool to test compounds and molecules for drug screening.

In fact, many compounds that efficiently prevent tau aggregation in mouse models do not work as well with human tau, so it is important to have an assay that is as physiologically relevant as possible.

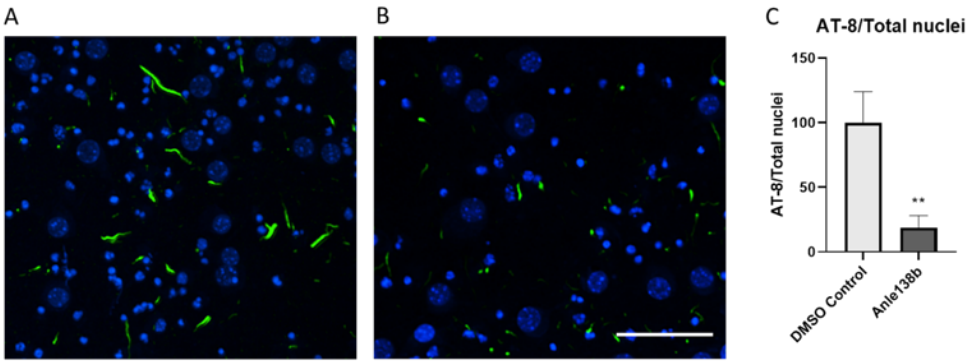


Figure 3.30: Anle138b can decrease AT-8 positive inclusions in hTau MFD cultures. *hTau neurons were plated in HT MF devices and they were treated at the propagation side with 10μM of Anle138b. AT-8 analysis at the propagation side shows that Anle138b (B) treatment induces a decrease of Tau aggregation and propagation in comparison with DMSO control (A). Statistical evaluation was performed using multiple t-test with p<0.01; (C) results are represented as mean +/- SEM of 2 independent experiments with 4 replicates for each condition.*

3.5.2 hTau HT microfluidic assay: the role of astrocytes in tau propagation and aggregation

Having developed a humanised version of the RCN microfluidic assay and having demonstrated that we can study tau propagation and test compounds and molecules specific for human tau we decided to run some preliminary experiments to study the role of other cell type in this culture. In fact, our cortical cell cultures plated in MF devices contained not only neurons, but a mixed population of cells that we never analysed in detail before.

We decided to investigate the nature of the other cell types by staining for both astrocytes (GFAP) and microglia (Iba-1 and CXCR3) after treating hTau neurons with increasing doses of hAD seed (0, 12, 18 and 25 nM).

We could not detect microglia with either Iba-1 or CXCR3 (data not shown) possibly due to the MeOH fixation that could have washed away or modified the antigen epitopes.

However, we observed a good GFAP signal (*Fig 3.31*) where intensity looked directly proportional to the seed concentration indicating that seed could induce glial activation and inflammation, in agreement with previous findings [261,262].

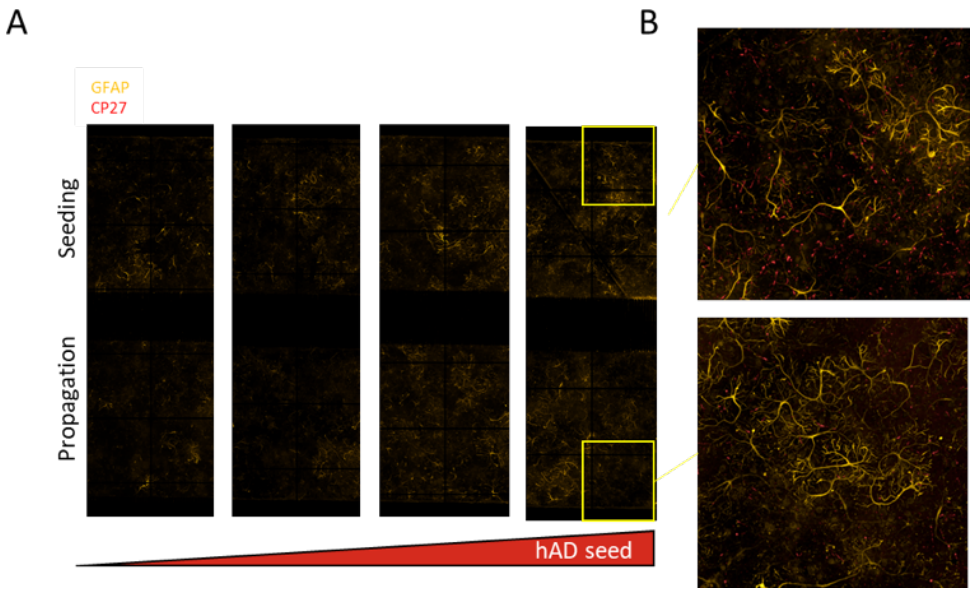


Figure 3.31: Astrocytes activation in response to hAD seed*. Four MFDevices were treated with increasing concertation of hAD seed and they were stained for CP27 and GFAP (A). Zoomed in image of the 24uM treatment that shows astrocytes surrounding CP27 inclusions.*

To further study this effect we ran additional preliminary experiments and seeded hTau neurons in MFDs, with Anle138b or DMSO only in the propagation side to reduce tau propagation and aggregation as previously shown.

We then studied the presence of astrocytes in these two conditions and observed that despite no difference in GFAP staining when comparing the control and Anle138b in the seeding side, we could see in the propagation side not only a reduction in tau signal (AT-8) but also a decrease in the astrocyte number compared to the DMSO control (*Fig 3.32, A*).

We also tried to characterize the glial population using makers for both progenitors and mature astrocytes: vimentin and ALDOC. We demonstrated that at DIV 21 there are both progenitors and mature astrocytes, probably indicating that there is a dynamic population that, in order to adapt to the culture condition can divide and promote the development of more mature and functional astrocytes (*Fig 3.32 B*).

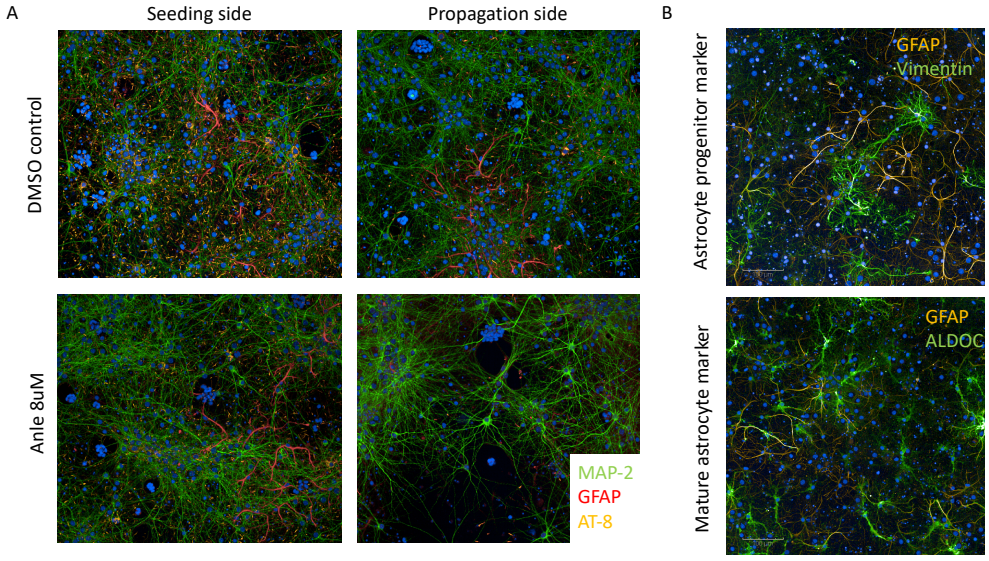


Figure 3.32: **Astrocyte activation and characterization**. *hTau neurons were treated at DIV7 with hAD seed at the seeding side and with DMSO or Anle138b at the propagation side. Cells were fixed at DIV21 and stained for GFAP, MAP-2 and AT-8 (A). To further characterize glial population, hTau neurons were stained for vimentin and ALDOC, markers of astrocyte progenitors and mature astrocytes (B).*

4. DISCUSSION & CONCLUSION

Alzheimer's disease is a progressive and complex neurodegenerative disease. It is the predominant cause of dementia worldwide, affecting circa 30% of the population over the age of 65 [263], with a clinical progression that evolves over the course of 8-10 years.

Currently there are 265 agents in clinical trials for the treatment of AD (including Mild Cognitive Impairment and FTD), (38 in Phase 1, 74 in Phase 2, 22 in Phase 3, 8 in Phase 4, 6 approved, and 117 inactive or discontinued), which represents an increase in the number of agents in each phase compared with the development pipeline from 2018 (Alzforum.org). Most of the agents in trials are molecules that target amyloid-beta production and aggregation, but approximately 8% of the molecular entities target tau. Some of these agents are small molecules (aggregation inhibitors), and others are biological therapies or a combination of targets, such as AADvac1: an active vaccine that induces the immune response by targeting multiple key epitopes in pathological forms of tau, thereby inhibiting tau aggregation and decreasing the formation of neurofibrillary tangles. Another antibody now in a clinical trials, Zagotenemab, is an anti-tau antibody engineered to capture and neutralize tau aggregates [264].

The recent increase in studies highlighting the importance of modifying tau propagation as potential treatment for AD has led to the development of antibody therapies that could prevent tau uptake in

healthy neurons. As such, it is vital to establish a robust *in vitro* model system that is able to recapitulate the cell-to-cell transmission of tau aggregates to test molecules before they progress to *in vivo* studies.

To that end, this study aimed to develop an *in vitro* neuronal model to study the aggregation and propagation of tau, with the goal to generate a model of physiological tau spreading for the systematic screening of molecules that target these mechanisms.

Aware of the importance of using a cell model that recapitulates the pathology in a physiological way, we decided to induce tau aggregation in rat cortical neurons first as a proof of principle. The assay was then modified to utilize transgenic hTau mouse cortical neurons that were seeded with hAD seed. This material is a sarkosyl insoluble extract derived from the brains of AD patients that can initiate the templated misfolding of endogenous tau, therefore inducing aggregation in a prion-like manner [125].

Initially, it was demonstrated that the procedure for generating hAD seed gives consistent results, with a similar concentration of insoluble tau obtained between different preparations. This is important because the yield of each preparation is limited and only covers a few experiments; confirming that different seed batches were capable of reproducing the same effect increased confidence when comparing experiments by eliminating concern about the source of the hAD seed.

When RCNs were seeded with hAD seed for 2 weeks, the endogenous rat tau protein aggregated, forming sarkosyl-insoluble inclusions that were T49 and AT-8 positive. As the seeding material was human tau, and T49 is a rodent tau-specific antibody, this finding indicates that the aggregates isolated from these neurons were made from endogenous rodent tau that was phosphorylated and insoluble.

Unlike other animal models, this process allows the induction of endogenous tau aggregation to recapitulate AD-like pathology [126]. The use of hAD material ensures it remains as similar to the human clinical presentation of disease as possible. In fact, it has recently been hypothesized that difficulties in generating significant tau pathology *in vitro* and *in vivo*, especially in non-Tg animals, were partly caused by suboptimal seeding materials [145]. Although artificially generated, heparin-induced tau fibrils have been used extensively in preclinical research, and it has been shown by cryo-EM that the macromolecular structure of this material is very different from the AD-patient brain extracts, which may account for the differences in seeding ability [125].

In this work, it has been demonstrated that it is possible to induce tau misfolding and aggregation in RCNs, and that there is a positive correlation between the concentration of the hAD seed used and the abundance of T49-positive aggregates. Moreover, it has been shown that the formation of detectable aggregates takes time and that, in accordance with the aggregation models that have been proposed to describe tau aggregation [107,109], the process includes different

steps. There is an initial, slow phase that lasts for 3-4 days, during which the seed is internalized and starts acting on the endogenous tau (aggregates in this phase are not visible yet). Subsequently, there is a second, fast phase where the aggregates (that can be detected with IF) can act as new seeds to induce new nucleation and elongation events, exponentially increasing the aggregate number. In fact, from day 14 to 21, the increase of threads is substantial, and the longer the neurons are kept in culture, the more T49 positive aggregates are observed.

To further test this assay platform, we used Anle138b, a compound that inhibits oligomer formation *in vitro* and *in vivo* [230,231]. In line with published data, a dose dependent decrease of tau aggregates in response to an increasing concentration of Anle138b was observed, showing that it is possible to manipulate tau aggregation and detect changes in this model.

After the aggregation assay was established, a propagation assay for studying tau propagation and testing compounds that could affect this crucial mechanism for tau spreading in AD was developed and optimised. There are several hypotheses regarding how tau can be released, taken up, and spread between cells [137]; however, it is still not clear which are the most relevant for AD progression in humans. One such hypothesis is that synaptic release of naked tau (not protected within exosomes) is one of the most important mechanisms that leads to tau transmission between neurons and that aggregates

can be transported to different brain areas along axonal projections [147]. Moreover, it is possible to target tau in the synaptic space using tau antibodies preventing its internalization [152].

To test this hypothesis, a qualitative and quantitative assay to recapitulate trans-neuronal synaptic tau spreading was developed using a novel microfluidic approach.

Microfluidic devices have been used previously as an *in vitro* model to study propagation of insoluble protein aggregates [147,180,246]. Features of their design make them ideal platforms to study interactions between two or more isolated cell populations. Indeed, in microfluidic devices, cell populations are separated not only physically, by microgroove barriers, but also hydrostatically, using a volume gradient of media that ensures that the transmission of aggregates is due to active cellular mechanisms and not passive diffusion.

Initially, commercially available 2-chamber devices from Xona were utilized to optimise the assay conditions for neuronal culture, as well as tau aggregation and propagation. Two neuronal populations were isolated with only axons able to pass through the microgrooves. It was demonstrated that when one side of the device (seeding side) was treated with hAD seed, aggregation of endogenous tau was induced in the neurons, which subsequently propagated the pathological tau into the second compartment (propagation side).

This was confirmed by the successful detection of T49-positive thread-like inclusions. To investigate the localization of these aggregates a variety of neuronal markers were used and it was shown that, in agreement with previous findings [125], they were not dendritic but axonal and somatic.

This *in vitro* propagation system uses a non-recombinant, hAD brain-derived form of seed to induce aggregation in WT RCNs. This is an improvement on other models that rely on overexpression of mutant tau [169,180] and gives credence to the argument that this is a more native and disease-relevant model, as neither overexpression of tau, nor mutations in the tau gene are causes of AD [265].

In this system, neurons form synaptic connections between the two compartments, supporting the hypothesis that aggregated tau moves anterogradely from the soma of the neurons in the seeding side to the axon in the propagation side, where aggregates are released and internalized by the second population of neurons. However, as suggested by some studies [147], the apparent propagation could also be due to retrograde transport of the aggregates if axons of neurons plated in the propagation side had projected into the seeding side, through the microgrooves; this possibility cannot be fully excluded with two-chamber devices.

To better elucidate the mechanism of propagation in these cells, both 3-chamber Xona devices and unidirectional devices (that only allow axons to grow in one direction) were used. These experiments, using the two different approaches, confirmed that misfolded, endogenous tau generated from the hAD seed in the seeding side is anterogradely transported through the axons into the propagation compartment, where it is trans-synaptically transferred to the second population and induces aggregation in a seed-dependent manner.

This body of work is in accordance with other studies [150,163], reaffirming the belief that synapses are fundamental for tau transmission. When the synaptic connection between the two neuronal populations in the microfluidic devices is lost, there is no transfer and, consequently, no aggregation of tau in the propagation side of the device.

An important feature of this platform is that, compared to previous reports, it is not only qualitative, but also quantitative and it allows a semi-automated image analysis of the whole microfluidic unit. The analysis pipeline for this assay employs both the Harmony software from Perkin Elmer, and another internally developed application, Cell Counter, which allows the separation of the seeding and propagation sides in our images for quantification. This enables comparisons of the number of neurons and tau aggregates present in each side. This is a very important component of this assay as it enables the comparison of treatments in a way that can be statistically assessed for therapeutic

effect. Most importantly, this assay was validated in collaboration with statisticians after having run multiple preliminary experiments assessing: seeding and fixing days; assay duration; and seeding concentrations. From these experiments it was observed that seeding on DIV3 resulted in a higher number of neuritic thread-like inclusions in both seeding and propagation compartments compared to seeding on DIV7. It is possible that neurons at DIV3 exhibit enhanced uptake or reduced clearance of hAD seed compared to DIV7, which could account for their enhanced response to seeding. Additionally, Wu et al. observed that neuronal activity enhances tau propagation and tau pathology *in vitro* and *in vivo* [246], therefore differences in neuronal activity between DIV3 and DIV7 could account for the different response to seeding observed at these timepoints. This hypothesis could be further explored using different techniques such as calcium imaging or electrophysiology to prove the different neuronal activity, or biochemical experiments to quantify the expression of receptors that are believed to be responsible for tau uptake such as LRP1 or HSPGs [160] as well as experiments to test the clearance ability of neurons at different time points by studying both autophagy and proteasome systems.

However, neurons at DIV3 are not fully mature and synapses form at DIV5-7 [255]. So, to improve the biological relevance of the assay, DIV7 was chosen for seeding to maximise neuronal maturation at the time of seeding.

As a result of the validation analysis, this assay format was determined to be fully quantitative and highly reproducible.

After having validated the MFD platform, Anle138b was used to investigate whether small molecules can inhibit tau aggregation. The compound showed an inhibition of tau aggregation, confirming previous findings [230,266]. The primary mechanism of action for Anle138b seems to be the inhibition of oligomer formation; it does not affect tau expression, ubiquitination or autophagy. Anle138b has been shown to act on a wide range of amyloidogenic peptides and proteins, and is thought to interfere with the formation of ordered β-sheet structures [231]. Our data in the MFD assay show an inhibitory effect of Anle138b on aggregation in both the seeding and propagation sides of the devices. Anle138b can only inhibit *de novo* tau aggregation and cannot cause the disaggregation of already formed aggregates (NMR unpublished data from our group). Therefore, the reduction of T49-positive inclusions observed in neurons on the propagation side after Anle138b application, confirms that aggregates being detected in the propagation side are actually present in those neurons. Aggregates present in the projecting axons of neurons from the seeding side would not be affected by the application of Anle138b, because they are formed in the somatic compartment and transported through the axons to the synapses. From this understanding, we can infer that this compound is affecting the new endogenous aggregation that has been induced in the neurons plated in the propagation compartment.

To characterise the species of tau that were propagated from neurons in the seeding side to the propagation compartment, conditioned media was collected from the propagation side. The conditioned media was subject to immunoprecipitation with the T49 antibody and a sarkosyl extraction, in order to concentrate the tau species present. However, no signal was detected by Western blot, possibly indicating that the level of tau is too low and that, in order to study these species, media may need to be pooled from more devices or more sensitive detection techniques need to be utilized, such as Quanterix Simoa or mass spectrometry.

Microfluidic devices have previously been used to study neuronal activity and communication *in vitro* [267]. Therefore, we sought to use this MFD assay platform for the same purpose. Calcium imaging experiments were performed using a ZEISS Axioscope that revealed not only that the neuronal populations are synchronized, and therefore synaptically connected, but also that the seeded cells are hyperexcitable relative to unseeded controls. These data strengthen the evidence from both human AD brain and transgenic AD mouse models where changes in channel properties and alteration in electrical excitability have been shown [268–270]. Moreover, it has recently been demonstrated that there is an increased AD-vulnerability and a preference of tau to aggregate within excitatory neurons, with respect to inhibitory neurons both in mouse models [138], and in AD hiPSC-derived 2D cultures and 3D cerebral organoids [271]. In line with previous findings, we have demonstrated that seed-treated

neurons are hyperexcitable compared to the unseeded controls and that excitatory neurons appear to be selectively vulnerable to tau aggregation in AD. Therefore, this model becomes more relevant in the study of tau aggregation and propagation and can be further used to help understand the causes and effects of excitatory neuronal vulnerability.

Using the Xona devices, a non-recombinant form of seed can be used to induce aggregation in non-Tg RCNs. The concentration of the hAD seed used in these experiments did not result in acute cellular toxicity, as revealed by nuclei count. Seeded pre-synaptic neurons were viable when transmitting the pathological forms of tau to post-synaptic neurons, suggesting that transmissibility of the inclusions is an event occurring prior to neuronal death. Moreover, calcium imaging demonstrated that the two populations were synchronized and functionally active. This finding is consistent with recent research that suggest that misfolded Tau does not directly cause neuronal death, but targets and impairs axonal transport and synaptic loss first [272]. Furthermore, at a more clinically relevant level, the spreading of tau precedes tangle formation in the brain [273].

In an effort to transform this system to a higher-throughput assay format, collaborators from the University of Strathclyde generated bespoke microfluidic systems that were each composed of 8 two-compartment devices, allowing higher throughput with the same device mechanics.

This process required further optimisation (plasma oven condition, coating material, neuronal density, seeding and fixing day, hAD seed concentration), but it was demonstrated that this model was valid and that the results, in terms of tau propagation, were robust. These plates can facilitate the testing of compounds as they provide more microfluidic units and require smaller volumes of compound and seed, relative to the Xona devices.

Tau propagation can also be decreased by alternative mechanisms, rather than directly targeting tau aggregation as demonstrated with Anle138b in the Xona devices. We decided to target mGluR2/3 receptors that are present in the presynaptic membrane and that have an important role in vesicle release, by modulating both voltage-sensitive calcium channels and the fusion of the snare complex with the presynaptic membrane [256,257]. Modulating mGluR2/3 with an agonist – thus preventing synaptic calcium influx and subsequent vesicle release – decreased the extent of tau propagation. This effect could be reversed using an antagonist. This confirms the role of neuronal activity in tau release; in fact, it has already been shown that neuronal activity promotes the propagation of extracellular tau *in vitro* and *in vivo* [170,172,246].

One of the most significant parts of this work was the humanisation of the microfluidic assay. As Manuel Moro (National Institution of Aging) said “There’s no perfect model for any disease; the only perfect model would be another human being, but of course that wouldn’t work. Each

model has advantages or disadvantages depending on what you're evaluating, depending what you're studying, depending what you're testing. In fact, you may have to use a combination of models to study a particular area of Alzheimer's disease" [274]. The structures of human and rodent tau are different and they exhibit different aggregation properties [182,258,275,276]. It is possible that the use of the wrong animal models has led some AD clinical trials to fail in human patients [228,277,278]. Therefore, it is crucial to consider and select the most optimal models to study this complex disease.

For this reason, we decided to humanise the microfluidic platform with a primary cell line that would express human tau. We used hTau mice, a mouse model where mouse tau has been replaced with GFP and has a human tau inserted into the genome [244]. Consequently, these neurons fluoresce green and express 3R and 4R human, wild type, tau. Due to the zygosity of the hTau allele, only 50% of littermates express hTau, and so a quick genotyping assay was developed to discriminate for tau expression. The hTau positive cells could be cultured in the small microfluidic devices, with the same viability as RCNs, and that they could be seeded with hAD seed. Moreover, endogenous tau aggregates were positive for both total tau and phosphorylated tau. Interestingly, the signal window in the hTau cultures was much larger than in the RCNs, possibly because, as previously demonstrated, the prion-like ability of aggregates to confer seeding is increased when proteins are from the same species [139,146,184]. These results reaffirmed that using a rodent tau-

expressing neurons is a limitation of the previous version of the assay; in fact, we may have lost some structural information and possibly obtained false positive effects of compound which could work on rodent tau but not on the human one. Anle138b showed a greater inhibitory effect on tau aggregation in the humanised model compared to the RCN model, emphasising the importance of using humanised models.

MFDs offer an ideal platform to study neuronal connectivity and spread of tau pathology. The number of publications involving their use in recent years supports their utility as an *in vitro* platform [150,163,180]. The architecture of microfluidic devices offers the potential to create even more complex *in vitro* systems, with respect to classic systems, which may better recapitulate the multifactorial nature of neurodegenerative diseases. The interplay between neuroinflammation and neurodegeneration has recently become clearer as it has been established that the pathological effects in AD are cell- and non-cell-autonomous and occur within the context of neurovascular or glioneuronal units [279]. For these reasons, preliminary experiments were conducted to investigate the presence of glial cells in our model and the effect of hAD seed on their activation. While microglial cells couldn't be detected, possibly due to the methanol fixation method that could have washed away or modified the antigen epitopes [280], the presence of astrocytes in these cultures was observed. Using an established marker for astrocyte activation [281], it was observed that the activation of astrocytes increased with

seed concentration and the number of aggregates formed in that culture condition. This preliminary finding is in line with previous studies demonstrating that the presence of aggregated tau induces an activation of glial cells and neuroinflammation [261,262].

It would be interesting in the future to investigate the role of neuroinflammation in tau propagation using astrocytes, oligodendrocytes and microglia. This could be achieved by measuring the release of proinflammatory cytokines from both populations of neurons in the propagation assay as a measure of the activation state of glial cells. Another potential assay could be to culture isolated oligodendrocytes, astrocytes and/or microglia in one of the microfluidic chambers and see how they affect or support tau propagation. For example, it has been shown that microglia can take up aggregated tau released by neurons to clear it and destroy seed competent species. Furthermore, when the pro-inflammatory state is dominant, the activity of these cells is compromised and they can potentially exacerbate the spread of tau pathology [282].

Another future study is to test different seeds, not only from AD brains but also from progressive supranuclear palsy (PSP) or corticobasal degeneration (CDB) since tau aggregates differently and in different cell types in each disease [78]; in AD 3R and 4R tau aggregates primarily in neurons, while in CBD and PSP 4R tau also aggregates in astrocytes and oligodendrocytes, although their morphology differs in each disease (astrocytic plaques in CBD and tufted astrocytes in

PSP). Moreover, glial cells can propagate tau aggregates independently of neuronal tau and oligodendrocytes can not only express but also transmit aggregated tau. Astrocytes do not express tau but can take it up from neurons and thereby likely contribute to the spreading [195].

In the effort to produce more disease relevant experimental models, microfluidic devices could also be used for the growth of human iPSC derived neuronal cultures that can be seeded and transmit seed-induced pathology [283].

Microfluidic devices provide multiple possibilities in terms of platform design. The ability to collaborate with Universities or companies that produce them is a big potential not only for exploratory research but also for drug discovery. For example, in future this assay could be further miniaturised into a device conforming to the dimensions of a 384-well plate that allows the handling of 80 two-chamber devices simultaneously (*Fig 4.1*).

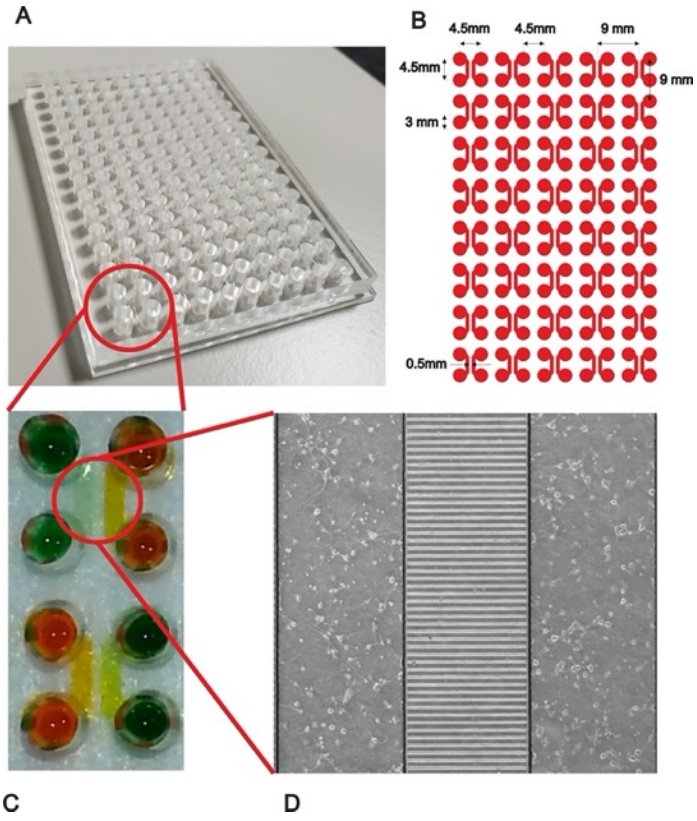


Figure 4.1: Microfluidic platform in a 384-well plate format. *Further miniaturization of the microfluidic platform (A) was obtained conforming to the dimensions of a 384-well plate (B), facilitating the handling of 80 two-chamber devices simultaneously. Zoomed view of the microfluidic layout (C) and brightfield image of a mixed hippocampal culture at DIV10 (D).*

Clearly, as all the *in-vitro* assays, this platform has limitations that are mainly practical. One is the cost that this type of experiment has; in fact, not only these devices are hand-made and consequently very expensive, but the plasma oven and the microscope needed for the imaging are not available in all the standard laboratories. Moreover, the handling must be very meticulous. It is not easy to plate the cells into the channels and it is very plausible to kill the neurons during this step of the protocol if is not taken enough care. These experiments are

also quite long and time consuming since the plating and all the media changes are manually done. However, it is possible to upgrade this system with a robot that automatically changes the media, but it would add another cost to the list of the expenses. Moreover, it would be possible to shorten the experiment length using primary neurons made from a mouse that expresses a mutated form of tau as P301S or P301L that would speed up the endogenous aggregation, but we would use a form of hTau that is not representative of the AD physiopathology. Finally, this is always an *in vitro* model so it is possible that the effect that we observe in the neurons plated on glass is not the same that naturally happens at brain level, but we have to find a compromise between what we can model and what we have to suppose.

Nevertheless, this microfluidic assay is a unique platform that can be used for specific questions such as protein propagation. Due to the costs and the length of the protocol it should be used wisely. As an example, once a new molecule is predicted as a possible tau aggregation and/or propagation inhibitor it should be first tested in the cheaper and easier 96-well RCNs assay that can not only show if the drug is actually able to reduce tau aggregation in a neuronal model but can also indicate the potency of the drug and suggest the best concentration to be used for the MFD assay. Only at this point we can use the MFD assay to test if the effect observed is related to a decrease in tau propagation that consequently leads to a decrease in the endogenous aggregation. If then the drug shows no effects

compared to the vehicle control it means that its acts on different mechanisms such as, as an example, elongation inhibition. If the drug shows effects, we can say for certain that it is an inhibitor of tau release and/or uptake and it can be further studied in collaboration with chemists to improve its physical and chemical characteristics in order to be ideal for *in vivo* treatments.

In conclusion, this work has established a robust and quantitative microfluidic assay that can model elements of sporadic human tauopathies, namely the transneuronal propagation of pathological tau. Using both RCNs and hTau cortical neurons seeded with hAD seed, it was possible to quantify the formation and propagation of endogenous tau inclusions and to test the effect of inhibitor molecules specifically targeting either rodent or human tau. It was demonstrated that this assay platform can be further utilised to perform exploratory studies, such as monitoring the functional activity and connectivity of neuronal cultures, as well as investigating the role of different cell types in aggregation and propagation.

5. BIBLIOGRAPHY

[1] R. Peters, Ageing and the brain., Postgrad. Med. J. 82 (2006) 84–88. https://doi.org/10.1136/pgmj.2005.036665.

[2] V. Galvan, K. Jin, Neurogenesis in the aging brain., Clin. Interv. Aging. 2 (2007) 605–610. https://doi.org/10.2147/cia.s1614.

[3] Y. Yan, H. Yang, Y. Xie, Y. Ding, D. Kong, H. Yu, Research Progress on Alzheimer's Disease and Resveratrol, Neurochem. Res. (2020). https://doi.org/10.1007/s11064-020-03007-0.

[4] Association, A.S. 2019 Alzheimer's disease facts and figures., Alzheimers Dement. 15 (2019) 321–387.

[5] H. Braak, E. Braak, Staging of alzheimer's disease-related neurofibrillary changes, Neurobiol. Aging. 16 (1995) 271–278. https://doi.org/10.1016/0197-4580(95)00021-6.

[6] J. Lewis, D.W. Dickson, W.L. Lin, L. Chisholm, A. Corral, G. Jones, S.H. Yen, N. Sahara, L. Skipper, D. Yager, C. Eckman, J. Hardy, M. Hutton, E. McGowan, Enhanced neurofibrillary degeneration in transgenic mice expressing mutant tau and APP, Science (80-.). 293 (2001) 1487–1491. https://doi.org/10.1126/science.1058189.

[7] E. Nichols, C.E. I Szoeke, S. Emil Vollset, N. Abbasi, F. Abd-Allah, J. Abdela, M. Taki Eddine Aichour, R.O. Akinyemi, F. Alahdab, S.W. Asgedom, A. Awasthi, S.L. Barker-Collo, B.T. Baune, Y. Bã, A.B. Belachew, D.A. Bennett, B. Biadgo, A. Bijani, M. Shahdaat Bin Sayeed, C. Brayne, D.O. Carpenter, L. Carvalho, E. Cerin, J.-Y.J. Choi, A. Kim Dang, M.G. Degefa, S. Djalalinia, M. Dubey, E. Ejeta Duken, D. Edvardsson, M. Endres, S. Eskandarieh, A. Faro, F. Farzadfar, S.-M. Fereshtehnejad, E. Fernandes, I. Filip, F. Fischer, A.K. Gebre, D. Geremew, M. Ghasemi-Kasman, E. V Gnedovskaya, R. Gupta, V. Hachinski, T.B. Hagos, S. Hamidi, G.J. Hankey, J.M. Haro, S.I. Hay, S.N. Sina Irvani, R.P. Jha, J.B. Jonas, R. Kalani, A. Kasaeian, Y. Saleh Khader, I.A. Khalil, E. Ahmad Khan, T. Khanna, T.A. M Khoja, J. Khubchandani, A. Kisa, K. Kissimova-Skarbek, M. KivimÃ, A. Koyanagi, K.J. Krohn, G. Logroscino, S. Lorkowski,

M. Majdan, R. Malekzadeh, W. Mã, G. Mengistu, A. Meretoja, M. Mohammadi, M. Mohammadi-Khanaposhtani, A.H. Mokdad, S. Mondello, G. Moradi, G. Nagel, M. Naghavi, G. Naik, L.H. Nguyen, T.H. Nguyen, Y.L. Nirayo, M.R. Nixon, R. Ofori-Asenso, F.A. Ogbo, A.T. Olagunju, M.O. Owolabi, S. Panda-Jonas, ria M. de Azeredo Passos, D.M. Pereira, G.D. Pinilla-Monsalve, M.A. Piradov, C.D. Pond, H. Poustchi, M. Qorbani, A. Radfar, R.C. Reiner Jr, S.R. Robinson, G. Roshandel, A. Rostami, T.C. Russ, P.S. Sachdev, H. Safari, S. Safiri, R. Sahathevan, Y. Salimi, M. Satpathy, M. Sawhney, M. Saylan, S.G. Sepanlou, A. Shafieesabet, M.A. Shaikh, M. Ali Sahraian, M. Shigematsu, R. Shiri, I. Shiue, P. Silva, M. Smith, S. Sobhani, D.J. Stein, R. TabarÃ, M.R. Tovani-Palone, B.X. Tran, T. Thanh Tran, A.T. Tsegay, I. Ullah, N. Venketasubramanian, V. Vlassov, Y.-P. Wang, J. Weiss, R. Westerman, T. Wijeratne, G.M. Wyper, Y. Yano, E.M. Yimer, N. Yonemoto, M. Yousefifard, Z. Zaidi, Z. Zare, T. Vos, V.L. Feigin, C.J. L Murray, D. Collaborators, Global, regional, and national burden of Alzheimer's disease and other dementias, 1990-2016: a systematic analysis for the Global Burden of Disease Study 2016, Lancet Neurol. 18 (2019) 88–106. https://doi.org/10.1016/S1474-4422(18)30403-4.

[8] F. Bermejo-Pareja, J. Benito-León, S. Vega, M.J. Medrano, G.C. Román, Incidence and subtypes of dementia in three elderly populations of central Spain., J. Neurol. Sci. 264 (2008) 63–72. https://doi.org/10.1016/j.jns.2007.07.021.

[9] G.G. Glenner, C.W. Wong, Alzheimer's disease and Down's syndrome: sharing of a unique cerebrovascular amyloid fibril protein., Biochem. Biophys. Res. Commun. 122 (1984) 1131–5. http://www.ncbi.nlm.nih.gov/pubmed/6236805 (accessed May 30, 2015).

[10] C. Wu, J. Scott, J.E. Shea, Binding of congo red to amyloid protofibrils of the alzheimer Aβ9-40 peptide probed by molecular dynamics simulations, Biophys. J. 103 (2012) 550–557. https://doi.org/10.1016/j.bpj.2012.07.008.

[11] D. Vilchez, I. Saez, A. Dillin, The role of protein clearance mechanisms in organismal ageing and age-related diseases,

Nat. Commun. 5 (2014). https://doi.org/10.1038/ncomms6659.

[12] P.A. Temussi, L. Masino, A. Pastore, From Alzheimer to Huntington: why is a structural understanding so difficult?, EMBO J. 22 (2003) 355–61. https://doi.org/10.1093/emboj/cdg044.

[13] J. Dorszewska, M. Prendecki, A. Oczkowska, M. Dezor, W. Kozubski, Molecular Basis of Familial and Sporadic Alzheimer's Disease, Curr. Alzheimer Res. 13 (2016) 952–963. https://doi.org/10.2174/1567205013666160314150501.

[14] D.J. Selkoe, Alzheimer's disease: genes, proteins, and therapy., Physiol. Rev. 81 (2001) 741–66. http://www.ncbi.nlm.nih.gov/pubmed/11274343 (accessed May 25, 2015).

[15] S.S. Sisodia, E.H. Koo, P.N. Hoffman, G. Perry, D.L. Price, Identification and transport of full-length amyloid precursor proteins in rat peripheral nervous system, J. Neurosci. 13 (1993) 3136–3142. https://doi.org/10.1523/jneurosci.13-07-03136.1993.

[16] H. Zheng, E.H. Koo, The amyloid precursor protein: beyond amyloid., Mol. Neurodegener. 1 (2006) 5. https://doi.org/10.1186/1750-1326-1-5.

[17] N. Miyashita, J.E. Straub, D. Thirumalai, Y. Sugita, Transmembrane structures of amyloid precursor protein dimer predicted by replica-exchange molecular dynamics simulations, J. Am. Chem. Soc. 131 (2009) 3438–3439. https://doi.org/10.1021/ja809227c.

[18] M.A. Meraz-Ríos, D. Franco-Bocanegra, D. Toral Rios, V. Campos-Peña, Early onset Alzheimer's disease and oxidative stress, Oxid. Med. Cell. Longev. 2014 (2014). https://doi.org/10.1155/2014/375968.

[19] T. V. Andreeva, W.J. Lukiw, E.I. Rogaev, Biological basis for amyloidogenesis in Alzheimer'S disease, Biochem. 82 (2017) 122–139. https://doi.org/10.1134/S0006297917020043.

[20] Q. Jiang, C.Y.D. Lee, S. Mandrekar, B. Wilkinson, P. Cramer, N. Zelcer, K. Mann, B. Lamb, T.M. Willson, J.L. Collins, J.C. Richardson, J.D. Smith, T.A. Comery, D. Riddell, D.M. Holtzman, P. Tontonoz, G.E. Landreth, ApoE Promotes the Proteolytic Degradation of Aβ, Neuron. 58 (2008) 681–693. https://doi.org/10.1016/j.neuron.2008.04.010.

[21] E.H. Corder, a M. Saunders, W.J. Strittmatter, D.E. Schmechel, P.C. Gaskell, G.W. Small, a D. Roses, J.L. Haines, M. a Pericak-Vance, Gene dose of apolipoprotein E type 4 allele and the risk of Alzheimer's disease in late onset families., Science. 261 (1993) 921–923. https://doi.org/10.1126/science.8346443.

[22] W.J. Strittmatter, A.M. Saunders, D. Schmechel, M. Pericak-Vance, J. Enghild, G.S. Salvesen, A.D. Roses, Apolipoprotein E: high-avidity binding to beta-amyloid and increased frequency of type 4 allele in late-onset familial Alzheimer disease., Proc. Natl. Acad. Sci. U. S. A. 90 (1993) 1977–1981. https://doi.org/10.1073/pnas.90.5.1977.

[23] J.C. Bis, X. Jian, B.W. Kunkle, Y. Chen, K.L. Hamilton-Nelson, W.S. Bush, W.J. Salerno, D. Lancour, Y. Ma, A.E. Renton, E. Marcora, J.J. Farrell, Y. Zhao, L. Qu, S. Ahmad, N. Amin, P. Amouyel, G.W. Beecham, J.E. Below, D. Campion, C. Charbonnier, J. Chung, P.K. Crane, C. Cruchaga, L.A. Cupples, J.F. Dartigues, S. Debette, J.F. Deleuze, L. Fulton, S.B. Gabriel, E. Genin, R.A. Gibbs, A. Goate, B. Grenier-Boley, N. Gupta, J.L. Haines, A.S. Havulinna, S. Helisalmi, M. Hiltunen, D.P. Howrigan, M.A. Ikram, J. Kaprio, J. Konrad, A. Kuzma, E.S. Lander, M. Lathrop, T. Lehtimäki, H. Lin, K. Mattila, R. Mayeux, D.M. Muzny, W. Nasser, B. Neale, K. Nho, G. Nicolas, D. Patel, M.A. Pericak-Vance, M. Perola, B.M. Psaty, O. Quenez, F. Rajabli, R. Redon, C. Reitz, A.M. Remes, V. Salomaa, C. Sarnowski, H. Schmidt, M. Schmidt, R. Schmidt, H. Soininen, T.A. Thornton, G. Tosto, C. Tzourio, S.J. van der Lee, C.M. van Duijn, B. Vardarajan, W. Wang, E. Wijsman, R.K. Wilson, D. Witten, K.C. Worley, X. Zhang, C. Bellenguez, J.C. Lambert, M.I. Kurki, A. Palotie, M. Daly, E. Boerwinkle, K.L. Lunetta, A.L. Destefano, J. Dupuis, E.R. Martin, G.D. Schellenberg, S. Seshadri, A.C. Naj, M. Fornage, L.A. Farrer, Whole exome

sequencing study identifies novel rare and common Alzheimer's-Associated variants involved in immune response and transcriptional regulation, Mol. Psychiatry. (2018). https://doi.org/10.1038/s41380-018-0112-7.

[24] E. Head, D. Powell, B.T. Gold, F.A. Schmitt, Alzheimer's Disease in Down Syndrome., Eur. J. Neurodegener. Dis. 1 (2012) 353–364.

[25] J.L. Down, Observations on an ethnic classification of idiots, Ment. Retard. 33 (1995) 54–56.

[26] A. Rovelet-Lecrux, D. Hannequin, G. Raux, N. Le Meur, A. Laquerrière, A. Vital, C. Dumanchin, S. Feuillette, A. Brice, M. Vercelletto, F. Dubas, T. Frebourg, D. Campion, APP locus duplication causes autosomal dominant early-onset Alzheimer disease with cerebral amyloid angiopathy., Nat. Genet. 38 (2006) 24–26. https://doi.org/10.1038/ng1718.

[27] M. Tanaka, Y.M. Kim, G. Lee, E. Junn, T. Iwatsubo, M.M. Mouradian, Aggresomes Formed by ??-Synuclein and Synphilin-1 Are Cytoprotective, J. Biol. Chem. 279 (2004) 4625–4631. https://doi.org/10.1074/jbc.M310994200.

[28] D.M. Mann, M.M. Esiri, The pattern of acquisition of plaques and tangles in the brains of patients under 50 years of age with Down's syndrome., J. Neurol. Sci. 89 (1989) 169–179. https://doi.org/10.1016/0022-510x(89)90019-1.

[29] C. Mori, E.T. Spooner, K.E. Wisniewski, T.M. Wisniewski, H. Yamaguchi, T.C. Saido, D.R. Tolan, D.J. Selkoe, C.A. Lemere, Intraneuronal Aβ42 accumulation in Down syndrome brain, Amyloid. 9 (2002) 88–102. https://doi.org/10.3109/13506120208995241.

[30] D.M. Wilcock, Neuroinflammation in the aging down syndrome brain; lessons from Alzheimer's disease., Curr. Gerontol. Geriatr. Res. 2012 (2012) 170276. https://doi.org/10.1155/2012/170276.

[31] P. Cras, M. Kawai, D. Lowery, P. Gonzalez-DeWhitt, B.

Greenberg, G. Perry, Senile plaque neurites in Alzheimer disease accumulate amyloid precursor protein, Proc. Natl. Acad. Sci. U. S. A. 88 (1991) 7552–7556. https://doi.org/10.1073/pnas.88.17.7552.

[32] M. Nicolas, B.A. Hassan, Amyloid precursor protein and neural development, Dev. 141 (2014) 2543–2548. https://doi.org/10.1242/dev.108712.

[33] M.P. Mattson, Cellular actions of beta-amyloid precursor protein and its soluble and fibrillogenic derivatives, Physiol Rev. 77 (1997) 1081–1132. http://physrev.physiology.org/content/77/4/1081 (accessed August 24, 2015).

[34] D.M. Hartley, D.M. Walsh, C.P. Ye, T. Diehl, S. Vasquez, P.M. Vassilev, D.B. Teplow, D.J. Selkoe, Protofibrillar intermediates of amyloid beta-protein induce acute electrophysiological changes and progressive neurotoxicity in cortical neurons., J. Neurosci. 19 (1999) 8876–84. http://www.ncbi.nlm.nih.gov/pubmed/10516307 (accessed August 25, 2015).

[35] L.C. Serpell, Alzheimer's amyloid fibrils: structure and assembly., Biochim. Biophys. Acta. 1502 (2000) 16–30. http://www.ncbi.nlm.nih.gov/pubmed/10899428 (accessed August 18, 2015).

[36] C.A. Ross, M.A. Poirier, Protein aggregation and neurodegenerative disease., Nat. Med. 10 Suppl (2004) S10-7. https://doi.org/10.1038/nm1066.

[37] R. Kayed, E. Head, J.L. Thompson, T.M. McIntire, S.C. Milton, C.W. Cotman, C.G. Glabe, Common structure of soluble amyloid oligomers implies common mechanism of pathogenesis., Science. 300 (2003) 486–9. https://doi.org/10.1126/science.1079469.

[38] G. Bitan, S.S. Vollers, D.B. Teplow, Elucidation of primary structure elements controlling early amyloid beta-protein oligomerization., J. Biol. Chem. 278 (2003) 34882–9.

https://doi.org/10.1074/jbc.M300825200.

[39] S.L. Chan, K. Furukawa, M.P. Mattson, Presenilins and APP in neuritic and synaptic plasticity: implications for the pathogenesis of Alzheimer's disease., Neuromolecular Med. 2 (2002) 167–96. https://doi.org/10.1385/NMM:2:2:167.

[40] Y.J. Wang, H.D. Zhou, X.F. Zhou, Clearance of amyloid-beta in Alzheimer's disease: progress, problems and perspectives, Drug Discov. Today. 11 (2006) 931–938. https://doi.org/10.1016/j.drudis.2006.08.004.

[41] H. Wolburg, W. Paulus, Choroid plexus: Biology and pathology, Acta Neuropathol. 119 (2010) 75–88. https://doi.org/10.1007/s00401-009-0627-8.

[42] M. Shibata, S. Yamada, S. Ram Kumar, M. Calero, J. Bading, B. Frangione, D.M. Holtzman, C.A. Miller, D.K. Strickland, J. Ghiso, B. V. Zlokovic, Clearance of Alzheimer's amyloid-β1-40 peptide from brain by LDL receptor-related protein-1 at the blood-brain barrier, J. Clin. Invest. 106 (2000) 1489–1499. https://doi.org/10.1172/JCI10498.

[43] F.C. Lam, R. Liu, P. Lu, A.B. Shapiro, J.M. Renoir, F.J. Sharom, P.B. Reiner, beta-Amyloid efflux mediated by p-glycoprotein., J. Neurochem. 76 (2001) 1121–1128. https://doi.org/10.1046/j.1471-4159.2001.00113.x.

[44] H. Kanemitsu, T. Tomiyama, H. Mori, Human neprilysin is capable of degrading amyloid beta peptide not only in the monomeric form but also the pathological oligomeric form., Neurosci. Lett. 350 (2003) 113–116. https://doi.org/10.1016/s0304-3940(03)00898-x.

[45] A. Caccamo, S. Oddo, M.C. Sugarman, Y. Akbari, F.M. LaFerla, Age- and region-dependent alterations in Abeta-degrading enzymes: implications for Abeta-induced disorders., Neurobiol. Aging. 26 (2005) 645–654. https://doi.org/10.1016/j.neurobiolaging.2004.06.013.

[46] J.A. Hardy, G.A. Higgins, J.A. Hardy, G.A. Higgins, Alzheimer '

s Disease : The Amyloid Cascade Hypothesis, Science (80-.). 256 (1992) 184–185.

[47] J.Y. Koh, L.L. Yang, C.W. Cotman, Beta-amyloid protein increases the vulnerability of cultured cortical neurons to excitotoxic damage., Brain Res. 533 (1990) 315–20. http://www.ncbi.nlm.nih.gov/pubmed/2289145 (accessed August 22, 2015).

[48] V.D. Bianca, S. Dusi, E. Bianchini, I. Dal Prà, F. Rossi, beta-amyloid activates the O-2 forming NADPH oxidase in microglia, monocytes, and neutrophils. A possible inflammatory mechanism of neuronal damage in Alzheimer's disease., J. Biol. Chem. 274 (1999) 15493–9. http://www.ncbi.nlm.nih.gov/pubmed/10336441 (accessed September 20, 2015).

[49] L. Meda, M.A. Cassatella, G.I. Szendrei, L. Otvos, P. Baron, M. Villalba, D. Ferrari, F. Rossi, Activation of microglial cells by beta-amyloid protein and interferon-gamma., Nature. 374 (1995) 647–50. https://doi.org/10.1038/374647a0.

[50] S.M. Dudek, M.F. Bear, Homosynaptic long-term depression in area CA1 of hippocampus and effects of N-methyl-D-aspartate receptor blockade, Proc. Natl. Acad. Sci. U. S. A. 89 (1992) 4363–4367. https://doi.org/10.1073/pnas.89.10.4363.

[51] Q.-S. Chen, W.-Z. Wei, T. Shimahara, C.-W. Xie, Alzheimer amyloid beta-peptide inhibits the late phase of long-term potentiation through calcineurin-dependent mechanisms in the hippocampal dentate gyrus., Neurobiol. Learn. Mem. 77 (2002) 354–371. https://doi.org/10.1006/nlme.2001.4034.

[52] D.M. Walsh, I. Klyubin, J. V Fadeeva, W.K. Cullen, R. Anwyl, M.S. Wolfe, M.J. Rowan, D.J. Selkoe, Naturally secreted oligomers of amyloid beta protein potently inhibit hippocampal long-term potentiation in vivo., Nature. 416 (2002) 535–9. https://doi.org/10.1038/416535a.

[53] J. Wu, R. Anwyl, M.J. Rowan, β-Amyloid selectively augments NMDA receptor-mediated synaptic transmission in rat

hippocampus, Neuroreport. 6 (1995). https://journals.lww.com/neuroreport/Fulltext/1995/11270/__Amyloid_selectively_augments_NMDA.31.aspx.

[54] H. Wang, A. Megill, K. He, A. Kirkwood, H.K. Lee, Consequences of inhibiting amyloid precursor protein processing enzymes on synaptic function and plasticity, Neural Plast. 2012 (2012). https://doi.org/10.1155/2012/272374.

[55] M. Brini, T. Calì, D. Ottolini, E. Carafoli, Neuronal calcium signaling: Function and dysfunction, Cell. Mol. Life Sci. 71 (2014) 2787–2814. https://doi.org/10.1007/s00018-013-1550-7.

[56] T.J.B. Simons, Calcium and neuronal function, Neurosurg. Rev. 11 (1988) 119–129. https://doi.org/10.1007/BF01794675.

[57] M.P. Mattson, S.L. Chan, Neuronal and glial calcium signaling in Alzheimer's disease., Cell Calcium. 34 385–97. http://www.ncbi.nlm.nih.gov/pubmed/12909083 (accessed September 20, 2015).

[58] S. Guntupalli, J. Widagdo, V. Anggono, Amyloid- β -Induced Dysregulation of AMPA Receptor Trafficking, Neural Plast. 2016 (2016). https://doi.org/10.1155/2016/3204519.

[59] K. Saito, J.S. Elce, J.E. Hamos, R.A. Nixon, Widespread activation of calcium-activated neutral proteinase (calpain) in the brain in Alzheimer disease: a potential molecular basis for neuronal degeneration., Proc. Natl. Acad. Sci. U. S. A. 90 (1993) 2628–32. http://www.pubmedcentral.nih.gov/articlerender.fcgi?artid=46148&tool=pmcentrez&rendertype=abstract (accessed August 20, 2015).

[60] D. Gabuzda, J. Busciglio, L.B. Chen, P. Matsudaira, B.A. Yankner, Inhibition of energy metabolism alters the processing of amyloid precursor protein and induces a potentially amyloidogenic derivative., J. Biol. Chem. 269 (1994) 13623–8. http://www.ncbi.nlm.nih.gov/pubmed/8175797 (accessed September 20, 2015).

[61] C.R.J. Jack, D.S. Knopman, W.J. Jagust, L.M. Shaw, P.S. Aisen, M.W. Weiner, R.C. Petersen, J.Q. Trojanowski, Hypothetical model of dynamic biomarkers of the Alzheimer's pathological cascade., Lancet. Neurol. 9 (2010) 119–128. https://doi.org/10.1016/S1474-4422(09)70299-6.

[62] C.R.J. Jack, D.S. Knopman, W.J. Jagust, R.C. Petersen, M.W. Weiner, P.S. Aisen, L.M. Shaw, P. Vemuri, H.J. Wiste, S.D. Weigand, T.G. Lesnick, V.S. Pankratz, M.C. Donohue, J.Q. Trojanowski, Tracking pathophysiological processes in Alzheimer's disease: an updated hypothetical model of dynamic biomarkers., Lancet. Neurol. 12 (2013) 207–216. https://doi.org/10.1016/S1474-4422(12)70291-0.

[63] D.W. Dickson, H.A. Crystal, L.A. Mattiace, D.M. Masur, A.D. Blau, P. Davies, S.H. Yen, M.K. Aronson, Identification of normal and pathological aging in prospectively studied nondemented elderly humans, Neurobiol. Aging. 13 (1992) 179–189. https://doi.org/10.1016/0197-4580(92)90027-U.

[64] A.D.C. Alonso, T. Zaidi, I. Grundke-Iqbal, K. Iqbal, Role of abnormally phosphorylated tau in the breakdown of microtubules in Alzheimer disease, Proc. Natl. Acad. Sci. U. S. A. 91 (1994) 5562–5566. https://doi.org/10.1073/pnas.91.12.5562.

[65] B. Eftekharzadeh, J.G. Daigle, L.E. Kapinos, A. Coyne, J. Schiantarelli, Y. Carlomagno, C. Cook, S.J. Miller, S. Dujardin, A.S. Amaral, J.C. Grima, R.E. Bennett, K. Tepper, M. DeTure, C.R. Vanderburgh, B.T. Corjuc, S.L. DeVos, J.A. Gonzalez, J. Chew, S. Vidensky, F.H. Gage, J. Mertens, J. Troncoso, E. Mandelkow, X. Salvatella, R.Y.H. Lim, L. Petrucelli, S. Wegmann, J.D. Rothstein, B.T. Hyman, Tau Protein Disrupts Nucleocytoplasmic Transport in Alzheimer's Disease, Neuron. 99 (2018) 925-940.e7. https://doi.org/10.1016/j.neuron.2018.07.039.

[66] M. Kidd, Paired helical filaments in electron microscopy of Alzheimer's Disease, Nature. 197 (1963) 192–193. https://doi.org/10.1038/197192b0.

[67] A.W.P. Fitzpatrick, B. Falcon, S. He, A.G. Murzin, G. Murshudov, H.J. Garringer, R.A. Crowther, B. Ghetti, M. Goedert, S.H.W. Scheres, Cryo-EM structures of tau filaments from Alzheimer's disease, Nature. 547 (2017) 185–190. https://doi.org/10.1038/nature23002.

[68] H. Braak, E. Braak, I. Grundke-Iqbal, K. Iqbal, Occurrence of neuropil threads in the senile human brain and in Alzheimer's disease: A third location of paired helical filaments outside of neurofibrillary tangles and neuritic plaques, Neurosci. Lett. 65 (1986) 351–355. https://doi.org/10.1016/0304-3940(86)90288-0.

[69] D.P. Perl, Neuropathology of Alzheimer's disease, Mt. Sinai J. Med. 77 (2010) 32–42. https://doi.org/10.1002/msj.20157.

[70] G.B. Witman, D.W. Cleveland, M.D. Weingarten, M.W. Kirschner, Tubulin requires tau for growth into microtubule initiating sites, Proc. Natl. Acad. Sci. U. S. A. 73 (1976) 4070–4074. https://doi.org/10.1073/pnas.73.11.4070.

[71] F. Liu, C.X. Gong, Tau exon 10 alternative splicing and tauopathies, Mol. Neurodegener. 3 (2008) 8. https://doi.org/10.1186/1750-1326-3-8.

[72] W. Noble, D.P. Hanger, C.C.J. Miller, S. Lovestone, The importance of tau phosphorylation for neurodegenerative diseases, Front. Neurol. 4 JUL (2013). https://doi.org/10.3389/fneur.2013.00083.

[73] R.L. Neve, P. Harris, K.S. Kosik, D.M. Kurnit, T.A. Donlon, Identification of cDNA clones for the human microtubule-associated protein tau and chromosomal localization of the genes for tau and microtubule-associated protein 2, Mol. Brain Res. 1 (1986) 271–280. https://doi.org/10.1016/0169-328X(86)90033-1.

[74] C. Conrad, J. Zhu, C. Conrad, D. Schoenfeld, Z. Fang, M. Ingelsson, S. Stamm, G. Church, B.T. Hyman, Single molecule profiling of tau gene expression in Alzheimer's disease, J. Neurochem. 103 (2007) 1228–1236.

https://doi.org/10.1111/j.1471-4159.2007.04857.x.

[75] D. Trabzuni, S. Wray, J. Vandrovcova, A. Ramasamy, R. Walker, C. Smith, C. Luk, J.R. Gibbs, A. Dillman, D.G. Hernandez, S. Arepalli, A.B. Singleton, M.R. Cookson, A.M. Pittman, R. de Silva, M.E. Weale, J. Hardy, M. Ryten, MAPT expression and splicing is differentially regulated by brain region: relation to genotype and implication for tauopathies., Hum. Mol. Genet. 21 (2012) 4094–103. https://doi.org/10.1093/hmg/dds238.

[76] S. Jeganathan, M. Von Bergen, H. Brutlach, H.J. Steinhoff, E. Mandelkow, Global hairpin folding of tau in solution, Biochemistry. 45 (2006) 2283–2293. https://doi.org/10.1021/bi0521543.

[77] S. Wegmann, I.D. Medalsy, E. Mandelkow, D.J. Müller, The fuzzy coat of pathological human Tau fibrils is a two-layered polyelectrolyte brush, Proc. Natl. Acad. Sci. U. S. A. 110 (2012) E313–E321. https://doi.org/10.1073/pnas.1212100110.

[78] V.M. Lee, M. Goedert, J.Q. Trojanowski, Neurodegenerative tauopathies., Annu. Rev. Neurosci. 24 (2001) 1121–59. https://doi.org/10.1146/annurev.neuro.24.1.1121.

[79] B. Falcon, W. Zhang, A.G. Murzin, G. Murshudov, H.J. Garringer, R. Vidal, R.A. Crowther, B. Ghetti, S.H.W. Scheres, M. Goedert, Structures of filaments from Pick's disease reveal a novel tau protein fold, Nature. 561 (2018) 137–140. https://doi.org/10.1038/s41586-018-0454-y.

[80] P. Poorkaj, T.D. Bird, E. Wijsman, E. Nemens, R.M. Garruto, L. Anderson, A. Andreadis, W.C. Wiederholt, M. Raskind, G.D. Schellenberg, Tau is a candidate gene for chromosome 17 frontotemporal dementia, Ann. Neurol. 43 (1998) 815–825. https://doi.org/10.1002/ana.410430617.

[81] M.G. Spillantini, J.R. Murrell, M. Goedert, M.R. Farlow, A. Klug, B. Ghetti, Mutation in the tau gene in familial multiple system tauopathy with presenile dementia, Proc. Natl. Acad. Sci. U. S. A. 95 (1998) 7737–7741.

https://doi.org/10.1073/pnas.95.13.7737.

[82] M.Y. Lee Virginia, V. Zhukareva, V. Vogelsberg-Ragaglia, Z. Wszolek, L. Reed, B.I. Miller, D.H. Geschwind, T.D. Bird, D. McKeel, A. Coate, J.C. Morris, K.C. Wilhelmsen, G.D. Schellenberg, J.Q. Trojanowski, V.M.Y. Lee, Mutation-specific functional impairments in distinct tau isoforms of hereditary FTDP-17, Science (80-.). 282 (1998) 1914–1917. https://doi.org/10.1126/science.282.5395.1914.

[83] S. Barghorn, Q. Zheng-Fischhofer, M. Ackmann, J. Biernat, M. Von Bergen, E.M. Mandelkow, E. Mandelkow, Structure, microtubule interactions, and paired helical filament aggregation by tau mutants of frontotemporal dementias, Biochemistry. 39 (2000) 11714–11721. https://doi.org/10.1021/bi000850r.

[84] G. Coppola, S. Chinnathambi, J.J. Lee, B.A. Dombroski, M.C. Baker, A.I. Soto-Ortolaza, S.E. Lee, E. Klein, A.Y. Huang, R. Sears, J.R. Lane, A.M. Karydas, R.O. Kenet, J. Biernat, L.-S. Wang, C.W. Cotman, C.S. Decarli, A.I. Levey, J.M. Ringman, M.F. Mendez, H.C. Chui, I. Le Ber, A. Brice, M.K. Lupton, E. Preza, S. Lovestone, J. Powell, N. Graff-Radford, R.C. Petersen, B.F. Boeve, C.F. Lippa, E.H. Bigio, I. Mackenzie, E. Finger, A. Kertesz, R.J. Caselli, M. Gearing, J.L. Juncos, B. Ghetti, S. Spina, Y.M. Bordelon, W.W. Tourtellotte, M.P. Frosch, J.P.G. Vonsattel, C. Zarow, T.G. Beach, R.L. Albin, A.P. Lieberman, V.M. Lee, J.Q. Trojanowski, V.M. Van Deerlin, T.D. Bird, D.R. Galasko, E. Masliah, C.L. White, J.C. Troncoso, D. Hannequin, A.L. Boxer, M.D. Geschwind, S. Kumar, E.-M. Mandelkow, Z.K. Wszolek, R.J. Uitti, D.W. Dickson, J.L. Haines, R. Mayeux, M.A. Pericak-Vance, L.A. Farrer, Alzheimer's Disease Genetics Consortium, O.A. Ross, R. Rademakers, G.D. Schellenberg, B.L. Miller, E. Mandelkow, D.H. Geschwind, Evidence for a role of the rare p.A152T variant in MAPT in increasing the risk for FTD-spectrum and Alzheimer's diseases., Hum. Mol. Genet. 21 (2012) 3500–12. https://doi.org/10.1093/hmg/dds161.

[85] M. Goedert, Tau gene mutations and their effects, Mov. Disord. 20 (2005) S45–S52. https://doi.org/10.1002/mds.20539.

[86] B.L. Goode, P.E. Denis, D. Panda, M.J. Radeke, H.P. Miller, L. Wilson, S.C. Feinstein, Functional interactions between the proline-rich and repeat regions of tau enhance microtubule binding and assembly, Mol. Biol. Cell. 8 (1997) 353–365. https://doi.org/10.1091/mbc.8.2.353.

[87] M. Goedert, M.G. Spillantini, Pathogenesis of the tauopathies, in: J. Mol. Neurosci., Springer, 2011: pp. 425–431. https://doi.org/10.1007/s12031-011-9593-4.

[88] P. Lei, S. Ayton, S. Moon, Q. Zhang, I. Volitakis, D.I. Finkelstein, A.I. Bush, Motor and cognitive deficits in aged tau knockout mice in two background strains, Mol. Neurodegener. 9 (2014) 29. https://doi.org/10.1186/1750-1326-9-29.

[89] M. Von Bergen, P. Friedhoff, J. Biernat, J. Heberle, E.M. Mandelkow, E. Mandelkow, Assembly of τ protein into Alzheimer paired helical filaments depends on a local sequence motif (306VQIVYK311) forming β structure, Proc. Natl. Acad. Sci. U. S. A. 97 (2000) 5129–5134. https://doi.org/10.1073/pnas.97.10.5129.

[90] A.D.C. Alonso, T. Zaidi, M. Novak, I. Grundke-Iqbal, K. Iqbal, Hyperphosphorylation induces self-assembly of τ into tangles of paired helical filaments/straight filaments, Proc. Natl. Acad. Sci. U. S. A. 98 (2001) 6923–6928. https://doi.org/10.1073/pnas.121119298.

[91] A. Schneider, J. Biernat, M. Von Bergen, E. Mandelkow, E.M. Mandelkow, Phosphorylation that detaches tau protein from microtubules (Ser262, Ser214) also protects it against aggregation into Alzheimer paired helical filaments, Biochemistry. 38 (1999) 3549–3558. https://doi.org/10.1021/bi981874p.

[92] A. Seitz, H. Kojima, K. Oiwa, E.E.M. Mandelkow, Y.H. Song, E.E.M. Mandelkow, Single-molecule investigation of the interference between kinesin, tau and MAP2c, 2002. https://doi.org/10.1093/emboj/cdf503.

[93] S. Millecamps, J.P. Julien, Axonal transport deficits and

neurodegenerative diseases, Nat. Rev. Neurosci. 14 (2013) 161–176. https://doi.org/10.1038/nrn3380.

[94] C.M. Cowan, A. Mudher, Are tau aggregates toxic or protective in tauopathies?, Front. Neurol. 4 AUG (2013) 114. https://doi.org/10.3389/fneur.2013.00114.

[95] C.A. Lasagna-Reeves, D.L. Castillo-Carranza, U. Sengupta, J. Sarmiento, J. Troncoso, G.R. Jackson, R. Kayed, Identification of oligomers at early stages of tau aggregation in Alzheimer's disease., FASEB J. Off. Publ. Fed. Am. Soc. Exp. Biol. 26 (2012) 1946–1959. https://doi.org/10.1096/fj.11-199851.

[96] A.D.C. Alonso, B. Li, I. Grundke-Iqbal, K. Iqbal, Polymerization of hyperphosphorylated tau into filaments eliminates its inhibitory activity, Proc. Natl. Acad. Sci. U. S. A. 103 (2006) 8864–8869. https://doi.org/10.1073/pnas.0603214103.

[97] B.R. Hoover, M.N. Reed, J. Su, R.D. Penrod, L.A. Kotilinek, M.K. Grant, R. Pitstick, G.A. Carlson, L.M. Lanier, L.L. Yuan, K.H. Ashe, D. Liao, Tau Mislocalization to Dendritic Spines Mediates Synaptic Dysfunction Independently of Neurodegeneration, Neuron. 68 (2010) 1067–1081. https://doi.org/10.1016/j.neuron.2010.11.030.

[98] L. Zhou, J. McInnes, K. Wierda, M. Holt, A.G. Herrmann, R.J. Jackson, Y.C. Wang, J. Swerts, J. Beyens, K. Miskiewicz, S. Vilain, I. Dewachter, D. Moechars, B. De Strooper, T.L. Spires-Jones, J. De Wit, P. Verstreken, Tau association with synaptic vesicles causes presynaptic dysfunction, Nat. Commun. 8 (2017) 15295. https://doi.org/10.1038/ncomms15295.

[99] H. Kadavath, M. Jaremko, Ł. Jaremko, J. Biernat, E. Mandelkow, M. Zweckstetter, Folding of the Tau Protein on Microtubules, Angew. Chemie Int. Ed. 54 (2015) 10347–10351. https://doi.org/10.1002/anie.201501714.

[100] C. Ballatore, V.M.Y. Lee, J.Q. Trojanowski, Tau-mediated neurodegeneration in Alzheimer's disease and related disorders, Nat. Rev. Neurosci. 8 (2007) 663–672. https://doi.org/10.1038/nrn2194.

[101] M. Kolarova, F. García-Sierra, A. Bartos, J. Ricny, D. Ripova, Structure and pathology of tau protein in Alzheimer disease, Int. J. Alzheimers. Dis. (2012). https://doi.org/10.1155/2012/731526.

[102] A. Del C. Alonso, I. Grundke-Iqbal, K. Iqbal, Alzheimer's disease hyperphosphorylated tau sequesters normal tau into tangles of filaments and disassembles microtubules, Nat. Med. 2 (1996) 783–787. https://doi.org/10.1038/nm0796-783.

[103] L.I. Binder, A.L. Guillozet-Bongaarts, F. Garcia-Sierra, R.W. Berry, Tau, tangles, and Alzheimer's disease, Biochim. Biophys. Acta - Mol. Basis Dis. 1739 (2005) 216–223. https://doi.org/10.1016/j.bbadis.2004.08.014.

[104] T.C. Gamblin, F. Chen, A. Zambrano, A. Abraha, S. Lagalwar, A.L. Guillozet, M. Lu, Y. Fu, F. Garcia-Sierra, N. LaPointe, R. Miller, R.W. Berry, L.I. Binder, V.L. Cryns, Caspase cleavage of tau: Linking amyloid and neurofibrillary tangles in Alzheimer's disease, Proc. Natl. Acad. Sci. U. S. A. 100 (2003) 10032–10037. https://doi.org/10.1073/pnas.1630428100.

[105] L. Fasulo, G. Ugolini, M. Visintin, A. Bradbury, C. Brancolini, V. Verzillo, M. Novak, A. Cattaneo, The neuronal microtubule-associated protein tau is a substrate for caspase-3 and an effector of apoptosis, J. Neurochem. 75 (2000) 624–633. https://doi.org/10.1046/j.1471-4159.2000.0750624.x.

[106] G. Meisl, T.C.T. Michaels, S. Linse, T.P.J. Knowles, Kinetic analysis of amyloid formation, in: Methods Mol. Biol., Humana Press Inc., 2018: pp. 181–196. https://doi.org/10.1007/978-1-4939-7816-8_12.

[107] M. Jucker, L.C. Walker, Self-propagation of pathogenic protein aggregates in neurodegenerative diseases, Nature. 501 (2013) 45–51. https://doi.org/10.1038/nature12481.

[108] R. Crespo, W. Koudstaal, A. Apetri, In vitro assay for studying the aggregation of tau protein and drug screening, J. Vis. Exp. 2018 (2018). https://doi.org/10.3791/58570.

[109] T. Eichner, S.E. Radford, A Diversity of Assembly Mechanisms of a Generic Amyloid Fold, Mol. Cell. 43 (2011) 8–18. https://doi.org/10.1016/j.molcel.2011.05.012.

[110] J.-Z. Wang, I. Grundke-Iqbal, K. Iqbal, Kinases and phosphatases and tau sites involved in Alzheimer neurofibrillary degeneration., Eur. J. Neurosci. 25 (2007) 59–68. https://doi.org/10.1111/j.1460-9568.2006.05226.x.

[111] I. Khlistunova, J. Biernat, Y. Wang, M. Pickhardt, M. Von Bergen, Z. Gazova, E. Mandelkow, E.M. Mandelkow, Inducible expression of tau repeat domain in cell models of tauopathy: Aggregation is toxic to cells but can be reversed by inhibitor drugs, J. Biol. Chem. 281 (2006) 1205–1214. https://doi.org/10.1074/jbc.M507753200.

[112] B. Bandyopadhyay, G. Li, H. Yin, J. Kuret, Tau aggregation and toxicity in a cell culture model of tauopathy, J. Biol. Chem. 282 (2007) 16454–16464. https://doi.org/10.1074/jbc.M700192200.

[113] V. Vogelsberg-Ragaglia, J. Bruce, C. Richter-Landsberg, B. Zhang, M. Hong, J.Q. Trojanowski, V.M.Y. Lee, Distinct FTDP-17 missense mutations in tau produce tau aggregates and other pathological phenotypes in transfected CHO cells, Mol. Biol. Cell. 11 (2000) 4093–4104. https://doi.org/10.1091/mbc.11.12.4093.

[114] M. Von Bergen, S. Barghorn, L. Li, A. Marx, J. Biernat, E.M. Mandelkow, E. Mandelkow, Mutations of Tau Protein in Frontotemporal Dementia Promote Aggregation of Paired Helical Filaments by Enhancing Local β-Structure, J. Biol. Chem. 276 (2001) 48165–48174. https://doi.org/10.1074/jbc.M105196200.

[115] P. Nacharaju, J. Lewis, C. Easson, S. Yen, J. Hackett, M. Hutton, S.H. Yen, Accelerated filament formation from tau protein with specific FTDP-17 missense mutations., FEBS Lett. 447 (1999) 195–9. https://doi.org/10.1016/s0014-5793(99)00294-x.

[116] H. Aoyagi, M. Hasegawa, A. Tamaoka, Fibrillogenic nuclei

composed of P301L mutant tau induce elongation of P301L tau but not wild-type tau, J. Biol. Chem. 282 (2007) 20309–20318. https://doi.org/10.1074/jbc.M611876200.

[117] T. Nonaka, S.T. Watanabe, T. Iwatsubo, M. Hasegawa, Seeded aggregation and toxicity of α-synuclein and tau: Cellular models of neurodegenerative diseases, J. Biol. Chem. 285 (2010) 34885–34898. https://doi.org/10.1074/jbc.M110.148460.

[118] N. Gustke, B. Trinczek, J. Biernat, E.M. Mandelkow, E. Mandelkow, Domains of τ Protein and Interactions with Microtubules, Biochemistry. 33 (1994) 9511–9522. https://doi.org/10.1021/bi00198a017.

[119] S.G. Greenberg, P. Davies, J.D. Schein, L.I. Binder, Hydrofluoric acid-treated τ(PHF) proteins display the same biochemical properties as normal τ, J. Biol. Chem. 267 (1992) 564–569.

[120] M. Goedert, R. Jakes, Expression of separate isoforms of human tau protein: correlation with the tau pattern in brain and effects on tubulin polymerization., EMBO J. 9 (1990) 4225–4230. https://doi.org/10.1002/j.1460-2075.1990.tb07870.x.

[121] B. Frost, R.L. Jacks, M.I. Diamond, Propagation of Tau misfolding from the outside to the inside of a cell, J. Biol. Chem. 284 (2009) 12845–12852. https://doi.org/10.1074/jbc.M808759200.

[122] M. Iba, J.L. Guo, J.D. McBride, B. Zhang, J.Q. Trojanowski, V.M.Y. Lee, Synthetic tau fibrils mediate transmission of neurofibrillary tangles in a transgenic mouse model of alzheimer's-like tauopathy, J. Neurosci. 33 (2013) 1024–1037. https://doi.org/10.1523/JNEUROSCI.2642-12.2013.

[123] E. Peeraer, A. Bottelbergs, K. Van Kolen, I.C. Stancu, B. Vasconcelos, M. Mahieu, H. Duytschaever, L. Ver Donck, A. Torremans, E. Sluydts, N. Van Acker, J.A. Kemp, M. Mercken, K.R. Brunden, J.Q. Trojanowski, I. Dewachter, V.M.Y. Lee, D. Moechars, Intracerebral injection of preformed synthetic tau fibrils initiates widespread tauopathy and neuronal loss in the brains of tau transgenic mice, 73 (2015) 83–95.

https://doi.org/10.1016/j.nbd.2014.08.032.

[124] J.L. Guo, V.M.Y. Lee, Neurofibrillary tangle-like tau pathology induced by synthetic tau fibrils in primary neurons over-expressing mutant tau, FEBS Lett. 587 (2013) 717–723. https://doi.org/10.1016/j.febslet.2013.01.051.

[125] J.L. Guo, S. Narasimhan, L. Changolkar, Z. He, A. Stieber, B. Zhang, R.J. Gathagan, M. Iba, J.D. McBride, J.Q. Trojanowski, V.M.Y. Lee, Unique pathological tau conformers from alzheimer's brains transmit tau pathology in nontransgenic mice, J. Exp. Med. 213 (2016) 2635–2654. https://doi.org/10.1084/jem.20160833.

[126] A. Crowe, M.J. Henderson, J. Anderson, S.A. Titus, A. Zakharov, A. Simeonov, A. Buist, C. Delay, D. Moechars, J.Q. Trojanowski, V.M.Y. Lee, K.R. Brunden, P.E. Fraser, Compound screening in cell-based models of tau inclusion formation: Comparison of primary neuron and HEK293 cell assays, J. Biol. Chem. 295 (2020) jbc.RA119.010532. https://doi.org/10.1074/jbc.ra119.010532.

[127] H. Braak, E. Braak, Neuropathological stageing of Alzheimer-related changes., Acta Neuropathol. 82 (1991) 239–259. https://doi.org/10.1007/BF00308809.

[128] B.T. Hyman, C.H. Phelps, T.G. Beach, E.H. Bigio, N.J. Cairns, M.C. Carrillo, D.W. Dickson, C. Duyckaerts, M.P. Frosch, E. Masliah, S.S. Mirra, P.T. Nelson, J.A. Schneider, D.R. Thal, B. Thies, J.Q. Trojanowski, H. V. Vinters, T.J. Montine, National Institute on Aging-Alzheimer's Association guidelines for the neuropathologic assessment of Alzheimer's disease, Alzheimer's Dement. 8 (2012) 1–13. https://doi.org/10.1016/j.jalz.2011.10.007.

[129] M. Schöll, A. Maass, N. Mattsson-Carlgren, N. Ashton, K. Blennow, H. Zetterberg, W. Jagust, Biomarkers for tau pathology, Mol. Cell. Neurosci. 97 (2018). https://doi.org/10.1016/j.mcn.2018.12.001.

[130] F. Clavaguera, I. Lavenir, B. Falcon, S. Frank, M. Goedert, M.

Tolnay, “Prion-Like” templated misfolding in tauopathies, in: Brain Pathol., 2013: pp. 342–349. https://doi.org/10.1111/bpa.12044.

[131] H. Braak, K. Del Tredici, The pathological process underlying Alzheimer’s disease in individuals under thirty, Acta Neuropathol. 121 (2011) 171–181. https://doi.org/10.1007/s00401-010-0789-4.

[132] A. Elobeid, H. Soininen, I. Alafuzoff, Hyperphosphorylated tau in young and middle-aged subjects., Acta Neuropathol. 123 (2012) 97–104. https://doi.org/10.1007/s00401-011-0906-z.

[133] B. Vasconcelos, I.C. Stancu, A. Buist, M. Bird, P. Wang, A. Vanoosthuyse, K. Van Kolen, A. Verheyen, P. Kienlen-Campard, J.N. Octave, P. Baatsen, D. Moechars, I. Dewachter, Heterotypic seeding of Tau fibrillization by pre-aggregated Abeta provides potent seeds for prion-like seeding and propagation of Tau-pathology in vivo, Acta Neuropathol. 131 (2016) 549–569. https://doi.org/10.1007/s00401-015-1525-x.

[134] U.R.M.O.H.B. DR Thal, D.R. Thal, U. Rüb, M. Orantes, H. Braak, Phases of Aβ-deposition in the human brain and its relevance for the development of AD, Neurology. 58 (2002) 1791–1800. https://doi.org/10.1212/WNL.58.12.1791.

[135] D. Thal, Sequence of Aβ-protein deposition in the human medial temporal lobe, J. Neuropathol. Exp. Neurol. 59 (2000) 733–748.

[136] J.O.G.H. DJ Surmeier, Selective neuronal vulnerability in Parkinson disease, Nat. Rev. Neurosci. 18 (2017) 101–113.

[137] V.L. JL Guo, Cell-to-cell transmission of pathogenic proteins in neurodegenerative diseases, Nat. Med. 20 (2014) 130–138.

[138] H. Fu, A. Possenti, R. Freer, Y. Nakano, N.C.H. Villegas, M. Tang, P.V.M. Cauhy, B.A. Lassus, S. Chen, S.L. Fowler, H.Y. Figueroa, E.D. Huey, G.V.W. Johnson, M. Vendruscolo, K.E. Duff, A tau homeostasis signature is linked with the cellular and regional vulnerability of excitatory neurons to tau pathology, Nat. Neurosci. 22 (2019) 47–56. https://doi.org/10.1038/s41593-018-

0298-7.

[139] S.J. Jackson, C. Kerridge, J. Cooper, A. Cavallini, B. Falcon, C. V. Cella, A. Landi, P.G. Szekeres, T.K. Murray, Z. Ahmed, M. Goedert, M. Hutton, M.J. O'Neill, S. Bose, Short fibrils constitute the major species of seed-competent tau in the brains of mice transgenic for human p301s tau, J. Neurosci. 36 (2016) 762–772. https://doi.org/10.1523/JNEUROSCI.3542-15.2016.

[140] H. Mirbaha, B.B. Holmes, D.W. Sanders, J. Bieschke, M.I. Diamond, Tau trimers are the minimal propagation unit spontaneously internalized to seed intracellular aggregation, J. Biol. Chem. 290 (2015) 14893–14903. https://doi.org/10.1074/jbc.M115.652693.

[141] H. Mirbaha, D. Chen, O.A. Morazova, K.M. Ruff, A.M. Sharma, X. Liu, M. Goodarzi, R. V. Pappu, D.W. Colby, H. Mirzaei, L.A. Joachimiak, M.I. Diamond, Inert and seed-competent tau monomers suggest structural origins of aggregation, Elife. 7 (2018) 1–29. https://doi.org/10.7554/eLife.36584.

[142] S. Narasimhan, Pathological tau strains from human brains recapitulate the diversity of tauopathies in nontransgenic mouse brain, J. Neurosci. 37 (2017) 11406–11423.

[143] F. Clavaguera, Brain homogenates from human tauopathies induce tau inclusions in mouse brain, Proc. Natl Acad. Sci. USA. 110 (2013) 9535–9540.

[144] S. Boluda, M. Iba, B. Zhang, K.M. Raible, V.M.Y. Lee, J.Q. Trojanowski, Differential induction and spread of tau pathology in young PS19 tau transgenic mice following intracerebral injections of pathological tau from Alzheimer's disease or corticobasal degeneration brains, Acta Neuropathol. 129 (2015) 221–237. https://doi.org/10.1007/s00401-014-1373-0.

[145] C. Peng, J.Q. Trojanowski, V.M.Y.M.-Y. Lee, Protein transmission in neurodegenerative disease., Nat. Rev. Neurol. 16 (2020) 199–212. https://doi.org/10.1038/s41582-020-0333-7.

[146] W. Zhang, B. Falcon, A.G. Murzin, J. Fan, R.A. Crowther, M.

Goedert, S.H.W.H. Scheres, Heparin-induced tau filaments are polymorphic and differ from those in alzheimer's and pick's diseases, Elife. 8 (2019) 1–24. https://doi.org/10.7554/eLife.43584.

[147] J. Wu, M. Herman, L. Liu, S. Simoes, C.M. Acker, H. Figueroa, J.I. Steinberg, M. Margittai, R. Kayed, C. Zurzolo, G. Di Paolo, K.E. Duff, Small misfolded tau species are internalized via bulk endocytosis and anterogradely and retrogradely transported in neurons, J. Biol. Chem. 288 (2013) 1856–1870. https://doi.org/10.1074/jbc.M112.394528.

[148] X. Chen, Y. Li, C. Wang, Y. Tang, S.A. Mok, R.M. Tsai, J.C. Rojas, A. Karydas, B.L. Miller, A.L. Boxer, J.E. Gestwicki, M. Arkin, A.M. Cuervo, L. Gan, Promoting tau secretion and propagation by hyperactive p300/CBP via autophagy-lysosomal pathway in tauopathy, Mol. Neurodegener. 15 (2020) 1–19. https://doi.org/10.1186/s13024-019-0354-0.

[149] J.W. Vogel, Y. Iturria-Medina, O.T. Strandberg, R. Smith, E. Levitis, A.C. Evans, O. Hansson, Spread of pathological tau proteins through communicating neurons in human Alzheimer's disease, Nat. Commun. 11 (2020) 2612. https://doi.org/10.1038/s41467-020-15701-2.

[150] Y. Wang, V. Balaji, S. Kaniyappan, L. Krüger, S. Irsen, K. Tepper, R. Chandupatla, W. Maetzler, A. Schneider, E.E.M. Mandelkow, E.E.M. Mandelkow, The release and trans-synaptic transmission of Tau via exosomes, Mol. Neurodegener. 12 (2017) 1–25. https://doi.org/10.1186/s13024-016-0143-y.

[151] S. Saman, W.H. Kim, M. Raya, Y. Visnick, S. Miro, S. Saman, B. Jackson, A.C. McKee, V.E. Alvarez, N.C.Y. Lee, G.F. Hall, Exosome-associated tau is secreted in tauopathy models and is selectively phosphorylated in cerebrospinal fluid in early Alzheimer disease, J. Biol. Chem. 287 (2012) 3842–3849. https://doi.org/10.1074/jbc.M111.277061.

[152] N. Kfoury, B.B. Holmes, H. Jiang, D.M. Holtzman, M.I. Diamond, Trans-cellular propagation of Tau aggregation by fibrillar species, J. Biol. Chem. 287 (2012) 19440–19451.

https://doi.org/10.1074/jbc.M112.346072.

[153] M. Medina, J. Avila, The role of extracellular Tau in the spreading of neurofibrillary pathology, Front. Cell. Neurosci. 8 (2014) 1–7. https://doi.org/10.3389/fncel.2014.00113.

[154] M. Audrain, J.V. Haure-Mirande, M. Wang, S.H. Kim, T. Fanutza, P. Chakrabarty, P. Fraser, P.H. St George-Hyslop, T.E. Golde, R.D. Blitzer, E.E. Schadt, B. Zhang, M.E. Ehrlich, S. Gandy, Integrative approach to sporadic Alzheimer's disease: deficiency of TYROBP in a tauopathy mouse model reduces C1q and normalizes clinical phenotype while increasing spread and state of phosphorylation of tau, Mol. Psychiatry. 24 (2019) 1383–1397. https://doi.org/10.1038/s41380-018-0258-3.

[155] S.C. Hopp, Y. Lin, D. Oakley, A.D. Roe, S.L. Devos, D. Hanlon, B.T. Hyman, The role of microglia in processing and spreading of bioactive tau seeds in Alzheimer's disease 11 Medical and Health Sciences 1109 Neurosciences, J. Neuroinflammation. 15 (2018) 1–15. https://doi.org/10.1186/s12974-018-1309-z.

[156] B.B. Holmes, S.L. DeVos, N. Kfoury, M. Li, R. Jacks, K. Yanamandra, M.O. Ouidja, F.M. Brodsky, J. Marasa, D.P. Bagchi, P.T. Kotzbauer, T.M. Miller, D. Papy-Garcia, M.I. Diamond, Heparan sulfate proteoglycans mediate internalization and propagation of specific proteopathic seeds, Proc. Natl. Acad. Sci. U. S. A. 110 (2013) 1–23. https://doi.org/10.1073/pnas.1301440110.

[157] K.J. McKelvey, K.L. Powell, A.W. Ashton, J.M. Morris, S.A. McCracken, Exosomes: Mechanisms of Uptake, J. Circ. Biomarkers. 4 (2015) 1–9. https://doi.org/10.5772/61186.

[158] S. Abounit, J.W. Wu, K. Duff, G.S. Victoria, C. Zurzolo, Tunneling nanotubes: A possible highway in the spreading of tau and other prion-like proteins in neurodegenerative diseases, Prion. 10 (2016) 344–351. https://doi.org/10.1080/19336896.2016.1223003.

[159] J.J. Chen, D.L. Nathaniel, P. Raghavan, M. Nelson, R. Tian, E. Tse, J.Y. Hong, S.K. See, S.A. Mok, M.Y. Hein, D.R.

Southworth, L.T. Grinberg, J.E. Gestwicki, M.D. Leonetti, M. Kampmann, Compromised function of the ESCRT pathway promotes endolysosomal escape of tau seeds and propagation of tau aggregation, J. Biol. Chem. 294 (2019) 18952–18966. https://doi.org/10.1074/jbc.RA119.009432.

[160] J.N. Rauch, G. Luna, E. Guzman, M. Audouard, C. Challis, Y.E. Sibih, C. Leshuk, I. Hernandez, S. Wegmann, B.T. Hyman, V. Gradinaru, M. Kampmann, K.S. Kosik, LRP1 is a master regulator of tau uptake and spread, Nature. (2020) 1–5. https://doi.org/10.1038/s41586-020-2156-5.

[161] F. Clavaguera, J. Hench, I. Lavenir, G. Schweighauser, S. Frank, M. Goedert, M. Tolnay, Peripheral administration of tau aggregates triggers intracerebral tauopathy in transgenic mice, 2014. https://doi.org/10.1007/s00401-013-1231-5.

[162] Z. Ahmed, J. Cooper, T.K. Murray, K. Garn, E. McNaughton, H. Clarke, S. Parhizkar, M.A. Ward, A. Cavallini, S. Jackson, S. Bose, F. Clavaguera, M. Tolnay, I. Lavenir, M. Goedert, M.L. Hutton, M.J. O'Neill, A novel in vivo model of tau propagation with rapid and progressive neurofibrillary tangle pathology: The pattern of spread is determined by connectivity, not proximity, Acta Neuropathol. 127 (2014) 667–683. https://doi.org/10.1007/s00401-014-1254-6.

[163] S. Calafate, A. Buist, K. Miskiewicz, V. Vijayan, G. Daneels, B. de Strooper, J. de Wit, P. Verstreken, D. Moechars, Synaptic Contacts Enhance Cell-to-Cell Tau Pathology Propagation, Cell Rep. 11 (2015) 1176–1183. https://doi.org/10.1016/j.celrep.2015.04.043.

[164] H. Braak, E. Braak, Development of Alzheimer-related neurofibrillary changes in the neocortex inversely recapitulates cortical myelogenesis, Acta Neuropathol. 92 (1996) 197–201. https://doi.org/10.1007/s004010050508.

[165] M.H. Yana, X. Wang, X. Zhu, M.H. Yan, X. Wang, X. Zhu, Mitochondrial defects and oxidative stress in Alzheimer disease and Parkinson disease, Elsevier Inc., 2013. https://doi.org/10.1016/j.freeradbiomed.2012.11.014.

[166] K.-A. Nave, H.B. Werner, Myelination of the Nervous System: Mechanisms and Functions, Annu. Rev. Cell Dev. Biol. 30 (2014) 503–533. https://doi.org/10.1146/annurev-cellbio-100913-013101.

[167] N. Maphis, G. Xu, O.N. Kokiko-Cochran, S. Jiang, A. Cardona, R.M. Ransohoff, B.T. Lamb, K. Bhaskar, Reactive microglia drive tau pathology and contribute to the spreading of pathological tau in the brain., Brain. 138 (2015) 1738–1755. https://doi.org/10.1093/brain/awv081.

[168] H. Asai, S. Ikezu, S. Tsunoda, M. Medalla, J. Luebke, T. Haydar, B. Wolozin, O. Butovsky, S. Kügler, T. Ikezu, Depletion of microglia and inhibition of exosome synthesis halt tau propagation, 18 (2015) 1584–1593. https://doi.org/10.1038/nn.4132.

[169] J.W. Wu, S.A. Hussaini, I.M. Bastille, G.A. Rodriguez, A. Mrejeru, K. Rilett, D. w. Sanders, C. Cook, H. Fu, R. Boonen, M. Herman, E. Nahmani, S. Emrani, H. Figueroa, M.I. Diamond, C. Clelland, S. Wray, K.E. Duff, Neuronal activity enhances tau propagation and tau pathology in vivo conducted the experiments and data analyses HHS Public Access Author manuscript, Nat Neurosci. 19 (2016) 1085–1092. https://doi.org/10.1038/nn.4328.

[170] K. Yamada, J.K. Holth, F. Liao, F.R. Stewart, T.E. Mahan, H. Jiang, J.R. Cirrito, T.K. Patel, K. Hochgräfe, E.M. Mandelkow, D.M. Holtzman, Neuronal activity regulates extracellular tau in vivo, J. Exp. Med. 211 (2014) 387–393. https://doi.org/10.1084/jem.20131685.

[171] A.M. Pooler, E.C. Phillips, D.H.W. Lau, W. Noble, D.P. Hanger, Physiological release of endogenous tau is stimulated by neuronal activity, EMBO Rep. 14 (2013) 389–394. https://doi.org/10.1038/embor.2013.15.

[172] M.K. Schultz, R. Gentzel, M. Usenovic, C. Gretzula, C. Ware, S. Parmentier-Batteur, J.B. Schachter, H.A. Zariwala, Pharmacogenetic neuronal stimulation increases human tau pathology and trans-synaptic spread of tau to distal brain

regions in mice, Neurobiol. Dis. 118 (2018) 161–176. https://doi.org/10.1016/j.nbd.2018.07.003.

[173] N.V. Mohamed, A. Desjardins, N. Leclerc, Tau secretion is correlated to an increase of Golgi dynamics, PLoS One. 12 (2017) e0178288. https://doi.org/10.1371/journal.pone.0178288.

[174] J.K. Holth, S.K. Fritschi, C. Wang, N.P. Pedersen, J.R. Cirrito, T.E. Mahan, M.B. Finn, M. Manis, J.C. Geerling, P.M. Fuller, B.P. Lucey, D.M. Holtzman, The sleep-wake cycle regulates brain interstitial fluid tau in mice and CSF tau in humans, Science (80-.). 363 (2019) 80–884. https://doi.org/10.1126/science.aav2546.

[175] H.-H. Sun, J.-B. Hu, J. Chen, X.-Y. Wang, X.-L. Wang, P.-L. Pan, C.-F. Liu, Abnormal Spontaneous Neural Activity in Parkinson's Disease With "pure" Apathy, Front. Neurosci. 14 (2020) 1–9. https://doi.org/10.3389/fnins.2020.00830.

[176] M. Asadollahi, M. Atazadeh, M. Noroozian, Seizure in Alzheimer's Disease: An Underestimated Phenomenon, Am. J. Alzheimers. Dis. Other Demen. 34 (2019) 81–88. https://doi.org/10.1177/1533317518813551.

[177] F. Clavaguera, Transmission and spreading of tauopathy in transgenic mouse brain, Nat. Cell Biol. 11 (2009) 909–913.

[178] A. Calignon, Propagation of tau pathology in a model of early Alzheimer's disease, Neuron. 73 (2012) 685–697.

[179] S.L.J.B.T.L.J.J. MJ Yetman, Transgene expression in the Nop-tTA driver line is not inherently restricted to the entorhinal cortex, Brain Struct. Funct. 221 (2016) 2231–2249.

[180] S. Dujardin, K. Lécolle, R. Caillierez, S. Bégard, N. Zommer, C. Lachaud, S. Carrier, N. Dufour, G. Aurégan, J. Winderickx, P. Hantraye, N. Déglon, M. Colin, L. Buée, Neuron-to-neuron wild-type Tau protein transfer through a trans-synaptic mechanism: Relevance to sporadic tauopathies, Acta Neuropathol. Commun. 2 (2014) 1–14. https://doi.org/10.1186/2051-5960-2-

14.

[181] S. Lee, C. Jung, G. Lee, G.F. Hall, Exonic point mutations of human tau enhance its toxicity and cause characteristic changes in neuronal morphology, tau distribution and tau phosphorylation in the lamprey cellular model of tauopathy, J. Alzheimer's Dis. 16 (2009) 99–111. https://doi.org/10.3233/JAD-2009-0954.

[182] D.W. Sanders, S.K. Kaufman, S.L. DeVos, A.M. Sharma, H. Mirbaha, A. Li, S.J. Barker, A.C. Foley, J.R. Thorpe, L.C. Serpell, T.M. Miller, L.T. Grinberg, W.W. Seeley, M.I. Diamond, Distinct tau prion strains propagate in cells and mice and define different tauopathies, Neuron. 82 (2014) 1271–1288. https://doi.org/10.1016/j.neuron.2014.04.047.

[183] A.M. Sharma, T.L. Thomas, D.R. Woodard, O.M. Kashmer, M.I. Diamond, Tau monomer encodes strains, Elife. 7 (2018) 1–20. https://doi.org/10.7554/eLife.37813.

[184] S.K. Kaufman, D.W. Sanders, T.L. Thomas, A.J. Ruchinskas, J. Vaquer-Alicea, A.M. Sharma, T.M. Miller, M.I. Diamond, Tau Prion Strains Dictate Patterns of Cell Pathology, Progression Rate, and Regional Vulnerability In Vivo, Neuron. 92 (2016) 796–812. https://doi.org/10.1016/j.neuron.2016.09.055.

[185] B.B. Holmes, J.L. Furman, T.E. Mahan, T.R. Yamasaki, H. Mirbaha, W.C. Eades, L. Belaygorod, N.J. Cairns, D.M. Holtzman, M.I. Diamond, Proteopathic tau seeding predicts tauopathy in vivo, Proc. Natl. Acad. Sci. U. S. A. 111 (2014) E4376–E4385. https://doi.org/10.1073/pnas.1411649111.

[186] T.K. Kerppola, Design and implementation of bimolecular fluorescence complementation (BiFC) assays for the visualization of protein interactions in living cells, Nat. Protoc. 1 (2006) 1278–1286. https://doi.org/10.1038/nprot.2006.201.

[187] W. Chun, G.S. Waldo, G.V.W. Johnson, Split GFP complementation assay for quantitative measurement of tau aggregation in situ, Methods Mol. Biol. 670 (2011) 109–123. https://doi.org/10.1007/978-1-60761-744-0_9.

[188] H. Tak, M.M. Haque, M.J. Kim, J.H. Lee, J.-H. Baik, Y.Y.K. Kim, D.J. Kim, R. Grailhe, Y.Y.K. Kim, Bimolecular fluorescence complementation; lighting-up tau-tau interaction in living cells., PLoS One. 8 (2013) e81682. https://doi.org/10.1371/journal.pone.0081682.

[189] I. Lopategui Cabezas, A. Herrera Batista, G. Pentón Rol, The role of glial cells in Alzheimer disease: potential therapeutic implications, Neurol. (English Ed. 29 (2014) 305–309. https://doi.org/10.1016/j.nrleng.2012.10.009.

[190] W. Luo, W. Liu, X. Hu, M. Hanna, A. Caravaca, S.M. Paul, Microglial internalization and degradation of pathological tau is enhanced by an anti-tau monoclonal antibody, Sci. Rep. 5 (2015) 11161. https://doi.org/10.1038/srep11161.

[191] H. Martini-Stoica, A.L. Cole, D.B. Swartzlander, F. Chen, Y.W. Wan, L. Bajaj, D.A. Bader, V.M.Y. Lee, J.Q. Trojanowski, Z. Liu, M. Sardiello, H. Zheng, TFEB enhances astroglial uptake of extracellular tau species and reduces tau spreading, J. Exp. Med. 215 (2018) 2355–2377. https://doi.org/10.1084/jem.20172158.

[192] R. Mancuso, G. Fryatt, M. Cleal, J. Obst, E. Pipi, J. Monzón-Sandoval, E. Ribe, L. Winchester, C. Webber, A. Nevado, T. Jacobs, N. Austin, C. Theunis, K. Grauwen, E. Daniela Ruiz, A. Mudher, M. Vicente-Rodriguez, C.A. Parker, C. Simmons, D. Cash, J. Richardson, D.N.C. Jones, S. Lovestone, D. Gómez-Nicola, V.H. Perry, CSF1R inhibitor JNJ-40346527 attenuates microglial proliferation and neurodegeneration in P301S mice, Brain. 142 (2019) 3243–3264. https://doi.org/10.1093/brain/awz241.

[193] R.E. Bennett, A. Bryant, M. Hu, A.B. Robbins, S.C. Hopp, B.T. Hyman, Partial reduction of microglia does not affect tau pathology in aged mice, J. Neuroinflammation. 15 (2018) 311. https://doi.org/10.1186/s12974-018-1348-5.

[194] D.R. Williams, A.J. Lees, Progressive supranuclear palsy: clinicopathological concepts and diagnostic challenges, Lancet Neurol. 8 (2009) 270–279. https://doi.org/10.1016/S1474-

4422(09)70042-0.

[195] S. Narasimhan, L. Changolkar, D.M. Riddle, A. Kats, A. Stieber, S.A. Weitzman, B. Zhang, Z. Li, E.D. Roberson, J.Q. Trojanowski, V.M.Y. Lee, Human tau pathology transmits glial tau aggregates in the absence of neuronal tau, J. Exp. Med. 217 (2020). https://doi.org/10.1084/jem.20190783.

[196] A.B. Shrirao, F.H. Kung, A. Omelchenko, R.S. Schloss, N.N. Boustany, J.D. Zahn, M.L. Yarmush, B.L. Firestein, Microfluidic platforms for the study of neuronal injury in vitro, Biotechnol. Bioeng. 115 (2018) 815–830. https://doi.org/10.1002/bit.26519.

[197] M. Tehranirokh, A.Z. Kouzani, P.S. Francis, J.R. Kanwar, Microfluidic devices for cell cultivation and proliferation, Biomicrofluidics. 7 (2013) 51502. https://doi.org/10.1063/1.4826935.

[198] S. Takeda, S. Wegmann, H. Cho, S.L. Devos, C. Commins, A.D. Roe, S.B. Nicholls, G.A. Carlson, R. Pitstick, C.K. Nobuhara, I. Costantino, M.P. Frosch, D.J. Muller, D. Irimia, B.T. Hyman, Neuronal uptake and propagation of a rare phosphorylated high-molecular-weight tau derived from Alzheimer's disease brain, Nat. Commun. 6 (2015) 8490. https://doi.org/10.1038/ncomms9490.

[199] S. Bersini, A. Miermont, A. Pavesi, R.D. Kamm, J.P. Thiery, M. Moretti, G. Adriani, A combined microfluidic-transcriptomic approach to characterize the extravasation potential of cancer cells, Oncotarget. 9 (2018) 36110–36125. https://doi.org/10.18632/oncotarget.26306.

[200] E. Moutaux, B. Charlot, A. Genoux, F. Saudou, M. Cazorla, An integrated microfluidic/microelectrode array for the study of activity-dependent intracellular dynamics in neuronal networks., Lab Chip. 18 (2018) 3425–3435. https://doi.org/10.1039/c8lc00694f.

[201] B. Deleglise, S. Magnifico, E. Duplus, P. Vaur, V. Soubeyre, M. Belle, M. Vignes, J.L. Viovy, E. Jacotot, J.M. Peyrin, B. Brugg, B-Amyloid Induces a Dying-Back Process and Remote Trans-

Synaptic Alterations in a Microfluidic-Based Reconstructed Neuronal Network, Acta Neuropathol. Commun. 2 (2014) 1–9. https://doi.org/10.1186/s40478-014-0145-3.

[202] Y.I. Wang, H.E. Abaci, M.L. Shuler, Microfluidic blood–brain barrier model provides in vivo-like barrier properties for drug permeability screening, Biotechnol. Bioeng. 114 (2017) 184–194. https://doi.org/10.1002/bit.26045.

[203] S. Maday, A.E. Twelvetrees, A.J. Moughamian, E.L.F. Holzbaur, Axonal Transport: Cargo-Specific Mechanisms of Motility and Regulation, Neuron. 84 (2014) 292–309. https://doi.org/10.1016/j.neuron.2014.10.019.

[204] K. Yanamandra, N. Kfoury, H. Jiang, T.E. Mahan, S. Ma, S.E. Maloney, D.F. Wozniak, M.I. Diamond, D.M. Holtzman, Article Anti-Tau Antibodies that Block Tau Aggregate Seeding In Vitro Markedly Decrease Pathology and Improve Cognition In Vivo, Neuron. 80 (2013) 402–414. https://doi.org/10.1016/j.neuron.2013.07.046.

[205] D. Yanagisawa, H.S. Hamezah, L.W. Durani, H. Taguchi, I. Tooyama, Study of tau pathology in male rTg4510 mice fed with a curcumin derivative Shiga-Y5, PLoS One. 13 (2018). https://doi.org/10.1371/journal.pone.0208440.

[206] X.W. Liu, X.L. Zhao, B. Blackman, X.M. Parmar, X.M.Y. Wong, X.T. Woo, F. Yu, M.J. Chiuchiolo, D. Sondhi, S.M. Kaminsky, R.G. Crystal, X.M. Paul, Vectored Intracerebral Immunization with the Anti-Tau Monoclonal Antibody PHF1 Markedly Reduces Tau Pathology in Mutant Tau Transgenic Mice, 36 (2016) 12425–12435. https://doi.org/10.1523/JNEUROSCI.2016-16.2016.

[207] C.K. Nobuhara, S.L. DeVos, C. Commins, S. Wegmann, B.D. Moore, A.D. Roe, I. Costantino, M.P. Frosch, R. Pitstick, G.A. Carlson, C. Hock, R.M. Nitsch, F. Montrasio, J. Grimm, A.E. Cheung, A.W. Dunah, M. Wittmann, T. Bussiere, P.H. Weinreb, B.T. Hyman, S. Takeda, Tau Antibody Targeting Pathological Species Blocks Neuronal Uptake and Interneuron Propagation of Tau in Vitro, Am. J. Pathol. 187 (2017) 1399–1412.

https://doi.org/10.1016/j.ajpath.2017.01.022.

[208] J. Cummings, G. Lee, A. Ritter, M. Sabbagh, K. Zhong, Alzheimer's disease drug development pipeline: 2019, Alzheimer's Dement. Transl. Res. Clin. Interv. 5 (2019) 272–293. https://doi.org/10.1016/j.trci.2019.05.008.

[209] M. Medina, An Overview on the Clinical Development of Tau-Based Therapeutics., Int. J. Mol. Sci. 19 (2018). https://doi.org/10.3390/ijms19041160.

[210] A. Schneider, E. Mandelkow, Tau-Based Treatment Strategies in Neurodegenerative Diseases, Neurotherapeutics. 5 (2008) 443–457. https://doi.org/10.1016/j.nurt.2008.05.006.

[211] J.M. Domínguez, A. Fuertes, L. Orozco, M. Del Monte-Millán, E. Delgado, M. Medina, Evidence for irreversible inhibition of glycogen synthase kinase-3β by tideglusib, J. Biol. Chem. 287 (2012) 893–904. https://doi.org/10.1074/jbc.M111.306472.

[212] L. Serenó, M. Coma, M. Rodríguez, P. Sánchez-Ferrer, M.B. Sánchez, I. Gich, J.M. Agulló, M. Pérez, J. Avila, C. Guardia-Laguarta, J. Clarimón, A. Lleó, T. Gómez-Isla, A novel GSK-3β inhibitor reduces Alzheimer's pathology and rescues neuronal loss in vivo, Neurobiol. Dis. 35 (2009) 359–367. https://doi.org/https://doi.org/10.1016/j.nbd.2009.05.025.

[213] S. Lovestone, M. Boada, B. Dubois, M. Hüll, J.O. Rinne, H.-J. Huppertz, M. Calero, M. V Andrés, B. Gómez-Carrillo, T. León, T. del Ser, A phase II trial of tideglusib in Alzheimer's disease., J. Alzheimers. Dis. 45 (2015) 75–88. https://doi.org/10.3233/JAD-141959.

[214] H.B. Nygaard, A.F. Wagner, G.S. Bowen, S.P. Good, M.G. MacAvoy, K.A. Strittmatter, A.C. Kaufman, B.J. Rosenberg, T. Sekine-Konno, P. Varma, K. Chen, A.J. Koleske, E.M. Reiman, S.M. Strittmatter, C.H. van Dyck, A phase Ib multiple ascending dose study of the safety, tolerability, and central nervous system availability of AZD0530 (saracatinib) in Alzheimer's disease., Alzheimers. Res. Ther. 7 (2015) 35. https://doi.org/10.1186/s13195-015-0119-0.

[215] C.H. van Dyck, H.B. Nygaard, K. Chen, M.C. Donohue, R. Raman, R.A. Rissman, J.B. Brewer, R.A. Koeppe, T.W. Chow, M.S. Rafii, D. Gessert, J. Choi, R.S. Turner, J.A. Kaye, S.A. Gale, E.M. Reiman, P.S. Aisen, S.M. Strittmatter, Effect of AZD0530 on Cerebral Metabolic Decline in Alzheimer Disease: A Randomized Clinical Trial., JAMA Neurol. 76 (2019) 1219–1229. https://doi.org/10.1001/jamaneurol.2019.2050.

[216] M. Medina, F. Hernández, J. Avila, New Features about Tau Function and Dysfunction., Biomolecules. 6 (2016). https://doi.org/10.3390/biom6020021.

[217] S.A. Yuzwa, X. Shan, M.S. Macauley, T. Clark, Y. Skorobogatko, K. Vosseller, D.J. Vocadlo, Increasing O-GlcNAc slows neurodegeneration and stabilizes tau against aggregation., Nat. Chem. Biol. 8 (2012) 393–399. https://doi.org/10.1038/nchembio.797.

[218] S.-W. Min, X. Chen, T.E. Tracy, Y. Li, Y. Zhou, C. Wang, K. Shirakawa, S.S. Minami, E. Defensor, S.A. Mok, P.D. Sohn, B. Schilling, X. Cong, L. Ellerby, B.W. Gibson, J. Johnson, N. Krogan, M. Shamloo, J. Gestwicki, E. Masliah, E. Verdin, L. Gan, Critical role of acetylation in tau-mediated neurodegeneration and cognitive deficits., Nat. Med. 21 (2015) 1154–1162. https://doi.org/10.1038/nm.3951.

[219] J.-H. Lee, J.-S. Liow, S. Paul, C.L. Morse, M.B. Haskali, L. Manly, S. Shcherbinin, J.C. Ruble, N. Kant, E.C. Collins, H.N. Nuthall, P. Zanotti-Fregonara, S.S. Zoghbi, V.W. Pike, R.B. Innis, PET quantification of brain O-GlcNAcase with [(18)F]LSN3316612 in healthy human volunteers., EJNMMI Res. 10 (2020) 20. https://doi.org/10.1186/s13550-020-0616-4.

[220] K.R. Brunden, B. Zhang, J. Carroll, Y. Yao, J.S. Potuzak, A.-M.L. Hogan, M. Iba, M.J. James, S.X. Xie, C. Ballatore, A.B. 3rd Smith, V.M.-Y. Lee, J.Q. Trojanowski, Epothilone D improves microtubule density, axonal integrity, and cognition in a transgenic mouse model of tauopathy., J. Neurosci. 30 (2010) 13861–13866. https://doi.org/10.1523/JNEUROSCI.3059-10.2010.

[221] Y. Matsuoka, Y. Jouroukhin, A.J. Gray, L. Ma, C. Hirata-Fukae, H.-F. Li, L. Feng, L. Lecanu, B.R. Walker, E. Planel, O. Arancio, I. Gozes, P.S. Aisen, A neuronal microtubule-interacting agent, NAPVSIPQ, reduces tau pathology and enhances cognitive function in a mouse model of Alzheimer's disease., J. Pharmacol. Exp. Ther. 325 (2008) 146–153. https://doi.org/10.1124/jpet.107.130526.

[222] B.H. Morimoto, D. Schmechel, J. Hirman, A. Blackwell, J. Keith, M. Gold, A double-blind, placebo-controlled, ascending-dose, randomized study to evaluate the safety, tolerability and effects on cognition of AL-108 after 12 weeks of intranasal administration in subjects with mild cognitive impairment., Dement. Geriatr. Cogn. Disord. 35 (2013) 325–336. https://doi.org/10.1159/000348347.

[223] A.L. Boxer, A.E. Lang, M. Grossman, D.S. Knopman, B.L. Miller, L.S. Schneider, R.S. Doody, A. Lees, L.I. Golbe, D.R. Williams, J.-C. Corvol, A. Ludolph, D. Burn, S. Lorenzl, I. Litvan, E.D. Roberson, G.U. Höglinger, M. Koestler, C.R. Jack Jr, V. Van Deerlin, C. Randolph, I. V Lobach, H.W. Heuer, I. Gozes, L. Parker, S. Whitaker, J. Hirman, A.J. Stewart, M. Gold, B.H. Morimoto, Davunetide in patients with progressive supranuclear palsy: a randomised, double-blind, placebo-controlled phase 2/3 trial, Lancet Neurol. 13 (2014) 676–685. https://doi.org/10.1016/S1474-4422(14)70088-2.

[224] B. Bulic, M. Pickhardt, E. Mandelkow, Progress and developments in tau aggregation inhibitors for Alzheimer disease., J. Med. Chem. 56 (2013) 4135–4155. https://doi.org/10.1021/jm3017317.

[225] C.M. Wischik, P.C. Edwards, R.Y. Lai, M. Roth, C.R. Harrington, Selective inhibition of Alzheimer disease-like tau aggregation by phenothiazines., Proc. Natl. Acad. Sci. U. S. A. 93 (1996) 11213–11218. https://doi.org/10.1073/pnas.93.20.11213.

[226] C.M. Wischik, R.T. Staff, D.J. Wischik, P. Bentham, A.D. Murray, J.M.D. Storey, K.A. Kook, C.R. Harrington, Tau aggregation inhibitor therapy: an exploratory phase 2 study in mild or moderate Alzheimer's disease., J. Alzheimers. Dis. 44 (2015)

705–720. https://doi.org/10.3233/JAD-142874.

[227] G.K. Wilcock, S. Gauthier, G.B. Frisoni, J. Jia, J.H. Hardlund, H.J. Moebius, P. Bentham, K.A. Kook, B.O. Schelter, D.J. Wischik, C.S. Davis, R.T. Staff, V. Vuksanovic, T. Ahearn, L. Bracoud, K. Shamsi, K. Marek, J. Seibyl, G. Riedel, J.M.D. Storey, C.R. Harrington, C.M. Wischik, Potential of Low Dose Leuco-Methylthioninium Bis(Hydromethanesulphonate) (LMTM) Monotherapy for Treatment of Mild Alzheimer's Disease: Cohort Analysis as Modified Primary Outcome in a Phase III Clinical Trial, J. Alzheimer's Dis. 61 (2018) 435–457. https://doi.org/10.3233/JAD-170560.

[228] S. Gauthier, H.H. Feldman, L.S. Schneider, G.K. Wilcock, G.B. Frisoni, J.H. Hardlund, H.J. Moebius, P. Bentham, K.A. Kook, D.J. Wischik, B.O. Schelter, C.S. Davis, R.T. Staff, L. Bracoud, K. Shamsi, J.M.D. Storey, C.R. Harrington, C.M. Wischik, Efficacy and safety of tau-aggregation inhibitor therapy in patients with mild or moderate Alzheimer's disease: a randomised, controlled, double-blind, parallel-arm, phase 3 trial, Lancet. 388 (2016) 2873–2884. https://doi.org/10.1016/S0140-6736(16)31275-2.

[229] F. van Bebber, D. Paquet, A. Hruscha, B. Schmid, C. Haass, Methylene blue fails to inhibit Tau and polyglutamine protein dependent toxicity in zebrafish., Neurobiol. Dis. 39 (2010) 265–271. https://doi.org/10.1016/j.nbd.2010.03.023.

[230] J. Wagner, S. Ryazanov, A. Leonov, J. Levin, S. Shi, F. Schmidt, C. Prix, F. Pan-Montojo, U. Bertsch, G. Mitteregger-Kretzschmar, M. Geissen, M. Eiden, F. Leidel, T. Hirschberger, A.A. Deeg, J.J. Krauth, W. Zinth, P. Tavan, J. Pilger, M. Zweckstetter, T. Frank, M. Bähr, J.H. Weishaupt, M. Uhr, H. Urlaub, U. Teichmann, M. Samwer, K. Bötzel, M. Groschup, H. Kretzschmar, C. Griesinger, A. Giese, Anle138b: A novel oligomer modulator for disease-modifying therapy of neurodegenerative diseases such as prion and Parkinson's disease, Acta Neuropathol. 125 (2013) 795–813. https://doi.org/10.1007/s00401-013-1114-9.

[231] J. Wagner, S. Krauss, S. Shi, S. Ryazanov, J. Steffen, C. Miklitz,

A. Leonov, A. Kleinknecht, B. Göricke, J.H. Weishaupt, D. Weckbecker, A.M. Reiner, W. Zinth, J. Levin, D. Ehninger, S. Remy, H.A. Kretzschmar, C. Griesinger, A. Giese, M. Fuhrmann, Reducing tau aggregates with anle138b delays disease progression in a mouse model of tauopathies, Acta Neuropathol. 130 (2015) 619–631. https://doi.org/10.1007/s00401-015-1483-3.

[232] M. Brendel, M. Deussing, T. Blume, L. Kaiser, F. Probst, F. Overhoff, F. Peters, B. von Ungern-Sternberg, S. Ryazanov, A. Leonov, C. Griesinger, A. Zwergal, J. Levin, P. Bartenstein, I. Yakushev, P. Cumming, G. Boening, S. Ziegler, J. Herms, A. Giese, A. Rominger, Late-stage Anle138b treatment ameliorates tau pathology and metabolic decline in a mouse model of human Alzheimer's disease tau., Alzheimers. Res. Ther. 11 (2019) 67. https://doi.org/10.1186/s13195-019-0522-z.

[233] A. Dominguez-Meijide, E. Vasili, A. König, M.-S. Cima-Omori, A. Ibáñez de Opakua, A. Leonov, S. Ryazanov, M. Zweckstetter, C. Griesinger, T.F. Outeiro, Effects of pharmacological modulators of α-synuclein and tau aggregation and internalization, Sci. Rep. 10 (2020) 12827. https://doi.org/10.1038/s41598-020-69744-y.

[234] J.T. Pedersen, E.M. Sigurdsson, Tau immunotherapy for Alzheimer's disease., Trends Mol. Med. 21 (2015) 394–402. https://doi.org/10.1016/j.molmed.2015.03.003.

[235] E. Kontsekova, N. Zilka, B. Kovacech, P. Novak, M. Novak, First-in-man tau vaccine targeting structural determinants essential for pathological tau-tau interaction reduces tau oligomerisation and neurofibrillary degeneration in an Alzheimer's disease model., Alzheimers. Res. Ther. 6 (2014) 44. https://doi.org/10.1186/alzrt278.

[236] P. Novak, N. Zilka, M. Zilkova, B. Kovacech, R. Skrabana, M. Ondrus, L. Fialova, E. Kontsekova, M. Otto, M. Novak, AADvac1, an Active Immunotherapy for Alzheimer's Disease and Non Alzheimer Tauopathies: An Overview of Preclinical and Clinical Development., J. Prev. Alzheimer's Dis. 6 (2019) 63–69. https://doi.org/10.14283/jpad.2018.45.

[237] C. Theunis, N. Crespo-Biel, V. Gafner, M. Pihlgren, M.P. López-Deber, P. Reis, D.T. Hickman, O. Adolfsson, N. Chuard, D.M. Ndao, P. Borghgraef, H. Devijver, F. Van Leuven, A. Pfeifer, A. Muhs, Efficacy and safety of a liposome-based vaccine against protein Tau, assessed in Tau.P301L mice that model tauopathy, PLoS One. 8 (2013). https://doi.org/10.1371/journal.pone.0072301.

[238] R. Alam, D. Driver, S. Wu, E. Lozano, S.L. Key, J.T. Hole, M.L. Hayashi, J. Lu, Preclinical Characterization of an Antibody [Ly3303560] Targeting Aggregated Tau, Alzheimer's Dement. 13 (2017) P592–P593. https://doi.org/10.1016/j.jalz.2017.07.227.

[239] M.L. Hayashi, J. Lu, S. Wu, S. Bose, Z. Ahmed, J. Cooper, T.K. Murray, S.J. Jackson, A. Cavallini, M. Ward, D. Driver, M. Goedert, R.B. Demattos, M.J. O'Neill, M. Hutton, Aggregate-Selective Anti-Tau Antibody Mc-1 Demonstrated Robust in Vitro and in Vivo Activity To Neutralize Transmissible Tau and Reduce Tau Pathology, Alzheimer's Dement. 13 (2017) P592. https://doi.org/10.1016/j.jalz.2017.07.226.

[240] T. West, Y. Hu, P.B. Verghese, R.J. Bateman, J.B. Braunstein, I. Fogelman, K. Budur, H. Florian, N. Mendonca, D.M. Holtzman, Preclinical and Clinical Development of ABBV-8E12, a Humanized Anti-Tau Antibody, for Treatment of Alzheimer's Disease and Other Tauopathies, J. Prev. Alzheimer's Dis. 4 (2017) 236–241. https://doi.org/10.14283/jpad.2017.36.

[241] K. Yanamandra, H. Jiang, T.E. Mahan, S.E. Maloney, D.F. Wozniak, M.I. Diamond, D.M. Holtzman, Anti-tau antibody reduces insoluble tau and decreases brain atrophy., Ann. Clin. Transl. Neurol. 2 (2015) 278–288. https://doi.org/10.1002/acn3.176.

[242] A. Cavallini, S. Brewerton, A. Bell, S. Sargent, S. Glover, C. Hardy, R. Moore, J. Calley, D. Ramachandran, M. Poidinger, E. Karran, P. Davies, M. Hutton, P. Szekeres, S. Bose, An unbiased approach to identifying tau kinases that phosphorylate tau at sites associated with Alzheimer's disease, (2013). https://doi.org/10.1074/jbc.M113.463984.

[243] R. Mayeux, Y. Stern, Epidemiology of Alzheimer disease., Cold Spring Harb. Perspect. Med. 2 (2012). https://doi.org/10.1101/cshperspect.a006239.

[244] C. Andorfer, Y. Kress, M. Espinoza, R. De Silva, K.L. Tucker, Y.A. Barde, K. Duff, P. Davies, Hyperphosphorylation and aggregation of tau in mice expressing normal human tau isoforms, J. Neurochem. 86 (2003) 582–590. https://doi.org/10.1046/j.1471-4159.2003.01879.x.

[245] S.G. Greenberg, P. Davies, A preparation of Alzheimer paired helical filaments that displays distinct τ proteins by polyacrylamide gel electrophoresis, Proc. Natl. Acad. Sci. U. S. A. 87 (1990) 5827–5831. https://doi.org/10.1073/pnas.87.15.5827.

[246] J.W. Wu, S.A. Hussaini, I.M. Bastille, G.A. Rodriguez, A. Mrejeru, K. Rilett, D.W. Sanders, C. Cook, H. Fu, R.A.C.M. Boonen, M. Herman, E. Nahmani, S. Emrani, Y.H. Figueroa, M.I. Diamond, C.L. Clelland, S. Wray, K.E. Duff, Neuronal activity enhances tau propagation and tau pathology in vivo, Nat. Neurosci. 19 (2016) 1085–1092. https://doi.org/10.1038/nn.4328.

[247] R. Renault, J.B. Durand, J.L. Viovy, C. Villard, Asymmetric axonal edge guidance: A new paradigm for building oriented neuronal networks, Lab Chip. 16 (2016) 2188–2191. https://doi.org/10.1039/c6lc00479b.

[248] E.D. Roberson, K. Scearce-Levie, J.J. Palop, F. Yan, I.H. Cheng, T. Wu, H. Gerstein, G.-Q. Yu, L. Mucke, Reducing Endogenous Tau Ameliorates Amyloid ß-Induced Deficits in an Alzheimer's Disease Mouse Model, Science (80-.). 316 (2007) 750–754. https://doi.org/10.1126/science.1141736.

[249] L.M. Ittner, Y.D. Ke, F. Delerue, M. Bi, A. Gladbach, J. van Eersel, H. Wölfing, B.C. Chieng, M.J. Christie, I.A. Napier, A. Eckert, M. Staufenbiel, E. Hardeman, J. Götz, Dendritic Function of Tau Mediates Amyloid-B Toxicity in Alzheimer's Disease Mouse Models, Cell. 142 (2010) 387–397. https://doi.org/10.1016/j.cell.2010.06.036.

[250] J.M. Decker, L. Krüger, A. Sydow, F.J. Dennissen, Z. Siskova, E. Mandelkow, E.-M. Mandelkow, The Tau/A152T mutation, a risk factor for frontotemporal-spectrum disorders, leads to NR2B receptor-mediated excitotoxicity., EMBO Rep. 17 (2016) 552–569. https://doi.org/10.15252/embr.201541439.

[251] S. Maeda, B. Djukic, P. Taneja, G.-Q. Yu, I. Lo, A. Davis, R. Craft, W. Guo, X. Wang, D. Kim, R. Ponnusamy, T.M. Gill, E. Masliah, L. Mucke, Expression of A152T human tau causes age-dependent neuronal dysfunction and loss in transgenic mice., EMBO Rep. 17 (2016) 530–551. https://doi.org/10.15252/embr.201541438.

[252] M.R. Hynd, H.L. Scott, P.R. Dodd, Glutamate-mediated excitotoxicity and neurodegeneration in Alzheimer's disease., Neurochem. Int. 45 (2004) 583–595. https://doi.org/10.1016/j.neuint.2004.03.007.

[253] D. Dewar, J. McCulloch, Abnormalities in Non-Cholinergic Neurotransmitter Systems in Alzheimer's Disease BT - Dementia, in: A. Burns, R. Levy (Eds.), Springer US, Boston, MA, 1994: pp. 159–183. https://doi.org/10.1007/978-1-4615-6805-6_11.

[254] A.W. Procter, Neurochemical Correlates of Dementia, Neurodegeneration. 5 (1996) 403–407. https://doi.org/https://doi.org/10.1006/neur.1996.0054.

[255] K. Gottmann, F.W. Krieger, H.D. Lux, The formation of glutamatergic synapses in cultured central neurons: selective increase in miniature synaptic currents, Dev. Brain Res. 81 (1994) 77–88. https://doi.org/10.1016/0165-3806(94)90070-1.

[256] W.P. Chen, A.L. Kirchgessner, Activation of group II mGlu receptors inhibits voltage-gated Ca2+ currents in myenteric neurons, Am. J. Physiol. - Gastrointest. Liver Physiol. 283 (2002). https://doi.org/10.1152/ajpgi.00216.2002.

[257] X. Zhang, C. Upreti, P.K. Stanton, Gβγ and the C Terminus of SNAP-25 Are Necessary for Long-Term Depression of Transmitter Release, PLoS One. 6 (2011) e20500.

https://doi.org/10.1371/journal.pone.0020500.

[258] F. Hernández, J. Merchán-Rubira, L. Vallés-Saiz, A. Rodríguez-Matellán, J. Avila, Differences Between Human and Murine Tau at the N-terminal End, Front. Aging Neurosci. 12 (2020) 11. https://doi.org/10.3389/fnagi.2020.00011.

[259] K. Duff, H. Knight, L.M. Refolo, S. Sanders, X. Yu, M. Picciano, B. Malester, M. Hutton, J. Adamson, M. Goedert, K. Burki, P. Davies, Characterization of pathology in transgenic mice over-expressing human genomic and cDNA tau transgenes, Neurobiol. Dis. 7 (2000) 87–98. https://doi.org/10.1006/nbdi.1999.0279.

[260] K.L. Tucker, M. Meyer, Y.A. Barde, Neurotrophins are required for nerve growth during development, Nat. Neurosci. 4 (2001) 29–32. https://doi.org/10.1038/82868.

[261] I. Ferrer, I. López-González, M. Carmona, L. Arregui, E. Dalfó, B. Torrejón-Escribano, R. Diehl, G.G. Kovacs, Glial and neuronal tau pathology in tauopathies: Characterization of disease-specific phenotypes and tau pathology progression, J. Neuropathol. Exp. Neurol. 73 (2014) 81–97. https://doi.org/10.1097/NEN.0000000000000030.

[262] C.E.G. Leyns, D.M. Holtzman, Glial contributions to neurodegeneration in tauopathies, Mol. Neurodegener. 12 (2017). https://doi.org/10.1186/s13024-017-0192-x.

[263] D.M. Holtzman, J.C. Morris, A.M. Goate, Alzheimer's disease: the challenge of the second century., Sci. Transl. Med. 3 (2011) 77sr1. https://doi.org/10.1126/scitranslmed.3002369.

[264] L.K. Huang, S.P. Chao, C.J. Hu, Clinical trials of new drugs for Alzheimer disease, J. Biomed. Sci. 27 (2020) 18. https://doi.org/10.1186/s12929-019-0609-7.

[265] M. Goedert, R. Jakes, Mutations causing neurodegenerative tauopathies, Biochim. Biophys. Acta - Mol. Basis Dis. 1739 (2005) 240–250. https://doi.org/10.1016/j.bbadis.2004.08.007.

[266] M. Wegrzynowicz, D. Bar-On, L. Calo', O. Anichtchik, M. Iovino,

J. Xia, S. Ryazanov, A. Leonov, A. Giese, J.W. Dalley, C. Griesinger, U. Ashery, M.G. Spillantini, Depopulation of dense α-synuclein aggregates is associated with rescue of dopamine neuron dysfunction and death in a new Parkinson's disease model, Acta Neuropathol. 138 (2019) 575–595. https://doi.org/10.1007/s00401-019-02023-x.

[267] R. Renault, N. Sukenik, S. Descroix, L. Malaquin, J.L. Viovy, J.M. Peyrin, S. Bottani, P. Monceau, E. Moses, M. Vignes, Combining microfluidics, optogenetics and calcium imaging to study neuronal communication in vitro, PLoS One. 10 (2015) 1–15. https://doi.org/10.1371/journal.pone.0120680.

[268] D.Y. Kim, B.W. Carey, H. Wang, L.A.M. Ingano, A.M. Binshtok, M.H. Wertz, W.H. Pettingell, P. He, V.M.Y. Lee, C.J. Woolf, D.M. Kovacs, BACE1 regulates voltage-gated sodium channels and neuronal activity, Nat. Cell Biol. 9 (2007) 755–764. https://doi.org/10.1038/ncb1602.

[269] J.J. Palop, L. Mucke, Network abnormalities and interneuron dysfunction in Alzheimer disease, Nat. Rev. Neurosci. 17 (2016) 777–792. https://doi.org/10.1038/nrn.2016.141.

[270] Z. Šišková, D. Justus, H. Kaneko, D. Friedrichs, N. Henneberg, T. Beutel, J. Pitsch, S. Schoch, A. Becker, H. vonderKammer, S. Remy, Dendritic structural degeneration is functionally linked to cellular hyperexcitability in a mouse model of alzheimer's disease, Neuron. 84 (2014) 1023–1033. https://doi.org/10.1016/j.neuron.2014.10.024.

[271] S. Ghatak, N. Dolatabadi, D. Trudler, X. Zhang, Y. Wu, M. Mohata, R. Ambasudhan, M. Talantova, S.A. Lipton, Mechanisms of hyperexcitability in alzheimer's disease hiPSC-derived neurons and cerebral organoids vs. Isogenic control, Elife. 8 (2019). https://doi.org/10.7554/eLife.50333.

[272] G. Hallinan, M. Vargas-Caballero, J. West, K. Deinhardt, Efficient propagation of misfolded tau between individual neurons occurs in absence of degeneration, BioRxiv. (2018) 372029. https://doi.org/10.1101/372029.

[273] S.L. DeVos, B.T. Corjuc, D.H. Oakley, C.K. Nobuhara, R.N. Bannon, A. Chase, C. Commins, J.A. Gonzalez, P.M. Dooley, M.P. Frosch, B.T. Hyman, Synaptic tau seeding precedes tau pathology in human Alzheimer's disease brain, Front. Neurosci. 12 (2018) 1–15. https://doi.org/10.3389/fnins.2018.00267.

[274] E.P. Neff, Animal models of Alzheimer's disease embrace diversity, Lab Anim. (NY). 48 (2019) 255–259. https://doi.org/10.1038/s41684-019-0377-8.

[275] Z. Joel, P. Izquierdo, D.A. Salih, J.C. Richardson, D.M. Cummings, F.A. Edwards, Improving mouse models for dementia. Are all the effects in tau mouse models due to overexpression?, Cold Spring Harb. Symp. Quant. Biol. 83 (2018) 151–161. https://doi.org/10.1101/sqb.2018.83.037531.

[276] Z. He, J.D. McBride, H. Xu, L. Changolkar, S. jung Kim, B. Zhang, S. Narasimhan, G.S. Gibbons, J.L. Guo, M. Kozak, G.D. Schellenberg, J.Q. Trojanowski, V.M.Y. Lee, Transmission of tauopathy strains is independent of their isoform composition, Nat. Commun. 11 (2020). https://doi.org/10.1038/s41467-019-13787-x.

[277] D. Mehta, R. Jackson, G. Paul, J. Shi, M. Sabbagh, Why do trials for Alzheimer's disease drugs keep failing? A discontinued drug perspective for 2010-2015., Expert Opin. Investig. Drugs. 26 (2017) 735–739. https://doi.org/10.1080/13543784.2017.1323868.

[278] A.C. Immune, A.C.I. Sa, R. Group, C.D. Rating-sum, C.- Sb, D.A.S. Subscale, A.- Cog, D. Cooperative, S. Group, D.L. Inventory, A. Pfeifer, A.C.I. Sa, PRESS RELEASE AC Immune Reports Top Line Results from TAURIEL Phase 2 Trial Evaluating Semorinemab in Early Alzheimer ' s Disease, (2020) 1–5.

[279] B. De Strooper, E. Karran, The Cellular Phase of Alzheimer's Disease, Cell. 164 (2016) 603–615. https://doi.org/10.1016/j.cell.2015.12.056.

[280] R.W.M. Hoetelmans, F.A. Prins, I.C. Velde, J. Van der Meer,

C.J.H. Van de Velde, J.H. Van Dierendonck, Effects of acetone, methanol, or paraformaldehyde on cellular structure, visualized by reflection contrast microscopy and transmission and scanning electron microscopy, Appl. Immunohistochem. Mol. Morphol. 9 (2001) 346–351. https://doi.org/10.1097/00022744-200112000-00010.

[281] S. Brahmachari, Y.K. Fung, K. Pahan, Induction of glial fibrillary acidic protein expression in astrocytes by nitric oxide, J. Neurosci. 26 (2006) 4930–4939. https://doi.org/10.1523/JNEUROSCI.5480-05.2006.

[282] S.C. Hopp, Y. Lin, D. Oakley, A.D. Roe, S.L. DeVos, D. Hanlon, B.T. Hyman, The role of microglia in processing and spreading of bioactive tau seeds in Alzheimer's disease, J. Neuroinflammation. 15 (2018) 1–15. https://doi.org/10.1186/s12974-018-1309-z.

[283] S. Gribaudo, P. Tixador, L. Bousset, A. Fenyi, P. Lino, R. Melki, J.M. Peyrin, A.L. Perrier, Propagation of α-Synuclein Strains within Human Reconstructed Neuronal Network, Stem Cell Reports. 12 (2019) 230–244. https://doi.org/10.1016/j.stemcr.2018.12.007.

6. SCIENTIFIC PRODUCTS

Publications:

- ***Quantitative propagation of assembled human Tau from Alzheimer's disease brain in microfluidic neuronal cultures.*** *A. Katsikoudi, **E. Ficulle**, A. Cavallini, G. Sharman, A. Guyot, M. Zagnoni, B. Eastwood, M. Hutton, and S. Bose. J. Biol. Chem. 22 Jul 2020, jbc.RA120.013325. doi:10.1074/jbc.RA120.013325*

- ***The selective disruption of presynaptic JNK2/STX1a interaction reduces NMDA receptor-dependent glutamate release***
  *Marcelli S, Iannuzzi F, **Ficulle E**, Mango D, Pieraccini S, Pellegrino S, Corbo M, Sironi M, Pittaluga A, Nisticò R, Feligioni M.*
  Sci Rep. 2019 May 9;9(1):7146. doi: 10.1038/s41598-019-43709-2.

- ***Hyperhomocysteinemia as a Risk Factor and Potential Nutraceutical Target for Certain Pathologies***
  *Tinelli C, Di Pino A, **Ficulle E**, Marcelli S, Feligioni M.*
  Front Nutr. 2019 Apr 24;6:49. doi: 10.3389/fnut.2019.00049. eCollection 2019. Review.

- ***MicroRNAs and mild cognitive impairment: A systematic review***
  *Piscopo P, Lacorte E, Feligioni M, Mayer F, Crestini A, Piccolo L, Bacigalupo I, Filareti M, **Ficulle E**, Confaloni A, Vanacore N, Corbo M.*
  Ageing Res Rev. 2019 Mar;50:131-141. doi: 10.1016/j.arr.2018.11.005. Epub 2018 Nov 22. Review.

- ***Aging-related SUMOylation pattern in the cortex and blood plasma of wild type mice***
  ***Ficulle E**, Sufian MDS, Tinelli C, Corbo M, Feligioni M.*
  Neurosci Lett. 2018 Mar 6;668:48-54. doi: 10.1016/j.neulet.2018.01.004. Epub 2018 Jan 8.

- ***An overview of the possible therapeutic role of SUMOylation in the treatment of Alzheimer's disease***
  *Marcelli S, **Ficulle E**, Piccolo L, Corbo M, Feligioni M.*
  Pharmacol Res. 2018 Apr; 130:420-437.
  Doi:10.1016/j.phrs.2017.12.023. Epub 2017 Dec26. Review.

Posters:

- ***SUMOylation and SUMO machinery profiling in the brain and blood plasma of ageing mice***
  *Md Shah Sufian, **E Ficulle**, M Corbo, M Feligioni.*
  4-6 December 2018, Milan.

7. DISCLOSURE INFORMATION

The availability of the results of this thesis has been possible through an agreement between Eli Lilly & Co. and the University of Milan.

8. PhD THESIS EVALUATION

This thesis was evaluated by 4 independent reviewers:

- Marco Feligioni, PhD, European Brain Research Institute (EBRI), Rome, Italy
- Sarah Pearce, PhD, Department of Physiology, Anatomy and Genetics, University of Oxford, UK
- Floriana Licitra, PhD, Evox, Oxford UK
- Oihana Errea Lorenzo, PhD, Cima Universidad de Navarra, Spain